NONLINEAR DYNAMICS OF TWO PENDULUMS

SUBTENDED BY AN ANGLE

CHAN KOK HONG, BEng.

Thesis submitted to the University of Nottingham for the

degree of Master of Philosophy

February 2017

Abstract

The work was based from previous analytical results that aims to facilitate rotations. It aims to initially use an elliptical track. However, from previous experimental observations, it was noted that addition of another pendulum, at an angle, instead of introducing a circular track, seemed more effective in inducing rotations.

The idea of inducing rotations with a higher range of frequency is intriguing, with rotations being one of the centerpiece of energy generations or mechanical motion. Rotations are used because there is a continuous translational energy as compared to oscillations where it loses energy on it's peak. If the experiment can induce rotations with impacts present and is still capable of rotating to generate electricity, it could lead to many more possibilities.

Renewable energy using vibration is the main approach of this work, and investigating ways to achieve such energy with rotations using electromechanical device is one of the initial conditions that have been chosen to act as a motivation.

Acknowledgements

I would like to express my deepest gratitude to my supervisor Dr. Ko-Choong Woo, in despite the fact that we have disagreements, and disputes. He have given me an opportunity to not only have me as his research student, but he guides me to his best potential and also gave me a chance to be his research assistant, his accomplice, his friend, his advisor. Through good and bad, he have accompanied me through the journey of a very dark tunnel that have allowed me to gain confidence in myself, as well as finding the true meaning of what I really want, and hence I am extremely grateful forever.

I would like to thank my fellow peers who have accompanied me in my journey despite leaving me alone to take care of the Rambutan. Dr. Teh Sze Hong, Dr. Davtalab Bashm, Dr. Jong Si Chung, for a remarkable experience of learning and provide me with the motivation to continue preserving. Though the lab that we work on NA16 has been moved to NB03, I will forever feel like the lab and our days in the lab as extremely enjoyable memories.

It is also my privilege to thank my parents, and my brothers who have supported me. Despite the hardships and draining process, they have always supported my decisions and thus I feel grateful for having them in my life

I would also like to thank my friends, juniors and seniors who have been there for me to keep my sanity and advice to continue.

Last, but not least. I would like to express my gratefulness to my girlfriend Lim Ying Yun and her family, for although we met quite late in the PhD. You have supported me, made me stronger, and always made me feel that there are no limits.

List of Figures

Chapter 6

Appendix

Tables

Nomenclature

θ Angular position of the pendulum body

γ Non-dimensional damping coefficient

p Non-dimensional excitation amplitude

ω Non-dimensional excitation frequency

t Non-dimensional time

ρ Imperfection term

δ Shaping factor

θ Angular position of the pendulum body

$\dot{\theta}$ Angular velocity of the pendulum body

X Position of the pendulum support in the vertical axis

$\dot{X}$ Position of the pendulum support in the vertical axis

φ The angle differences from the center between each pendulums.

R Resistance placed on the circuit

L Inductance

L_0 Inductance of the solenoid without the conductor

Z_0 The initial length of the spring

Z The length of the spring when extended.

z The extension of the spring

k Stiffness of the spring

y Vertical displacement travelled by the conductor / pendulum support.

P_{ctrl} Factor to control the vertical motion by solid state relay.

g Gravitational acceleration

c_y Damping coefficient of the vertical displacement

c_θ Damping coefficient of the angular motion

M Total mass of the pendulum support with the conductor

m_1 Mass of the first pendulum

m_2 Mass of the second pendulum.

M_b Mass of the conductor within the solenoid

M_p Mass of the pendulum support inclusive holder of the encoder.

D_s Part of the pendulum equation (sine state)

D_c Part of the pendulum equation (cosine state)

l_1 length of the first pendulum

l_2 length of the second pendulum

j_1 inertia of the first pendulum

j_2 inertia of the second pendulum

f_y non-linear friction forces acting against the vertical motion

f_θ non linear friction torque acting against the angular motion of pendulum

F_i impact force when vertical oscillation reaches an upper limit

Ω The frequency of the main power supply

V_s Voltage supply

f_{ctrl} Control frequency of the solid state relay

ξ Damping ratio

A coefficient to measure inductance L

B standard deviation to measure inductance L

F_m Static force applied by the solenoid to pull the pendulum support.

i Current supplied by the solenoid

Chapter 4

θ Angular position of the pendulum body

$\dot{\theta}$ Angular velocity of the pendulum body

φ The angle differences from the center between each pendulums.

R Resistance placed on the circuit

L Inductance

L_0 Inductance of the solenoid without the conductor

k Stiffness of the spring

$K_{1,2,3}$ Stiffness of spring 1 , 2, and 3.

y Vertical displacement travelled by the pendulum support.

P_{ctrl} Factor to control the vertical motion by solid state relay.

g Gravitational acceleration

c_y Damping coefficient of the vertical displacement

c_θ Damping coefficient of the angular motion

M Total mass of the pendulum support with the conductor

m_1 mass of the first pendulum

m_2 mass of the second pendulum.

M_b mass of the conductor within the solenoid

M_p mass of the pendulum support inclusive holder of the encoder.

D_s Part of the pendulum equation (sine state)

D_c Part of the pendulum equation (cosine state)

l_1 length of the first pendulum

l_2 length of the second pendulum

j_1 inertia of the first pendulum

j_2 inertia of the second pendulum

f_y non-linear friction forces acting against the vertical motion

f_θ non linear friction torque acting against the angular motion of pendulum

F_i impact force when vertical oscillation reaches an upper limit

Ω The frequency of the main power supply

V_s Voltage supply

f_{ctrl} Control frequency of the solid state relay

ξ Damping ratio

A coefficient to measure inductance L

B standard deviation to measure inductance L

F_m Static force applied by the solenoid to pull the pendulum support.

i Current supplied by the solenoid

Chapter 5

θ Angular position of the pendulum body

φ The angle differences from the center between the two pendulums.

R Resistance placed on the circuit

$L1$ Length of the pendulum attached to the cart

$L2$ Length of the pendulum attached to the bearing inside the circular track.

k Stiffness of the spring

x Vertical displacement travelled by the pendulum support.

Chapter 6

θ Angular position of the pendulum body

$\dot{\theta}$ Angular velocity of the pendulum body

φ The angle differences from the center between each pendulums.

R Resistance placed on the circuit

L Inductance

L_0 Inductance of the solenoid without the conductor

k Stiffness of the spring

X Position of the pendulum support in the vertical axis

$\dot{X}$ Position of the pendulum support in the vertical axis

Table of Contents

Chapter 1

Introduction

1.1 Background

Energy harvesting to generate electricity by means of rotational motion is a practical and effective way [3], the direction for this research is to deploy a pendulum and harvest energy through rotations. However, when pendulums were made to rotate [2], the range of frequencies for which stable and robust rotations exist is limited.

The rate of electrical energy generated from rotations of pendulums has been measured by Teh *et al* [2] for a finite range of excitation frequencies. Related work [4] has entailed a system comprising two pendulums, such that rotational solutions are synchronized. The pendulums rotate independently while sharing the same forcing. Xu *et al* [5] has carried out numerical and experimental study of the parametrically excited pendulum subject to electromechanical excitation. Xu and Wiercigroch [6] have explained the existence of rotational attractors in parameter space. Horton *et al* [7] proposed a parameter identification of a pendulum experimental rig and recorded

experimental tumbling chaos. . Xu *et al*. [8] studied the effect of interactions between the excited pendulum and electrodynamic shaker. In addition, Xu and Wiercigroch [9] obtained closed form analytical expressions by a first order perturbation method for rotary solutions, which was then expanded to the higher order terms and extensively studied by Lenci *et al*. [10] A classification of the complex responses of the parametric pendulum by the recurrence plots was proposed by Litak *et al.* [109].

This chapter introduces the objective of the research, what motions would affect the contribution by introducing a new configuration to be tested experimentally in order to widen the frequency range for which rotations exist, to identify the availability of rotations when forcing is aperiodic, either stochastic or chaotic. The vertical mode of electromechanical excitation is similar to that of Teh *et al* [2]. The effectiveness of this new configuration is observed experimentally under different forcing conditions which may be similar to real-life situations such as vibrating vehicles or sea waves.

The difference in this configuration is that it uses a solenoid which carries high current for a low voltage supply of about 15 V and is connected to a circuit similar to that reported by Jong *et al* [11].

A main feature of this experimental rig is two pendulums subtending at a fixed angle. The reproducibility and the type of rotations, as well as the angles are investigated and tested.

In this thesis, the experimental rig which is the main focus of the thesis, will be discussed in chapter 4. It focuses more on the subtended angles of the pendulum of the setup.

An earlier rig involving a circular track, which has been disassembled, will be discussed in Chapter 6 together with the findings from this experiment.

1.2 Research Statement

This new experimental configuration allows the pendulum to rotate easily over a larger range of excitation frequencies which are reproducible. Electrical energy may then be generated from such rotations through a load. Existing configurations of pendulums mostly oscillate and rotate within very specific values of system parameters. Even when such rotations are created, a control system or an initial pick up power is required to sustain such kinematic motions. The configuration studied in this experiment expects to increase range of continuous rotations so that energy can be extracted from it.

Oscillations of pendulums experience energy dissipation due to inherent damping and also possibly, air resistance. Periodic oscillations have frequencies related to a forcing frequency. The current configuration is able to maintain stable rotations even for slight variations in forcing frequency or the displacement of the vertical forcing. This is a crucial feature for future investigations in using the configuration for energy harvesting in natural environments, say in the ocean or a rough river. An electro-mechanical means of vertical excitation assumes the form of a solenoid which is compact and effective. Periodic excitation frequencies vary around a nominal value of 2 Hz and voltage values are varied by a Variac.

Prior to the final experimental rig, two configurations have been tested: the first of which is (a) a double pendulum such that where pendula are connected at a pivot, a

circular track is in place, and the second is (b) which is similar to (a), except that the first pendulum is constrained to small oscillations due to elastic constraints. A motivation for this work is to increase the basin of attraction for pendulum rotations, ideally with minimal amount of control, or even without it. Moreover, deployment of such system to harness energy from vibrations or sea waves would be an elegant solution to current concerns with depleting oil reserves. As such, identification of system parameters required for stable rotational motion is a necessary component of this work.

1.3 Motivation for work

An initial idea for this work was from previous analytical results which suggested that, if a pendulum pivot was free to move on an elliptical track, rotations would be facilitated. This would have been an interesting piece of experimental work based on previous theoretical results. However, from previous experimental observations, it was noted that addition of another pendulum, at an angle, instead of introducing a circular track, seemed more effective in inducing rotations.

The idea of inducing rotations with a higher range of frequency is intriguing, with rotations being one of the centerpiece of energy generations or mechanical motion. It is a must to use rotations as one of the generators, rotations are used because there is a continuous translational energy as compared to oscillations where it loses energy on it's peak. If the experiment can induce rotations with impacts present and is still capable of rotating to generate electricity, it could lead to many more possibilities. Renewable energy using vibration is the main approach of this work, and investigating ways to

achieve such energy with rotations using electromechanical device is one of the initial conditions that have been chosen to act as a motivation.

The experiment involving the circular track will be discussed in depth in chapter 6, which was the initial configuration before the study of the configuration in chapter 4 was made.

1.4 Methodology

System design:

The experimental rig is assembled and tested to ensure that the electromechanical means of exciting the system vertically results in stable rotations.

Since oscillations are much easier to obtain as compared to rotations, this experimental rig serves as a platform to observe both oscillatory and rotational attractors. Therefore initial conditions and system parameter values had to be identified for each oscillatory and rotational attractor. An example of a change in the system's qualitative response is period-two oscillations which could form the basis for future work in bifurcational analysis. Data from a numerical solution of Duffing's equation as well as a random stochastic signal was used to generate a form of chaotic and random vertical excitation.

Parametric studies were performed by modifying the values such as displacement, spring constant and solenoid type. Other parameter values include angles between the pendulums, the frequency of periodic excitation and supplied voltage.

Rotations in the form of tumbling chaos were observed to occur most frequently, which required impacts between vertical oscillatory conductor and mechanical limiters.

Angular displacement was measured using a Avagotech (AEAT − 6012) Magnetic absolute encoder was used together with an Arduino Uno to acquire the angular displacement. Opto NCDT NLD 1700 Laser was used to collect data for vertical displacement.

A mathematical model is needed to numerically predict system dynamic responses so as to correlate with experimental data. In this way, the extent of experimental correlation may be ascertained so that the mathematical model can be further improved to accurately describe system characteristics and dynamics responses.

An electromagnetic solenoid will be switched on and off either by a frequency generator or a WAVETEK arbitrary waveform generator model 75. Time intervals between instants in time when solenoid is switched on are varied in a stochastic manner, and in another case, a chaotic variation. This is made possible by the WAVETEK arbitrary waveform generator. At the same time, a suitable piece of software available from National Instruments is NI Max. This facilitates the transfer of numerical data from a personal computer to the arbitrary waveform generator. Measurement of vertical oscillations will be performed by using an accelerometer so that data pertaining to acceleration will be acquired and displacement calculated from successive integration. Angular displacement of pendulum will be measured using a rotary encoder. Measurement of vertical oscillations will be achieved by using a Laser sensor (OPTO NCDT 1700 Laser sensor). The justification of the selection of the sensor will be discussed in chapter 3 section 4.1.

To identify the different qualitative system responses, data from magnetic encoder (AEAT-6012-A06) was acquired in terms of time histories so that phase planes

may be constructed to depict period-one rotations, period-two oscillations, sub harmonic motion or chaotic rotations.

Data was analyzed primarily in Originlab software which supports curve fitting to mathematical functions and other analysis. A bandpass filter was used to remove signal noise so as to obtain the real signal.

Below are brief introductions of the phrases that will be frequently used within the thesis:

Period one signals:

Period one is a harmonic motion of the respective data which moves at the same frequency as the forcing frequency, and hence having a proportional relationship behavior.

Period-two signals:

Period two motion indicates a sub harmonic motion that is proportional to the forcing frequency, with a constant of 2. The period two signal, being half of the forcing frequency, showed that there are certain factors that contributed to the slowing down of the motion. Purpose of getting this data is to determine the relationship behavior between frequency and the response of the system.

The purpose of obtaining and analyzing period-one and period-two signals is to determine the relationship behavior between frequency and the response of the system.

Tumbling chaos:

A topology of the attractor, in which it will bifurcates between oscillations and rotations. At the same time the directions of the rotations will be changing directions between clockwise and anti-clockwise.

Stochastic:

A random input signal that has a random probability distribution or pattern that may be analyzed statistically but may not be predicted. It is widely used to depict the unpredictability of sea waves and vibrations. [84]

Chaotic:

A random input signal that has unpredictable distribution, be it in the motion of the vertical displacement or the vertical reaction of the conductor due to external factors such as the power of the solenoid.

Phase Plane:

A graphical presentation of the velocity against displacement, the graph result will reveal a circular connection, and if there are more than one circular points it can be determined as a different nature, period one, period two, chaotic , stochastic nature is determined after previewing the phase plane of the respective data.

The purpose is to determine the behavior of the system.

In order to determine the frequency in which it mostly occurs, the FFT under the analysis tool is used in the respective displacement. The graph that will then be controlled to see within a certain range of it's axis.

This is done to identify the overall frequency responses.

Lyapunov Exponent:

Identifying the characteristics with a quantity that determines the rate of separation of trajectories, and identifying whether the result is periodic or chaotic.

1.5 List of Publication

S. H-. Teh, K. H-. Chan, K. C. Woo, H. Demrdash, "Rotating a pendulum with an electromechanical excitation," *International Journal of Non- Linear Mechanics, ,* **70** 2014 pp 73 - 84.

Chapter 2

Past Work

2.1 Control of pendulum subjected to periodic forcing

It would be useful to review past work on pendulum rotations because it is difficult to maintain rotations, hence the aim is to accumulate methods to develop a pendulum system to induce rotations for energy harvesting,

Parametric pendulum model was already extensively investigated in the research area of non-linear dynamics for a long time, in order to quantify the non-linear characteristics and dynamic responses of the model. The non-dimensional form of the parametric pendulum is given by Thompson *et al* [100].

$$\ddot{\theta} + \gamma\dot{\theta} + \big(1 + pcos(\omega t)\big)\sin(\theta) = 0 \tag{2.1}$$

Where θ is the angular displacement, γ is the non-dimensional damping coefficient, p is the non-dimensional excitation amplitude, ω is the non-dimensional excitation frequency and t is the non-dimensional time.

The pendulum's motion has already been found to behave chaotically for certain parameter intervals in an early numerical study by Leven and Koch [12] in 1981. The

chaotic nature was assessed with the use of Lyapunov characteristics exponents and the power spectrum. They also numerically approached the boundaries of subharmonic and homoclinic bifurcation [82], using Melnikov's method and averaging methods, thus connect numerical and analytical results. The studies of rotating solutions of the parametrically excited pendulum has been gaining attention in recent years. Subharmonic rotating solutions were also studied by Koch and Leven [81]. Aside from theoretical analysis, early experimental work was performed by Koch *et al* [82] and Leven *et al* [88] to investigate experimental bifurcation of the parametrically excited pendulum. Experimental evidence was obtained for chaotic behavior of the parametric pendulum in [82], where attractors were shown by Poincaré maps. The details were reported in [88], which also showed that increasing driving amplitude and decreasing damping coefficient. The parametric pendulum could exhibit period-doubling, where the chaotic motion of pendulum was preceded by periodic motions.

Analytical investigation of a weakly damped pendulum was presented by Bryant and Miles [64 , 65, 16] using three different forcing, namely applied torque , horizontal forcing as well as vertical forcing. Resonance curves and stability boundaries were presented for each forcing case for downwards and inverted positions, and their occurrence in parameter space were discussed. A harmonic balance method and critical velocity criterion were applied by Clifford and Bishop [72] to analytically approximate the escape zone of the parametrically excited pendulum. Clifford and Bishop also located oscillatory orbits of the parametrically excited pendulum through numerical approach [18] by using the horse shoe structure formed by the manifolds of two saddles.

The rotating orbits of the parametrically excited pendulum were investigated and classified by Clifford and Bishop [74]. The classification were denoted in the letters *(n,r)* to describe a period-*n* orbit which makes *r* complete rotations in *n* periods. In

11

addition, the term "tumbling chaos" was introduced to denote an erratic alteration of rotations, rotating clockwise, counter-clockwise and oscillations. The classification was then classified by Garira and Bishop [69] into four categories. "Purely rotating orbits" denotes that the pendulum rotation is only in a single direction, whether clockwise or counter clockwise. "Oscillating orbits" denotes that the trajectory completes a fixed number of oscillations within a potential well before crossing a potential maximum into the next potential energy by rotational motion. "Straddling rotating orbits" exhibit a similarity to oscillating orbits, where it exhibits a mixture of oscillations and rotations but their response only straddle within one, two or three wells. Lastly "large amplitude rotating orbits" straddles within one, two or three wells, but do not make oscillations within potential well.

Chaotic motion of a parametrically pendulum were investigated by Bishop and Clifford [61]. The chaotic behaviors of the pendulum were distinguished into three types, namely tumbling chaos, oscillating chaos and rotating chaos, which studies the parameter space thoroughly. Furthermore the occurrences of a specific type of tumbling chaos of a parametric pendulum were investigated numerically by Szemplińska-Stupnicka and Tyrkiel [23]. It was found that the fractal structure of the basins of attraction of the oscillating and rotating attractors in the angular phase plane can identify the occurences of transient tumbling chaos of a parametric pendulum. The transients includes rotations with altering directions as well as oscillatory motion. Similarly distinct properties of the oscillation-rotations attractors of a dissipative parametric pendulum as well as their bifurcational structures were elucidated in another paper by Szemplińska-Stupnicka and Tyrkiel [107] via the numerical study of parameter regions of different attractors, coexistence of attracts and structure of basin boundaries. Resonant rotations of a weakly damped parametric pendulum were

analytically studied by Miles [91] in applying a harmonic balance method. The stable states in the parameter space were determined, where the resonant states are stable only in small frequency intervals.

Horton *et al* [7] proposed a technique to identify the friction parameters of the pendulum with coulomb friction as well as linear viscous dissipation. The identification was improvised from an earlier work by [67] which reported on modelling a spring-mass-damper system with coulomb friction and linear viscous dissipation. The experimental measurements of the time history of free oscillations were recorded, and the peak displacement amplitude was used to compute the unknown damping parameter values.

Litak *et al* [109] employed recurrence plot technique to analyze time histories of experimental parametric pendulum. The method is by using the recurrence quantification analysis (RQA), which is capable of distinguishing oscillations, rotations as well as transient chaotic vibrations for relatively short time histories using the same system frequency.

Lenci *et al* [84] conducted experiments of a pendulum parametrically excited by wave motion of water in a wave flume. Rotations were detected under the tested range of amplitude and frequency of water wave, as well as different initial conditions. This represents the experimental robustness of the rotation in both the parameter space as well as the phase space. The findings consist of the preliminary experimental proof of the feasibility of the concept: extracting energy from sea waves. It was further presented by Lenci and Rega [86], that the observed main rotations existed only in a precise subset of their theoretical region of existence, in the parameter space. By comparing the experimental data and their theoretical region of existence in the

parameter space, and comparing experimental data with constructed dynamical integrity profiles. It was concluded that the experimental rotations would only occur when it is high enough to sustain experimental imperfections.

The investigation of dynamics of parametric pendulum with imperfection symmetry, which imposes a horizontal forcing to the pendulum pivot, was identified in the circular track. The imperfection of symmetry can be included into the parametric pendulum model by adding an imperfection term into Equation (2.1)

$$\ddot{\theta} + \gamma\dot{\theta} + \big(1 + pcos(\omega t)\big)\sin(\theta) + \rho = 0 \qquad (2.2)$$

Where ρ represents the imperfection term. Sofroniou and Bishop [110] described the imperfection term is in the form of $\Delta\sigma$, where σ is a parameter value, and Δ is either +1 or -1. Sofroniou and Bishop [110] also reported that with an increasing value of imperfection term, the minimum forcing amplitude required to escape from the local potential well reduces for the same forcing frequency. This brings us to the parametric pendulum model subjected to elliptical excitation which influences stable rotation region in the parameter space, which was investigated numerically and analytically by Horton *et al* [1] and Pavloskaia *et al* [111]. For an elliptical excitation, ρ is in the form of $e\rho \sin(\omega t) \cos(\theta)$, where e is the ration between the horizontal and vertical diameter of the upright ellipse traced by the pendulum pivot for every period. [1] and [111] concludes that the effects of the elliptic motion are beneficial for rotations, increasing the region of stable pendulum rotations. Not to mention, smaller forcing is required to felicitate pendulum rotations when the ellipticity increases if the pendulum and pivot point is in the same direction. If the case where the excitation is along a tilted axis, the addition of the horizontal component results in a larger region when rotations

are supported [111]. For excitation along a tilted axis, ρ is in the form of $e\rho\sin(\omega t + \delta)\cos(\theta)$ where δ is the shaping factor of the forcing.

2.2 Dynamics of pendulum subjected to aperiodic forcing

The term aperiodic forcing is the study of the dynamics and the interaction of the pendulum with real life vibrations. It can be classified as stochastic or chaotic in nature.

There are a few researches that reported the investigations of the dynamics of pendulum subject to stochastic excitation. In the study, the effects of noise on the lifetimes of chaotic transients [63] was studied by Blackburn *et al*. Adding a stochastic forcing of a Gaussian distribution to the forced pendulum model, and it's effect in stabilizing and destabilizing the periodic motion of a parametric pendulum was investigated by Blackburn [61] and Litak *et al* [109]. They also Investigated the effect of noise on rotational motion of parametrically excited pendulum numerically. The noise which has a Wiener process, was introduced by a random phase in the parametric forcing term. The study indicates that the average rotational velocity of pendulum could still remain unchanged in a large interval of increasing noise level. Intermittent transition to chaos induced by noise was observed during the process of searching for rotating solutions.

Horton and Wiercigroch [75] proposed two wave excitation models by superimposing a stochastic component onto the standard harmonic parametric excitation. The first model, includes a stochastic noise term as addictive noise to parametric forcing component. The second model, includes the stochastic noise term as

the time varying amplitude and the phase angle to the parametric forcing. The effect of superimposing a stochastic component onto the harmonic parametric excitation on the stable rotational motion of the pendulum was numerically and experimentally by Najdecka *et al* [95]. The rotational motion of the parametric and planar pendulum subjected to stochastic wave excitation in the view of energy harvesting from sea wave excitation.

Yurchenko *et al* [113] studied numerically the rotational motion of a non-linear Mathieu equation, with a narrow-band stochastic excitation, integration technique was used to obtain the probability density function of the response, which was then used to identify the domains of the rotational motion in parameter space. Yurchenko *et al* [113] also reported that large values of damping could enlarge the rotational domain under stochastic excitation and that higher noise intensity could decrease the size of domain with dominant rotational motion. A single-degree-of-freedom filter was introduced intermediate to the actual wave excitation and the pendulum in [98], it was shown that the resulting filtered excitation allows widening the regions of dominant rotation motion.

Despite the fact that chaos is considered as an unwanted phenomenon without any implications for real life applications, the study on the domain of chaos is undertaken. Chaos has always been considered hazardous for the operation of real physical systems, and is aim to be avoided [114]. The study however, takes into account that the occurrence is likely to occur in real life and it is worthy to look into the effect of imposing a chaotic excitation and perhaps exploiting the occurrence for energy harvesting opportunities.

2.3 Dynamics of pendulum attached to a forced oscillator.

The type of experimental pendulum systems considered in this thesis belongs to the subclass of auto parametric systems, the pendulum is excited as it experiences auto parametric resonance with the electromechanically excited mass-spring damper system (vertical oscillator) [108]. An autoparametric system is a vibrating system which consists of at least two subsystems. For instance, it may consist of a primary subsystem which is generally in a vibrating state and a secondary subsystem which is excited indirectly and is couple to the primary subsystem in a non-linear way such that the secondary subsystem can be at rest while the oscillator is a vibrating [55]. This is the type of system that can also result in energy transfer between different vibration modes, and even resonances [83], possible only in this specific problem.

The study is motivated by the fact that pendulum attached to a forced oscillators has many applications that can be used in real life occurences. An example is that the pendulum attached to a force oscillator is used as a modification of the classical tune mass absorber [70, 108]. The pendulum are also used to fine tune mass dampers mounted in buildings to offset movements of buildings caused by Earthquakes [115]. The response of a linear oscillator with a parametrically excited pendulum attached to it has a main application as a dynamic vibration absorber system, this application was numerically and analytically investigated by Song *et al* [116, 117]. Warminski and Kecik introduced to the vertical oscillator by adding a non-linear spring [118, 119].

2.4 Electromechanical actuation using solenoid

The insight of electromechanical actuation using solenoid, which is the cause of the vertical actuation of pendulum in this thesis, as well as their applications, will be explained in this section. An experimental linear reluctance of self-oscillating motor operated based on resonance in an RLC stator circuit was developed by Mendrela and Pudlowski [100]. Under this configuration a conductor was oscillated within the magnetic field produced by the coil. As the configuration in chapter 4 required only voltages of maximum 24 V, the capacitor was removed, since it only allows voltages of at least 50 V.

A similar work was also reported by Blakley [63]. It was found that the coil inductance and the magnetic force varied with stator current rotor relocation. A few examples of short actuators driven by the electric circuits are devices like polarized magnetic valve, gripping device with compliant mechanism and planar moving actuators as reported by Kallenbach [78], linear electromagnetic actuator for mechatronic adaptonic system [69]. Its application in electro vibro-impact system was studied extensively by Jong [11], Nguyen *et al* [102]. Nguyen and Woo [103, 104], Ho et al. [29, 71].

Electromechanical excitation has been achieved by means of a solenoid which had been instrumental to an electro – vibro impact system [11]. Switching the solenoid on and off at both equal and unequal time intervals effects a repetitive as well as random excitation of pendulum respectively. The electromechanical excitation will generate through high current, nominal forcing frequencies and different rotating capabilities.

Xu *et al* [8] conducted experiments on pendulum using an electro- dynamical shaker. Quasi-periodic rotations were found experimentally to be co-existing with period-one rotations, which was not predicted using the mathematical model of the classical parametric pendulum. To address this weak correlation, the dynamic interactions between a parametric pendulum and an electro-dynamical shaker was investigated by taking the model shaker was investigated by taking the model of the electro-dynamical shaker into account, and the comparisons between theoretical and experimental results were discussed.

2.5 Dynamics of multiple pendulum

In this thesis, the idea of using multiple pendulums study initialized from Horton *et al* [1], the system is investigated with a similar aim to harvest energy with from regular and even irregular excitations. The system of two pendulums subtending a fixed angle is introduced to find a different approach. A circular track, being a special form of ellipse, has been manufactured for experimental testing, under periodic and aperiodic forcing conditions. However, this circular track was discarded because it did not seem to have a significant effect on experimental rotations

The study of rotating states of parametric pendulum has been extended by investigating the synchronization of rotation motions of more than one parametric pendulum, with the view of energy harvesting, in respect to the unbalanced forces effect introduced to the system by a single rotating pendulum [93]. Wiercigroch *et al* [4] investigated numerically and experimentally the dynamics of the parametric double pendulums attached to a common elastic support under harmonic excitation.

Synchronized rotational responses were focused with the aim of achieving a synchronized counter rotation of both pendulums. Delayed- feedback method was employed to assist the experimental pendulums separately in initiating and maintaining the desired rotational responses of the pendulums via servomotors. In a similar work, Najdecka *et al.* [96] numerically applied delay-feedback method to maintain the rotation of one of the pendulums (independent controller) and synchronize the second pendulum with the first one by using the computed velocity difference between the pendulums as an control input for the second pendulum (dependent controller). The robustness and sensitivity of the delayed-feedback method to change of frequency and amplitude of excitation, added noise to the control signal and mechanical disturbance was experimentally investigated by Vaziri et al [112]. Detailed theoretical and experimental investigation on the synchronization phenomenon of two rotating parametric pendulums attached to a common elastic support under harmonic excitation was reported by Najdecka et al [94]. It was also demonstrated that synchronization of pendulums rotating in antiphase is more favourable from an energy scavenging viewpoint than the synchronization in phase. Particularly, synchronization of pendulums rotating in antiphase has a property of damping lateral vibrations of the supporting structure, which is desirable for minimizing energy input to initate and maintain rotating states of the pendulum system.

N-pendulum system design, another variant of a pendulum system, was proposed by Yurchenko and Alevras [101] to address the sizing issue of a single pendulum system when it is operated at low frequency regime. By equally spacing the *N* pendulums and connecting them to a common ring. It was reported to be capable of achieving low frequencies staying relatively small in size, as well as being able to control its natural frequency and the created torque by manipulating the position of the

lump masses on their respective pendulums. Probability density function of the response was also generated numerically to show the viability of this variant, particularly in a tri-pendulum system, in generating rotational response. A corresponding experimental investigation was conducted by Alevras *et al*. [56] to demonstrate the capability of the design in establishing rotating response in experimental environment. It echoed the outcome in [99] that the tri-pendulum would provide an equivalent rotational response with not only realistic size but a multiplicity of configurations. Besides the experiments revealed the capability of the tri-pendulum in regulating its response by just changing its configuration. Which is advantageous for energy harvesting application.

The study of multiple pendulums was studied by Yurchenko [99] and it has come to a case where *n*-pendulums can be used to generate energy by rotations with the use of waves. In this thesis, a closer look at two pendulums will be rotated experimentally with an approach at how different angles will be the factors effecting the pendulum.

It has been seen from past work that it is difficult to implement rotations of pendulum in experiment, unless there is a control strategy [2]. As such, this thesis presents a case for inducing such rotational orbits without a need for additional external forcing input.

Chapter 3

Parameter Identification

3.1 Introduction

The experimental rig was based on a forcing from vertical oscillations to generate rotations. System characteristics such as Coulomb friction and viscous damping coefficient have to be quantified. Other physical quantities would include spring stiffness's, lengths and masses.

The chapter describes how the unknown coefficients were determined from experimental empirical means.

Inductance variation of the solenoid was measured using a meter and transient oscillations, which are useful for estimating the damping coefficients.

Electrical resistances were measured with a multimeter. Time histories of transient response of angular displacement were fitted to curves, and Vernier calipers were used to measure lengths.

This chapter also includes methods in how data is acquired through devices such as laser sensor, and Arduino UNO. It also includes a subchapter to indicate the devices to acquire results in chapter 6 that have been done earlier on, and was disassembled.

3.2 Spring Constant

The spring constant is identified with the use of multiple mass and three similar springs. A mass of 50 g after the first 100 g is added consecutively and the results of the extension of the spring is recorded.

Table 3. 1 Spring Constant table

Spring Constant

$Z_0 = 62$ $c = l_0$

Mass(kg)	Z	z(mm)	Nm^{-1}	X(mm)
0	62	0	0	0
0.1	62	0	0.981	0
0.15	62	0	1.4715	0
0.2	62	0	1.962	0
0.25	62	0	2.4525	0
0.3	62	0	2.943	0
0.35	62	0	3.4335	0
0.4	62	0	3.924	0
0.45	63	1	4.4145	0.001
0.5	65	3	4.905	0.003
0.55	68	6	5.3955	0.006
0.6	73	11	5.886	0.011
0.65	78	16	6.3765	0.016
0.7	83	21	6.867	0.021
0.75	89	27	7.3575	0.027

0.8	95	33	7.848	0.033
0.85	101	39	8.3385	0.039
0.9	107	45	8.829	0.045
0.95	111	49	9.3195	0.049
1	118	56	9.81	0.056
1.05	120	58	10.3005	0.058
1.1	126	64	10.791	0.064
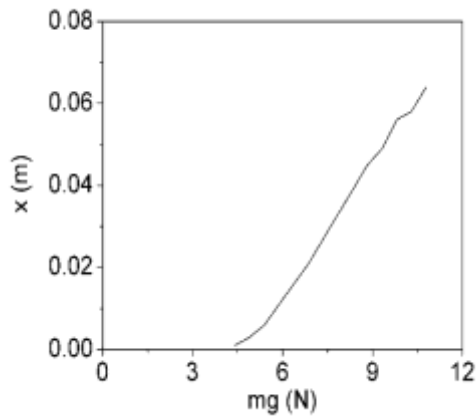
(a)   (b)
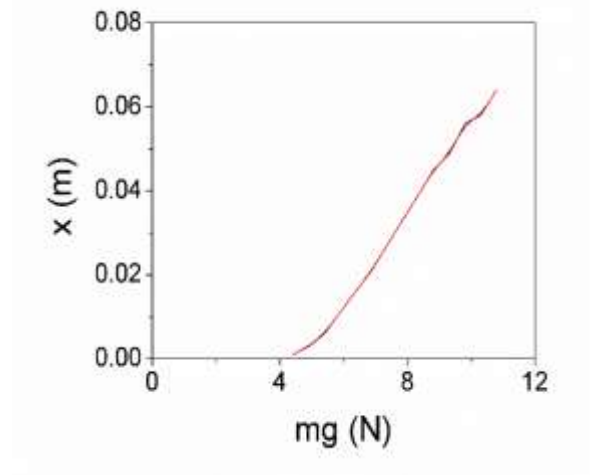
Fig 3.1 Spring constant diagram (a) represents the real curve, (b) represents a straight line.

After the spring diagram is drawn, the line was curve fitted using the equation, $y = kz + c$, where the values of $k = 0.0108$ and $c = -0.0519$, achieved by using curve fitting. The value of spring constant is calculated by $\frac{1}{k}$, where it results in 92.6 Nm^{-1}.

3.3 Generation of switching function for solenoid

The configuration will be excited by a random frequency and a software (NI MAX) was required to generate the signals to indicate on and off. The signals are generated using different equations.
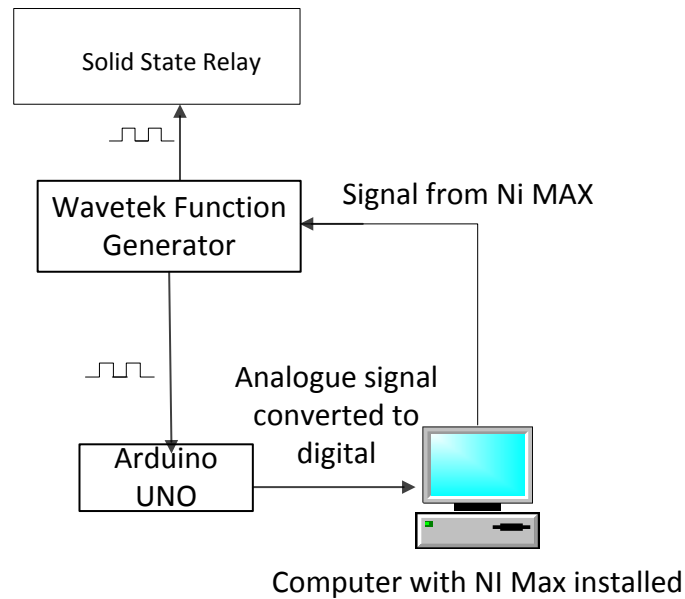
Fig 3.2 How the code is transferred to the function generator from the computer with the help of the software NI MAX

The signal was generated with reference to the Duffing's equation, in order to provide an unstable vertical motion to the system. The software "NI MAX" was used in order to send data signals to the Wavetek 75 arbitary waveform generator. The generator can return 2096 points, in which 756 data points were used to depict periodic switching, where repetitive square waves occurred at 11.21 mHz. For example, 3 data points were used for every signal indicating on and off for 756 data points. The remaining 1240 points depict chaotic switching. During chaotic switching, the oscillations and rotations of the pendulums could stop, this is due to the loss of energy

through impacts and stopping motion. The oscillations and rotations can be reinitiated after approximately 20 seconds as soon as continuous impacts occur.

The intention of this work is to investigate the effects of the exertion of an electromechanical excitation on the pendulum assembly. This was made possible by varying the timing for switching the solenoid on-and-off according to a specific profile [30]. Thus, two profiles, chaotic and stochastic, for generating input signals to the solid-state relay were proposed in this work for achieving the objectives.

The purpose of obtaining the chaotic response is to use the data for solenoid behavior. The chaotic profile involves the usage of the Duffing's equation in [52], which can be expressed as follows:

$$\ddot{x} + \alpha\dot{x} + \beta x + \gamma x^3 = A\sin\omega t \qquad (3.1)$$

where α, β, γ, A, and ω are the parameters of Eq. (3.1), and they are selected from [51] as $0.168, -0.5, 0.5, 0.177$ and 100π, respectively, for generating chaotic response. Eq. (3.1) was solved numerically in MATLAB by using ode45s. These values were chosen as it was recommended by Rao [52], and the results obtained from MATLAB showed that the data are chaotic. The data were then normalized with respect to magnitude of the input signal to the solid-state relay, which is between 0 V and 1 V, where 0 V indicates the "off" state and 1 V indicates the "on" state. For instances where $x \leq 0$, the value of x was rounded off to 0 or "off" state; likewise the value of x was rounded off to 1 or "on" state when $x > 0$.

On the other hand, a probability distribution function to generate the values of 0 and 1 was employed for creating the stochastic profile. A random number generator was designed and it utilized the "rand" command in MATLAB for generating the values from 0 and 1 according to the continuous uniform distribution. Similar to the chaotic

profile, if the generated value x was less than or equal to 0.5, it will be rounded off to 0 or "off" state; likewise if the generated value is greater than to 0.5, it will be rounded off to 1.

For those two profiles, the generated arrays of values of 0 and 1 were exported to the National Instruments Measurement & Automation Explorer (NI MAX) software which provides a graphical user interface to communicate with a NI General Purpose Interface Bus (GPIB) controller (model: NI GPIB-USB-HS). The controller receives the data from the computer system via an USB connection, and it outputs the corresponding signal to the arbitrary waveform generator via the GPIB connection. The arbitrary waveform generator in turn generates an external voltage, ranging from 0 V to 1 V, based on the signal from the GPIB controller to close and open the RL circuit of the AC solenoid.

In a similar case, a signal was generated in order to provide stochastic motion for the system. The equation used (3.2) for this system was referred to normal random distribution in Fig 3.3, and the vertical oscillation was according to the generated data provided by the equation shown below. The dashed lines were acquired with the use of random number generator which was directly modified and provided by the MATLAB software, the distribution was defined from the numerical expression as identified below:

$$f(x) = \begin{cases} \frac{1}{b-a}, & for\ a \leq x \leq b \\ 0, & for\ x < a\ or\ x > b \end{cases} \tag{3.2}$$
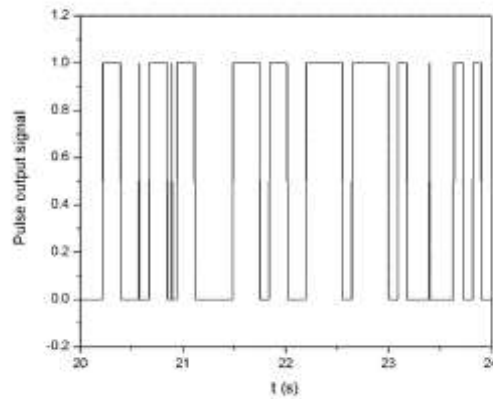
Fig 3.3 Signal pulse generated using the Arbitary waveform generator captured by Arduino.

3.4 Data acquisition

3.4.1 Angular position

The sensor used in order to acquire data for angular position is the Magnetic absolute encoder (AEAT6012A06). The parts connected to the magnetic encoder include a Molex 5 way receptacle housing of 1.25 mm pitch and Molex Picoblade 50056 female crimp, which is used to attach the connectors to the Magnetic encoder.

A jumper cable was attached to the picoblade and inserted into the housing to be connected to the magnetic encoder junction. The jumper cable was soldered to the picoblade to secure it, and a receptor that must be followed by the picoblade must follow in order to fit inside the housing.

Each of the encoder junctions have different uses, which can be viewed from Fig 3.3 below:

28

Electrical Connections
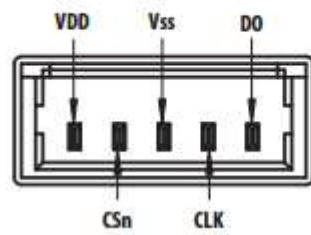
Pin	Symbol	Description
1	VDD	5V Supply Voltage
2	CSn	Chip Select – Input (See Figure 2)
3	VSS	Supply Ground
4	CLK	Serial Clock - Input (See Figure 2)
5	DO	Serial Data - Output. (See Figure 2)

(b)

Fig 3.4 Electrical connections[M1] (a) represents the connection from the supplier and (b) represents the pins configured in the equipment.

Fig 3.4 (a) is taken from the manual provided from the supplier. The cables are connected to each of the pins indicated, and then connected to an Arduino UNO that controls the encoder.

VDD indicates the voltage supplied from the Arduino UNO, CSn is the input data to provide data as well as control the input, the clock (CLK) indicates the timer in which it is switched on and off, and DO is the indicated data output in which the Chip or the position of the pendulum. The assembled version can be seen in Fig 3.5 and Fig 3.9.

Fig 3.5 Connector input to the encoder.

To connect the wires and pin, 5 wires were used to connect each junction. The wire was connected to the picoblade and was fitted and clamped to the cable by means of a crimp. The picoblade was crimped to the wire with a small amount of space on the edge to allow the tip of the magnetic encoder to be attached to the picoblade directly. The connection for each cable was then further soldered to make the connection sturdy. The cables were then aligned to follow the instructions as given from the identification of ports as can be seen from Fig 3.4.

The other end of each wire was attached to a connector that allows a connection to the Arduino UNO. Many sets were made in order to be tested for the sustainability of heavy impacts and vibrations. The connecting wire was force fitted to the housing so that the data acquired from the system can be more accurate, and also to ensure that it will not fall off especially during impacts. Impacts may cause the wires to be cut off at a certain point, therefore assuring the connection to be robust is a minimum requirement to acquire uninterrupted data from the system.

The experimental rig was configured to have one side of the pendulum connected to a magnetic indicator in order to indicate the position of the pendulum. The pendulum was modelled further to hold the extension in such a way that the magnetic encoder was prevented from directly affecting the pendulum, whereby the magnetic encoder cap was lifted away from the encoder itself.

Timing Characteristics

Notes:
1. Please refer to Table 4 for Timing Characteristics.
2. For 12 bits version; the Positional Data Bits will start with D11 instead and end at D0.
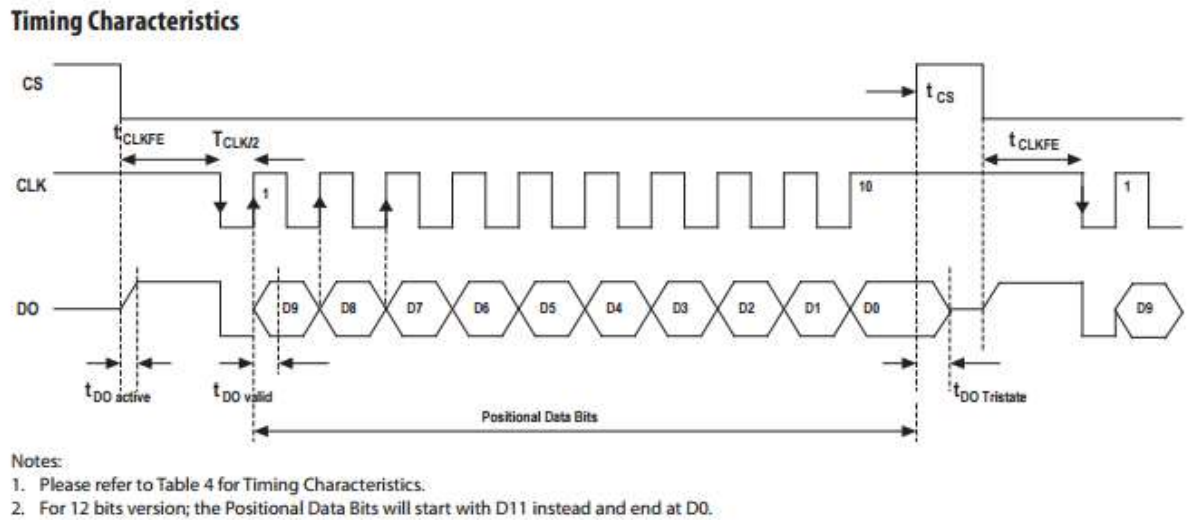
Figure 2. Timing Diagram for 10 bit Magnetic Encoder

Fig 3.6 Timing diagram [M1]

The figure is extracted from the manual of the encoder, which provides information such as identification in order to be coded, the programming of the encoder and the logic function which is provided in order to acquire data from the pendulum.
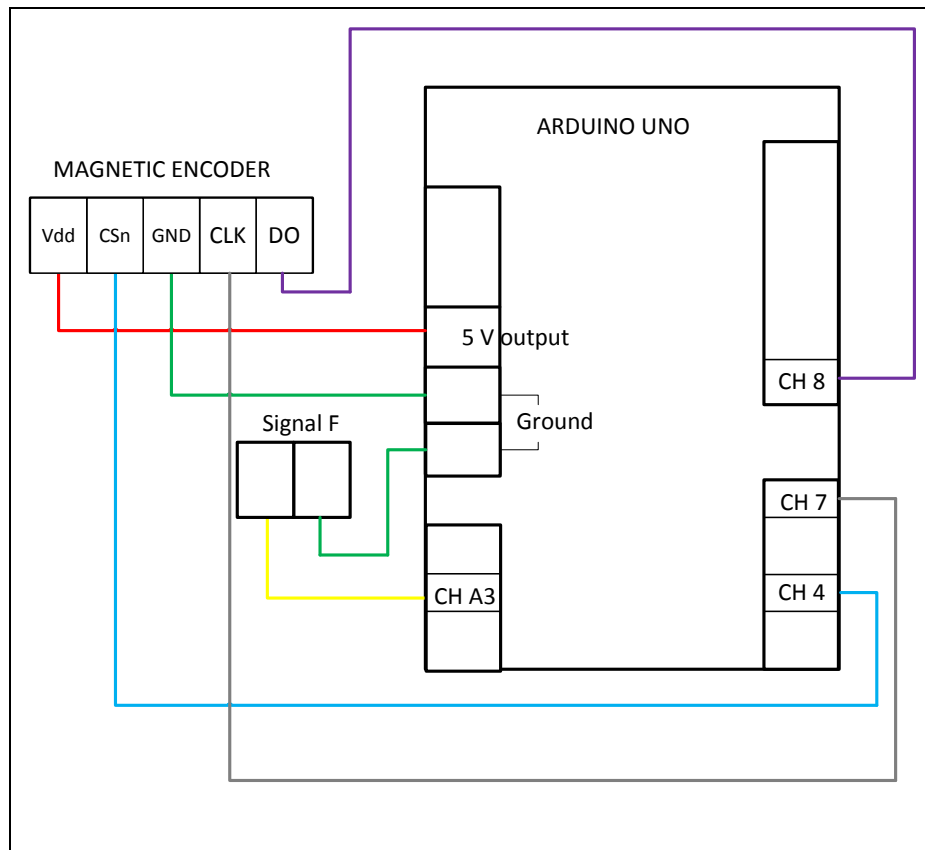
Fig 3.7 Circuit diagram for the connections of the Encoder and Function generator to the Arduino Uno.

(a)   (b)
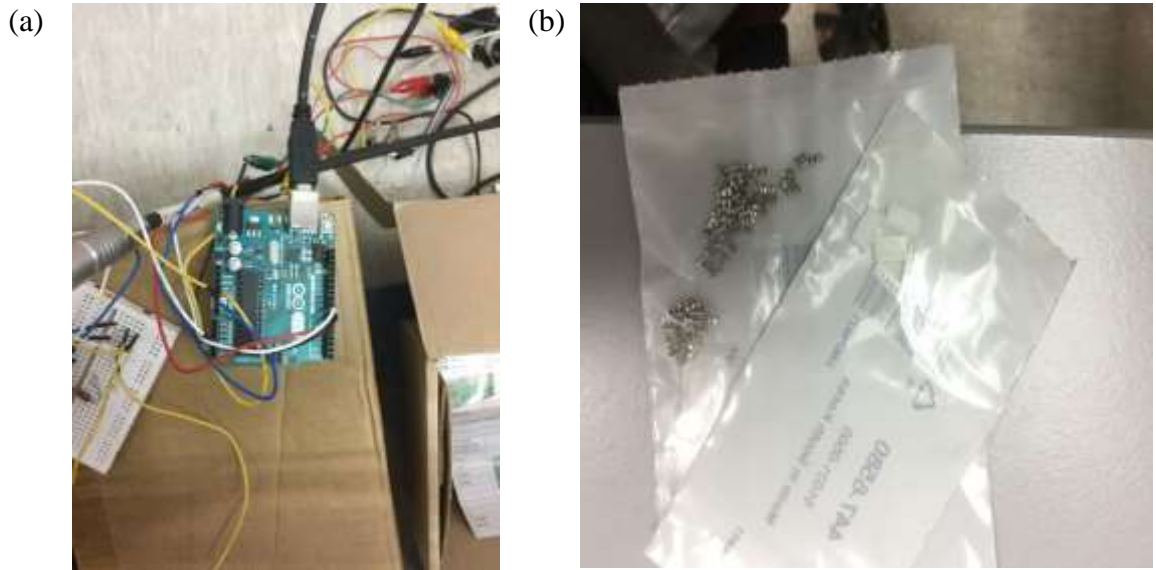
Fig 3.8 (a) connection of the cables to the Arduino and (b) housing and the picoblade

suitable for the magnetic encoder.

Fig 3.9 The wiring connection attached to the magnetic encoder with the use of the

housing.

Table A.7 indicates the code written in the Arduino Uno, using the software

"Arduino Software (IDE)" downloaded from the website Arduino.cc [120]. The code

selects the channels and assigns the function of the encoder to the respective assigned ports. The connections can be found in Fig 3.4. The connections indicated are mapped on the table below for better clarity.

Magnetic Encoder Connection	Arduino UNO connection
Vdd	5 V
CSn	Channel 4
GND	GROUND
CLK	Channel 7
DO	Channel 8

Table 3. 2 Connection relay

The wiring of the circuit to the Arduino UNO board has to follow the code in Table A. 7, hence each channel was indicated and aligned according to Table 3. 2. coloured wiring was used to provide a clear indication for each wire and the correlating junction, as represented in Fig 3.7. The analogue signal from Channel A3 (CH A3) is output from the function generator, which is in turn connected in parallel to the RL circuit, so that square waves may switch the solenoid on and off. Restructure of previous sentence: Channel A3 (CH A3) was used as an intermediary between the function generator and the RL circuit, where Channel A3 received the output of the function generator and the analogue signal was sent to the RL circuit in the form of square waves used to switch the solenoid on and off.

When the solenoid was switched on, an electromagnetic force was exerted on the conductor which caused it to oscillate vertically. Since data can not be recorded by Arduino data directly, an external software known as Cool Term [105] was used to acquire data from the Arduino. Instance in time at which data occur are generated by

identifying the sampling rate which was 370 points per second. This number was calculated from a toggle function generator present in the software, the number of activations and deactivations was determined such that the signal pulse can be generated for each second.

As the sampling rate is not know, it has to be defined by using a 1 Hz sinusoidal square wave, where 1023 is "on" and 0 is "off". With this method, the number of points for one cycle can be determined. In order to eliminate initial inconsistencies, data sampling was started after three consecutive cycles of 1023, and 0.

The acquired data was then saved as a text file and imported to a Microsoft Excel spreadsheet. Since data points were numbered to start at 0 and end at 1023, 1024 data points corresponded to a full rotation of 360°. The angle was then reposition to between $-180°$ and $180°$

The signal pulse captured from the analogue channel 3 assumed a value of either 0 or 1023 corresponding to the "off" or "on" state respectively. The value of 1023 was then calibrated to 1, indicating that a closed circuit, whereas a value of 0 then indicates an open circuit. The circuit was switched on and off using a solid state relay.

3.4.2 Vertical position

The equipment was selected instead of linear variable differential transformer (LVDT) or an accelerometer because there will be no contact to the device and thus, would not have an effect on the motion. However, this laser sensor was designed to measure static distances. In this work, the distances were changing in real time,

therefore inaccuracy when measured with a laser sensor is to be expected to a certain degree.

On the other hand, although an accelerometer measures the physical quantity, acceleration precisely, when subjected to impacts there is a possibility of the accelerometer failing, this could be uneconomical as it has to be replaced repeatedly. Therefore, the accelerometer was not used in this work. As a linear variable differential transformer (LVDT) requires a mechanical connection in order to follow the movement of the vertical oscillation, this will result in additional friction due to misalignment causing the rotations to be irregular and more variables will take place. As such, the laser sensor was then selected for measurement of vertical oscillations without contact.

The laser sensor NLD 1700, is attached to a micro – RS 422/ USB converter, and configured by a local supplier of this product. The software used for data acquisition is ILD 1700 Multi-channel tool which can be downloaded from a website of the manufacturer [106].

The laser sensor is clamped to a stationary system isolated from the experimental configuration, as can be seen from Fig 3.10 below:

Fig 3.10 Laser sensor was clamped to a stationary object.

The laser sensor was detected by the computer with the use of software shown below in the figure:
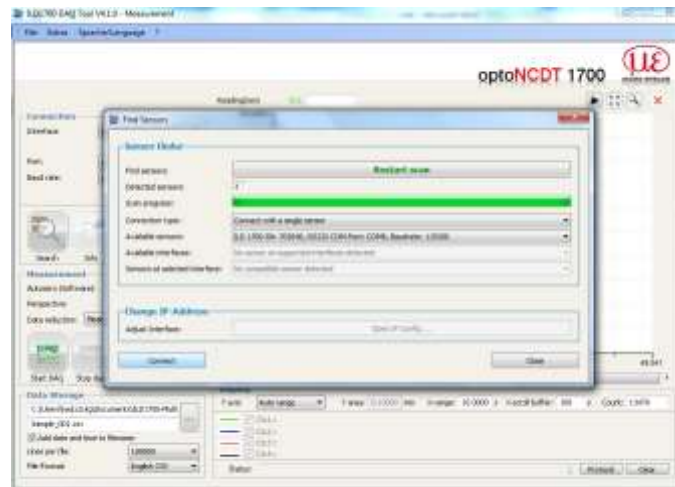
Fig 3.11 Laser sensor scanning and identifying of the equipment.

Upon connecting the laser sensor to the personal computer and starting data acquisition, a typical screen shot is shown in Fig 3.11.
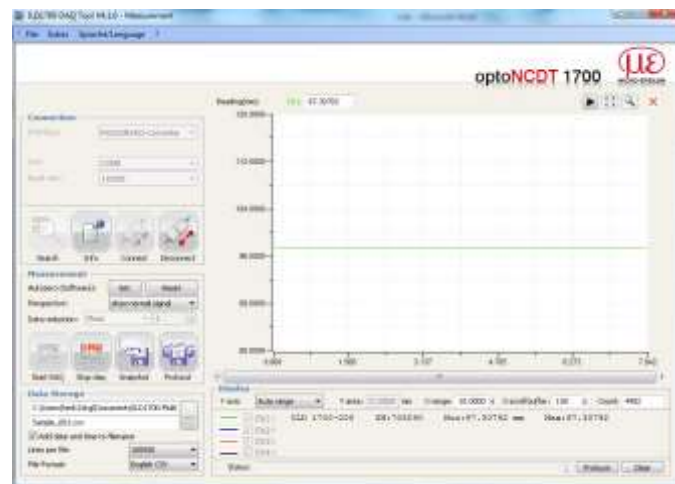
Fig 3.12 Connecting the laser sensor to identify the position of the pendulum support.

The data acquired shows the method in which the system was able to identify and calibrate the ideal position of the pendulum support. The body that holds the bottom spring was adjusted and the position between the solenoid and the conductor was also

adjusted. The adjustment method which brought about the calibration of the position of where the pendulum support should be can be seen in the appendix.

Since the laser sensor is positioned 97.35 mm under the pendulum support, in order to make the result more accurate, the system read is set to 0 mm removing the extra distance by using the software button set located within the measurement box, beside the Autozero(software). By pressing this button, the data acquired will be calibrated to 0 mm before being analyzed.
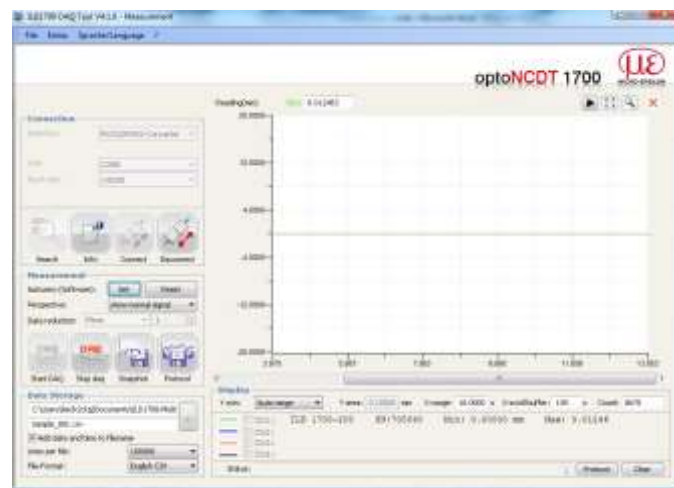
Fig 3.13 Zeroing the data or calibrating the reading data to 0 mm for more accurate reading.

Data acquisition can be started by clicking the virtual button on the screen. The data will be saved in a .csv file, which can be imported into Microcal Origin to plot time histories and other graphs. These graphs will then be used to identify the qualitative response of the pendulum in the vertical direction.

3.5 Inductance measurement

The solenoid used in the experiment is a pull action solenoid (Mechetronics Manufacture part No. SD119A99P1). The inductance of the solenoid was measured using a programmable automatic RCL Meter PM6304, which can be seen in Fig A. 1, and Fig A. 2. The solenoid was connected in series to a constant voltage supply of 2V as can be seen in Fig A. 3.

The circuit can be viewed in Fig A. 2, showing how the mechanical displacement was measured using a pair of Vernier calipers, and the frequency of voltage was set to coincide with the mains frequency supplied to the variac at 50 Hz. The resistance and inductance was measured by the RCL meter. The position of the conductor is denoted by the variable, y.

Electrical resistance is represented by R, and L the inductance:

Table 3. 3 Inductance Measurement using RCL meter for the solenoid

Position, y (m)	$R(\Omega)$	L (mH)
0	4.49	4.194
0.002	3.76	3.707
0.004	2.8	3.231
0.006	2.05	2.763
0.008	1.685	2.570
0.010	1.373	2.410
0.012	1.187	2.212

0.014	0.9433	2.068
0.016	0.7887	1.994
0.018	0.7552	1.948
0.020	0.6837	1.942
0.022	0.6281	1.925
0.024	0.5712	1.895
0.026	0.5155	1.908
0.028	0.4931	1.942
0.030	0.4701	1.974
0.032	0.4587	1.987

(a)   (b)
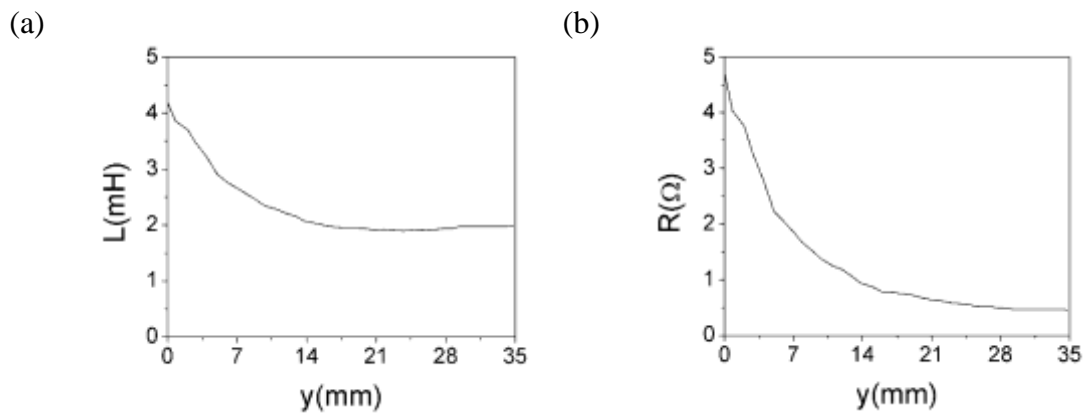
Fig 3.14 The quantities of the solenoid. (a) shows the inductance against displacement, (b) shows resistance against displacement.

(a)   (b)
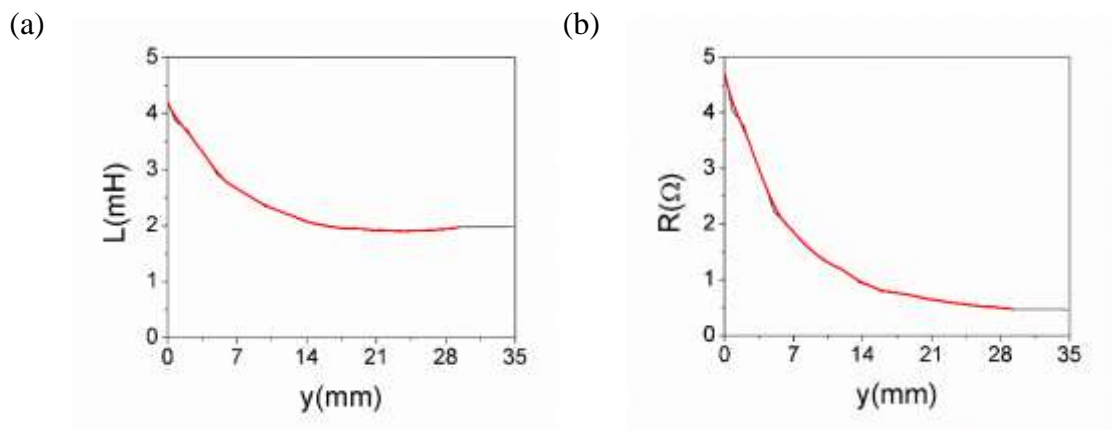
Fig 3.15 The quantities of the solenoid with a smoother curve. (a) shows the inductance against displacement, (b) shows resistance against displacement.

3.6 Damping Coefficient

θ(°)
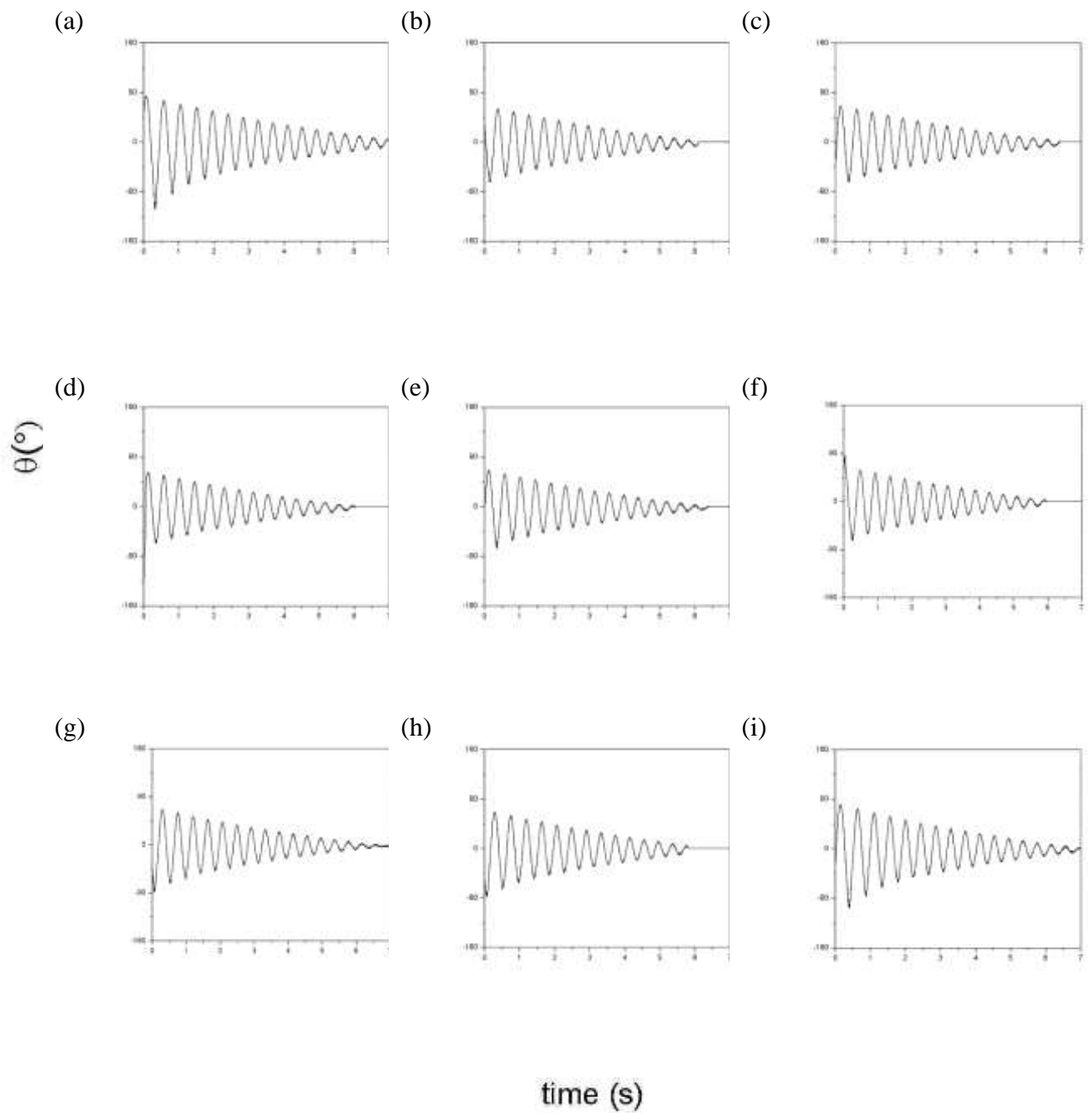
Fig 3.16 A zero initial velocity and non – zero initial angular displacement starts each

time history to estimate damping characteristics from a transient response

Fig 3.16 (g) was used to identify the damping coefficient from non-linear curve-fitting to a governing equation of motion. The damping coefficient has been calculated to be 0.0015 for a few sets of data using a formula derived by B. Horton *et al* [1].

Curve fitting was performed in Origin lab to the following function:

$$y = P_1 e^{\frac{P_2}{x}} \sin(y + P_4) + P_3 e^{\frac{P_2}{x}} \sin(y - P_4) \qquad (3.3)$$

Where the values are determined from the system where P_4 is equivalent to the value of the angle between the two pendulums.

(a)
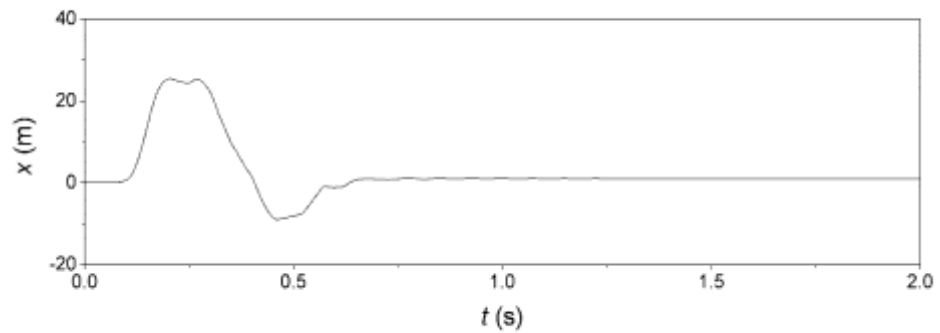
(b)
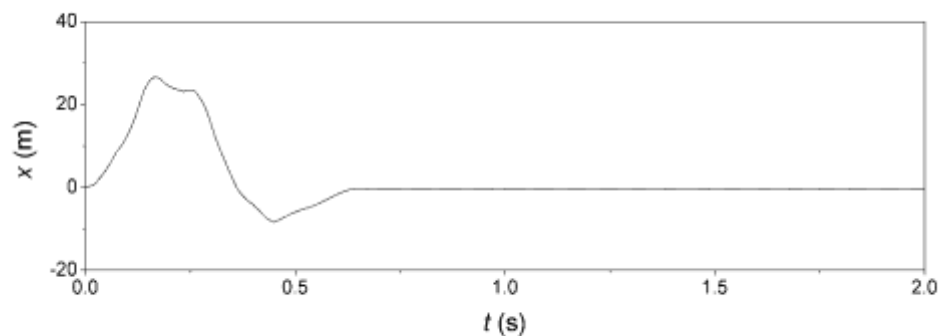
Fig 3.17 A zero initial velocity and non – zero initial vertical displacement starts each time history to estimate damping characteristics from a transient response

Fig 3.17 (b) was used to identify the damping coefficient from non-linear curve-fitting to a governing equation of motion. The damping coefficient has been calculated to be 0.2793 using a formula derived by B. Horton *et al* [1].

Curve fitting was performed in Originlab to the following function:

$$y = P_1 e^{P_2 x} + P_3 e^{P_2 x} \tag{3.4}$$

Where the values were determined from the system.

3.7 Acquiring data signals for circular track.

This chapter discusses how data signals were acquired for circular track experiment in chapter 6, which is the earlier version of the experiment described in Chapter 4.

The equipment used for this part of the experiment is further discussed in this Chapter 6. The equipment used for this experiment is using the accelerometer when it is still feasible to mount it to the rig designed at [2]. At this point the experimental rig has no encoder feasible to read the angular position of the pendulum's rotation and can only be observed. However, the main key for this experiment is that the pendulum's result causing the differences to the vertical displacement.

The vertical displacement is recorded with the use of National Instruments NI-USB 4432 (Fig 3.19) with the help of an accelerometer Kistler Type 8776A50 (Fig 3.18) connected to a high performance cable specifically for the accelerometer.

Fig 3.18 Accelerometer Kistler

Fig 3.19 National Instrument NI-USB 4432 signal box

The Accelerometer is mounted to the pendulum cart shown in Fig 5. 2 (b). The results were then recorded with the use the National Instruments NI- USB 4432 as discussed before with the use of the Labview software, which was then imported to OriginLab to present the experimental time history of the vertical displacement.

Fig 3.19 was also used to acquire results from the motor generator, using a BNC connecter connected to the motor. The signal was also taken with the use of Labview

software with a controlled sampling rate. The experimental results were then imported to MATLAB for calculation of the energy resultant.

3.8 Conclusions

This chapter has introduced all the equipment's required to acquire the experimental time history of the pendulums motion. It identifies the devices used for data acquisition as well as how it should be attached to the experimental configuration.

The equipment that are used to contribute to the results are also identified in order to define the parameters that will be used for simulation results. Results such as spring constant, solenoid inductance directly affects the vertical motion of the pendulum, it is analyzed so that it can also contribute to another similar configuration or a pendulum study.

The method of supplying a signal wave form is also discussed in this chapter and have always been used to generate stochastic waves, and chaotic waves for this experimental configuration. This is just one of the sources that can generate such waves which uses the same connection to the circuit that is similar to a frequency generator.

The laser sensor, and absolute magnetic encoder were used to acquire the experimental results. The connection of the magnetic encoder to the pendulum can be further improved to acquire accurate results, even when the pendulum is stationary the results buffer within a secluded range, causing the analytical results to have a difficult accuracy problem and thus difficulty in identifying the bifurcation of topologies as well as plotting a bifurcation table. The laser sensor on the other hand only has a limitation

of acquiring results up to a certain degree, as compared to a mounted accelerometer which can identify even a very small bifurcation in the system.

Chapter 4

Numerical Analysis

4.1 **Introduction**

The circuit was obtained from the study of Jong *et al* [11]. The mathematical model equation is taken and derived from Teh *et al* [2], which was then restructured further. And the dynamical properties of the classical parametrically driven pendulum, such as potential well, symmetry-breaking, periodic and chaotic attractors have been explored in detail experimentally:

One of the main objective of this study is to facilitate the numerical analysis of the experimental pendulum system and validate the experimental system with the mathematical model.

In this chapter, the equations of motion that describe the experimental pendulum setup presented in the previous chapter are derived. The system equations consist of

expressions that govern the mechanical behavior of the pendulum together with its suspension. In addition, description is made of the dynamics of the RL circuit of the solenoid. Coupling of mechanical system with the electrical circuit is due to an expression of non-linear electromagnetic force. The system parameters are identified appropriately for the mathematical model. Numerical results are then generated using the developed mathematical model and the identified parameters, their correlation with experimental observations will be discussed.

4.2 Mathematical Model
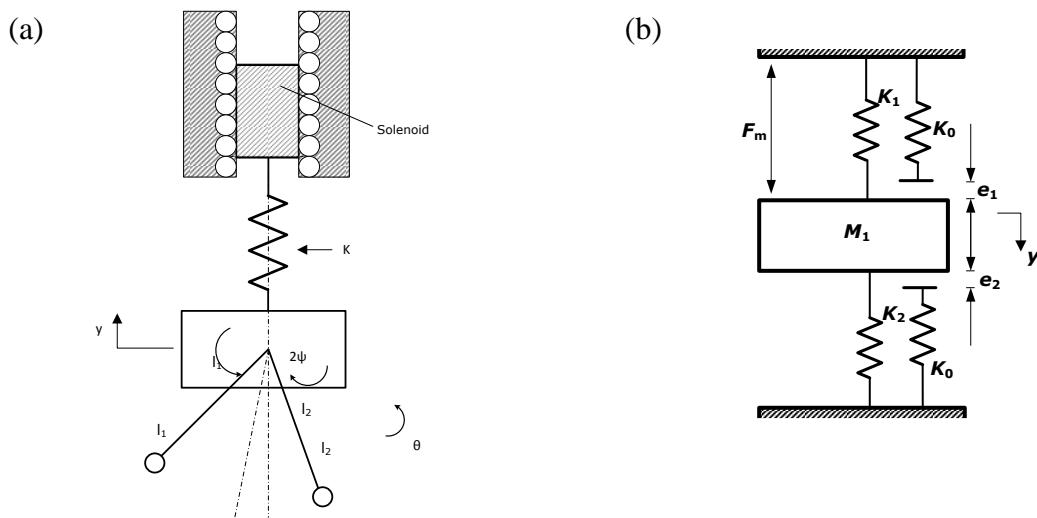
Fig 4. 1 (a) represents the dynamic motion of the pendulum.

A mathematical model has been derived to describe the experimental rig. Fig 4. 1 **(a) represents the dynamic motion of the pendulum** (a) shows the physical model of the parametric pendulum, and Fig 6.4 shows where the mechanical parts and RL circuit present.

The derivation of the equation is as follows:

$$V = m_1 g \Delta y + m_2 g \Delta y + M g y + \frac{1}{2} y^2 (K_1 + K_2$$

$$+ K_3)$$

(5.1)

$$K_1 = K_2 = K_3 = K$$

(5.2)

For a case of equal stiffness, Potential energy may be expressed alternatively as

$$V = m_1 g \Delta y_1 + m_2 g \Delta y_2 + M g y + \frac{3}{2} y^2 K$$

$$= m_1 g \big((l_1 cos\theta + y) - l_1 cos(\theta + \varphi) \big)$$

$$+ m_2 g \big((l_2 cos\theta + y) - l_2 cos(\theta - \varphi) \big)$$

(5.3)

$$+ M g y + \frac{3}{2} y^2 K$$

To quantify kinetic energy, an energy component for the first pendulum is determined as:

$$KE_1 = \frac{1}{2} m_1 (\Delta \dot{x}_1 + \Delta \dot{y}_1)^2$$

$$= \frac{1}{2} m_1 (\dot{\theta}^2 l_1{}^2 + 2 \dot{y} l_1 sin(\theta + \varphi) + \dot{y}^2)$$

(5.4)

For the second pendulum, the energy is determined as:

$$KE_2 = \frac{1}{2} m_2 (\Delta \dot{x}_2 + \Delta \dot{y}_2)^2$$

$$= \frac{1}{2} m_2 (\dot{\theta}^2 l_2{}^2 + 2 \dot{y} l_2 \dot{\theta} sin(\theta - \varphi) + \dot{y}^2)$$

(5.5)

A contribution from the moment of inertia

$$KE_{1i,2i} = \frac{1}{2}I_{1,2}\dot{\theta}^2$$

The moment of inertia are equivalent due to being two identical pendulums.

$$C\_z = 0.2793$$

The total Kinetic energy:

$$T = KE = KE_1 + KE_2 + KE_{1i} + KE_{2i}$$

$$= m\left(\dot{\theta}^2 L^2 + 2\dot{y}l\dot{\theta}\left(sin(\theta + \varphi) + sin(\theta - \varphi)\right) + \dot{y}^2\right) + I\dot{\theta}^2 \qquad (5.6)$$

Using Lagrangian Function

$$Y = 2\ddot{y}m + ml(\ddot{\theta}\left(sin(\theta + \varphi) + sin(\theta - \varphi)\right) + \dot{\theta}^2\left(cos(\theta + \right.$$

$$\left.\varphi) + cos(\theta - \varphi)\right) + 2mg + 3Ky + C\_z \qquad (5.7)$$

Where Y is the rate of change of momentum

$$\Theta = 2\ddot{\theta}(ml + I) + ml\ddot{y}\left(sin(\theta + \varphi) + sin(\theta - \varphi)\right)$$

$$+ mgl\left(sin(\theta + \varphi) + sin(\theta - \varphi)\right) \qquad (5.8)$$

There are four discrete masses in the physical system, one of which is that of the beam, M_b . The mass of conductor within the solenoid, and pendulum support inclusive of holder for the encoder is denoted by M_p. The mass of the first pendulum inclusive of the bob is represented by m_1, and the mass of the second pendulum inclusive of its bob is represented by m_2. The length of the two pendulums are denoted

51

as l_1, and l_2 respectively. A non linear electromagnetic force, F_m, is generated within the solenoid as a result of the interaction between the metal conductor and current-induced magnetic field of the solenoid. The stiffness of each tension spring is denoted as K. 2φ represents the subtended angles between the two pendulums. Angular displacement of the pendulum, θ, and the vertical displacement of the pendulum support, y, are used to describe the mechanical coordinates of the system, The equations of motion of the mechanical system derived using the Lagrangian approach are as follows:

$$\Sigma M \ddot{y} = \ddot{\theta} D_s + \dot{\theta}^2 D_c + 3Ky - \Sigma Mg - f_z + F_m - F_i \tag{5.9}$$

$$\Sigma J \ddot{\theta} = \ddot{y} D_s + g D_s - f_\theta \tag{5.10}$$

$$\Sigma M = m_1 + m_2 + M_b + M_p \tag{5.11}$$

$$\Sigma J = +j_1 + j_2 + m_1 l_1^2 + m_2 l_2^2 \tag{5.12}$$

$$D_s = m_1 l_1 \sin(\theta + \varphi) + m_2 l_2 \sin(\theta - \varphi) \tag{5.13}$$

$$D_s = m_1 l_1 \cos(\theta + \varphi) + m_2 l_2 \cos(\theta - \varphi) \tag{5.14}$$

where g is the gravitational acceleration and the dot denotes the differentiation of the coordinates with respect to time t. In Equations (14) and (15), the non-linear friction forces acting against the vertical motion of pendulum assembly, f_y, and the non-linear friction torque acting against the angular motion of pendulum, f_θ, are described. F_i represents the impact force when vertical oscillation reaches an upper limit.

$$f_y = C_y \dot{y} \tag{5.15}$$

$$f_\theta = C_\theta \dot{\theta} \tag{5.16}$$

$$\text{Impact Force} = F_i = \begin{cases} k_0(y + e) & \text{if } y > -e \\ 0 & \text{otherwise,} \end{cases} \qquad (5.17)$$

where C_y is the damping coefficient of the vertical axis, C_θ is the damping coefficient of the angular axis. It is assumed that the non-linear friction of the mechanical system comprises only linear damping and non-linear dry friction for both the vertical and angular axes.

The electric circuit is made up of a pure resistor, R, and inductance characteristic, L, and they are connected in a series configuration as shown in Fig 6.5. The electric circuit is powered by an externally supplied time dependent voltage, $V(t)$, and an electronic switch, solid state relay, is connected in series with other electrical components to activate and deactivate the electric circuit according to the input signal. The current of the circuit I, is used to describe the electrical variation of the system and the displacement of the metal conductor moving vertically inside the solenoid is directly correlated to the value of y. The equation describing the dynamics of the electric circuit is based on electromagnetic principles as follows:

$$L\frac{d^2i}{dt^2} + \left[R + 2\dot{y}\frac{dL}{dy}\right]\frac{di}{dt} + \left[\frac{d^2L}{dy^2}\dot{y}^2 + \frac{dL}{dy}\ddot{y}\right]i = a\frac{dV(t)}{dt} \qquad (5.18)$$

where a is the command signal generated by waveform generator to the solid state relay. As the electrical circuit is powered by alternating current (AC) power supply, $V(t)$ can be explicitly expressed as follows:

$$V(t) = V_s \sin(\Omega t) \qquad (5.19)$$

where V_s is the amplitude and the Ω is the frequency of the AC power supply.

Hence, the derivative of V(t) with respect to t is:

$$\frac{dV(t)}{dt} = \Omega \, V_s \cos(\Omega t) \tag{5.20}$$

in the case where periodic forcing is required from the solenoid, the command signal

will be in the form of a train of rectangular pulses with a control frequency of f_{ctrl}:

$$P = \begin{cases} -1 \ \ if \ t \ (mod \ \left(\dfrac{1}{f_{ctrl}}\right) < \dfrac{1}{2f_{ctrl}} \\ \quad 0 \qquad \qquad otherwise, \end{cases} \tag{5.21}$$

where the units of f_{ctrl} are in Hz.

The non − linear relationship between the inductance of the coils and the displacement of the metal conductor moving within the solenoid can be sufficiently described using the following Gaussian form, as reported in Ho *et al.* [30]

The right side of Equation (5.11) is the derivative of voltage supply with respect to time under the switching effect of Solid State Relay Logic (SSRL) which is connected to Solenoid 2. The AC power is supplied by VARIAC (CAROLL AND MAYNELL 480 VA output, 240 V) which adopts the waveform of common household main electric supply. The magnitude of the AC power is adjusted using the amplifier, fixed at V_s= 14 V in this experiment.

Measurements of Inductance L, may be curve fitted to

$$L = L_0 + \frac{A}{B\sqrt{\pi/2}} e^{-2(\frac{y}{B})^2} \tag{5.22}$$

where L_0 is the inductance of the solenoid without the metal conductor placed inside the solenoid, A is a coefficient of the above function and B is a standard deviation.

The single and double derivatives of Eq. (5.13) with respect to y are shown as follows:

$$\frac{dL}{dy} = \frac{-4Ay}{B^3\sqrt{\pi/2}}e^{-2(\frac{y}{B})^2} \tag{5.23}$$

and

$$\frac{d^2L}{dy^2} = \frac{-4A(1-(\frac{2y}{B})^2)}{B^3\sqrt{\pi/2}}e^{-2(\frac{y}{B})^2} \tag{5.24}$$

The non-linear electromagnetic force generated using the RL circuit is derived from energy conservation principles by considering the transformation of magnetic energy stored inside the solenoid into useful work that actuates the movable core as follows:

$$F_m = \frac{1}{2}i^2\frac{dL}{dy} \tag{5.25}$$

The above expression couples the mechanical system with the electrical circuit besides completing the mathematical description of the system.

4.3 Simulation Results
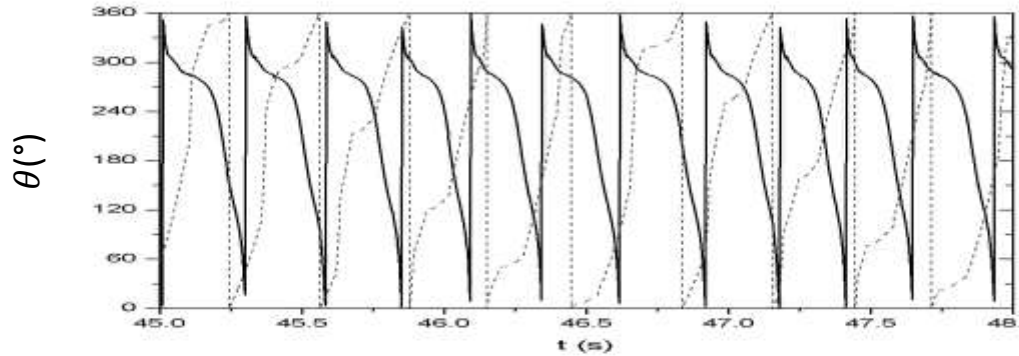
Fig 4. 2 Numerical prediction from the mathematical model is based on the same frequency value as that reported in Figure 3.18. However, the direction of the rotation is opposite as compared to the experimental system, this is due to the initial perturbation.

While the figure has been reported to achieve rotations. There are a lot of enquiries with the mathematical model. In the comparison of the graphs. The shape of the rotational motion is not the same as one that was compared to experimental result. Many initial conditions were given in order to compare accuracy with the system for example. In the integrator attached to the system for vertical axis, the initial starting position is 0.007 m. The vertical displacement moves within a range of 34 mm.

Initial angular velocity was also provided with an approximate angular velocity of $\frac{\pi}{2}$ to the system so as to have the same condition of the flick by the hand to the pendulum.

(a)
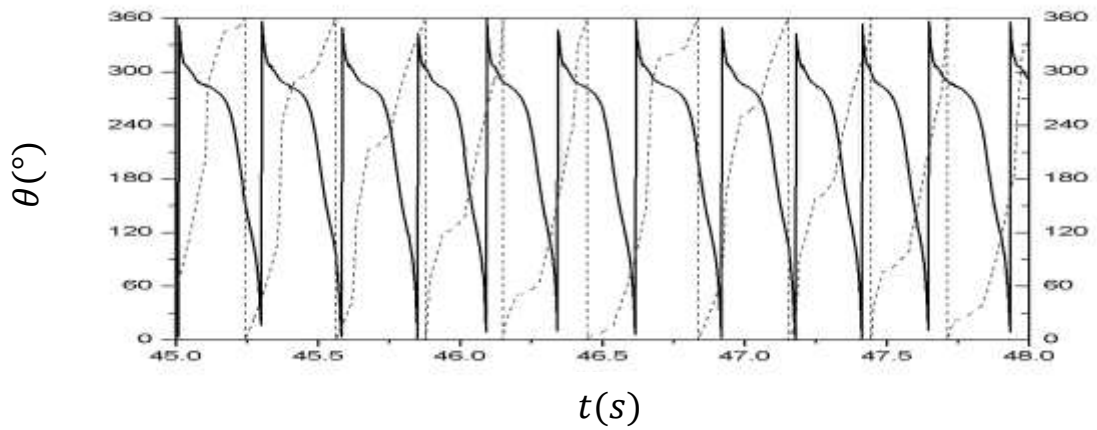
(b)
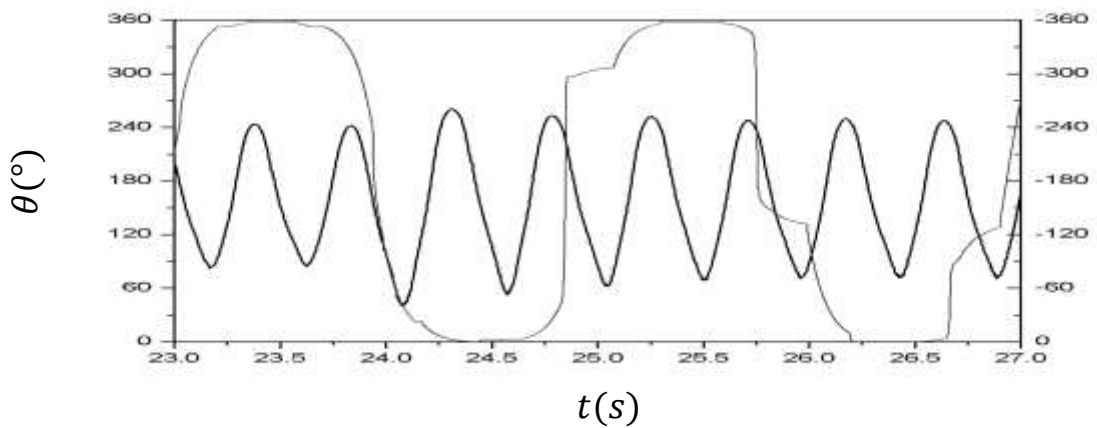
Fig 4.3 Numerical predictions for this mathematical model are for the same frequency (a) 3.5 Hz. However, the direction of the rotation is opposite to that of the experimental system, which may have been caused by the initial perturbation. (b) An excitation frequency of 2.196 Hz had resulted in oscillations with impact. In particular, period 2 motion was observed. Direct numerical integration was solved by Simulink using an ode15s solver.

The simulation results was run at two different states, oscillations and rotations. When the initial conditions were given for the rotations, and (b) oscillation.

4.4 Conclusion

The mathematical model running in the MATLAB shows difficulty in determining the solution. The model was solved by ode15s. This causes the data to not achieve smooth curves and exact shape when compared to the experimental data.

The simulation work has not reached the objective and managed to only identify the derivation, as well as the connection between the parameters of the experimental configuration. The simulated data, is not synced to the experimental work nor comparable. The positive outcome of this chapter is that Simulink has been learnt to model the dynamics of the pendulum.

Dynamics software have also been introduced however, there were difficulties in generating the equation. This may be due to unfamiliar discontinuity and a more in depth research in the analytical dynamics for the configuration will be needed for computational purpose.

Experimental correlation between the simulated results requires a further analysis with a different set of equations. The dynamics of the equation should be looked more closely with a wider parameter understanding.

The numerical predictions for the frequency shows that it can validate rotations, however not oscillations. Since the mathematical model is derived to correlate between the experimental and the simulated results, more parameter identification will be required.

Chapter 5

Experimental Rig with circular track

5.1 Introduction

B. Horton *et al* [1], has introduced a new identical method for pendulum to rotate, it has been known that motion of a point of suspension in an elliptical track facilitates pendulum rotations. Recent studies also simulated the experimental configuration and thus from these study, a circular track in the form of an ellipse, has been manufactured for experimental testing, under periodic and aperiodic forcing conditions to sought Rotational orbits.

Electromechanical excitation has been achieved by means of a solenoid which had been part of an electro–vibro impact system [2]. Switching the solenoid on and off at both equal and unequal time intervals effects a repetitive as well as random excitation of pendulum respectively.

Two configurations have been tested, the first of which is (a) a double pendulum such that where pendula are connected, a circular track is in place. The second is (b) similar, except that the first pendulum is constrained to small oscillations because of elastic supports. A motivation for this work is to increase the basin of attraction for pendulum, rotations, ideally with a minimal amount of control, or even without it. Moreover, deployment of such system to harness energy from vibrations or sea waves would be an elegant solution to current concerns with depleting oil reserves. As such, identification of system parameters required for stable rotational motion is a main outcome of this work.
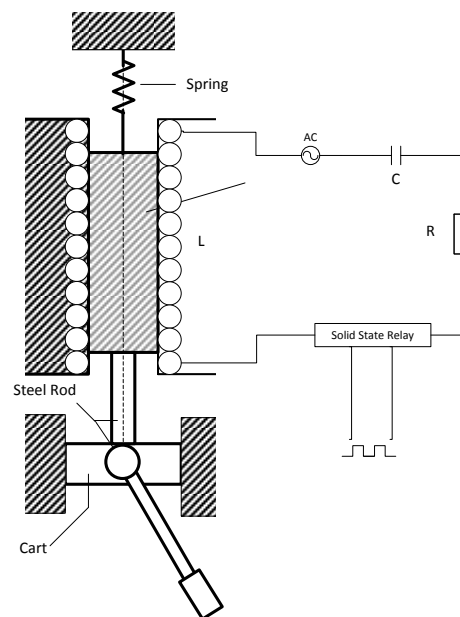
5.2 Experimental configuration

Fig 5. 1 Design of the pendulum actuated by electromechanical device based on Teh *et al* **[2]**.

Electromechanical actuation is similar to that described in the experimental setup which is made possible by use of a solenoid which is connected to an RLC circuit

which is switched on and off according to a function generator by means of a solid state relay.

An inertia capable of vertical motion is constrained by two smooth acrylic plates. The pendulum consists of an aluminium rod supported by a shaft is capable of free rotation. At the end of the rod, a bob is mechanically attached to a circular track on which a second pendulum rotates. An accelerometer is attached to the inertia to measure vertical accelerations. It is connected to a Kistler 8776A50 accelerometer which acquires data for storage in a personal computer PXI – 1031. A rotary encoder, Autonics E4086 – 1000-6–L-5, records angular displacement of the first pendulum. Data is then acquired by National Instruments NI – USB – 4432.

Fig 5. 2 and Fig 5. 3 show schematics and photographs of the experimental rig.

(a)   (b)
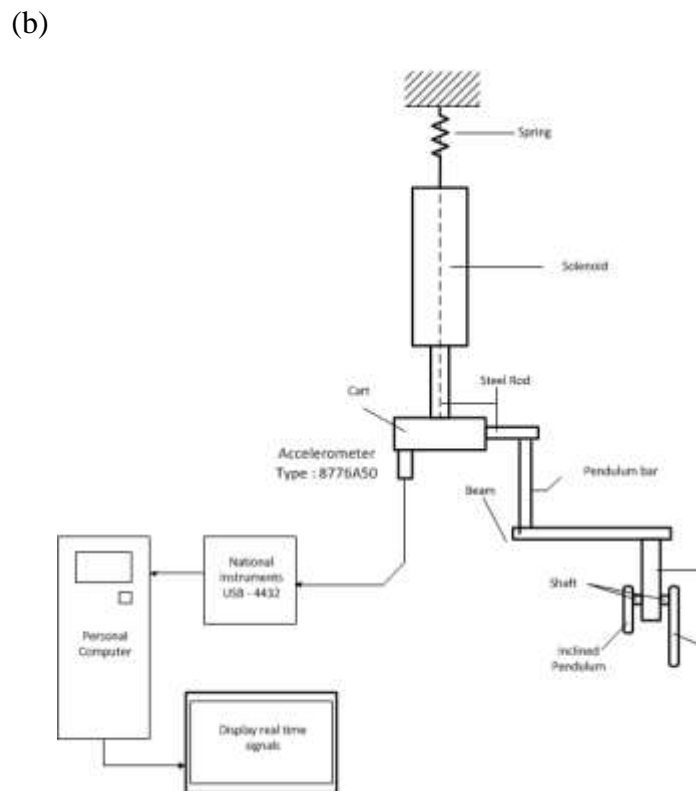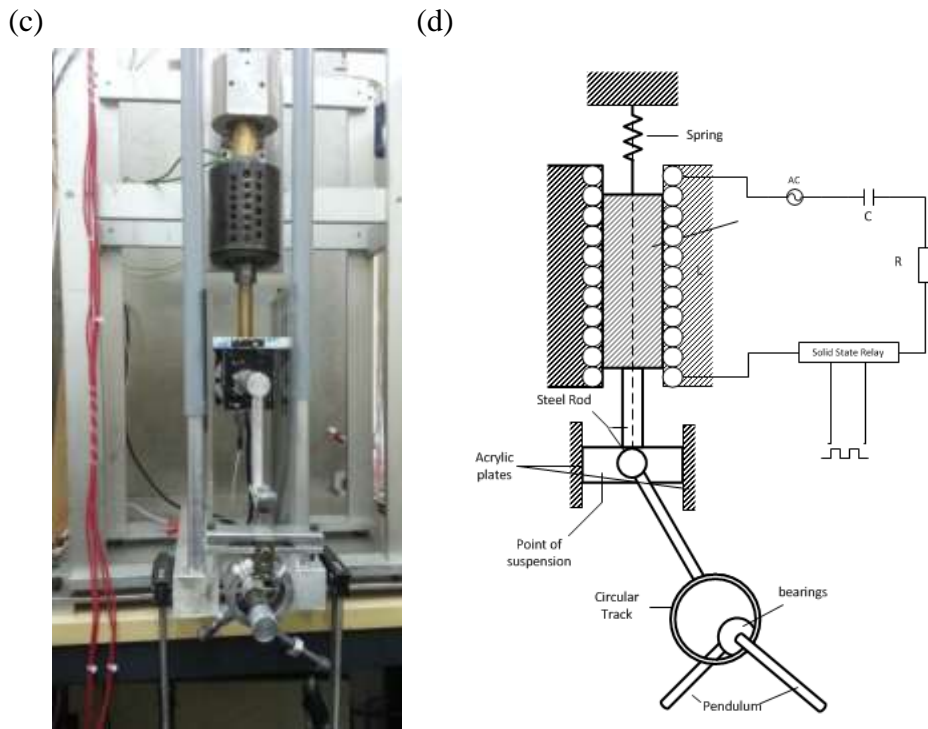
Fig 5. 2 A schematic of the system such that the first pendulum is free to move, side and front views illustrated by (b) and (d) respectively. Corresponding photographs are shown in (a) and (c), also respectively.

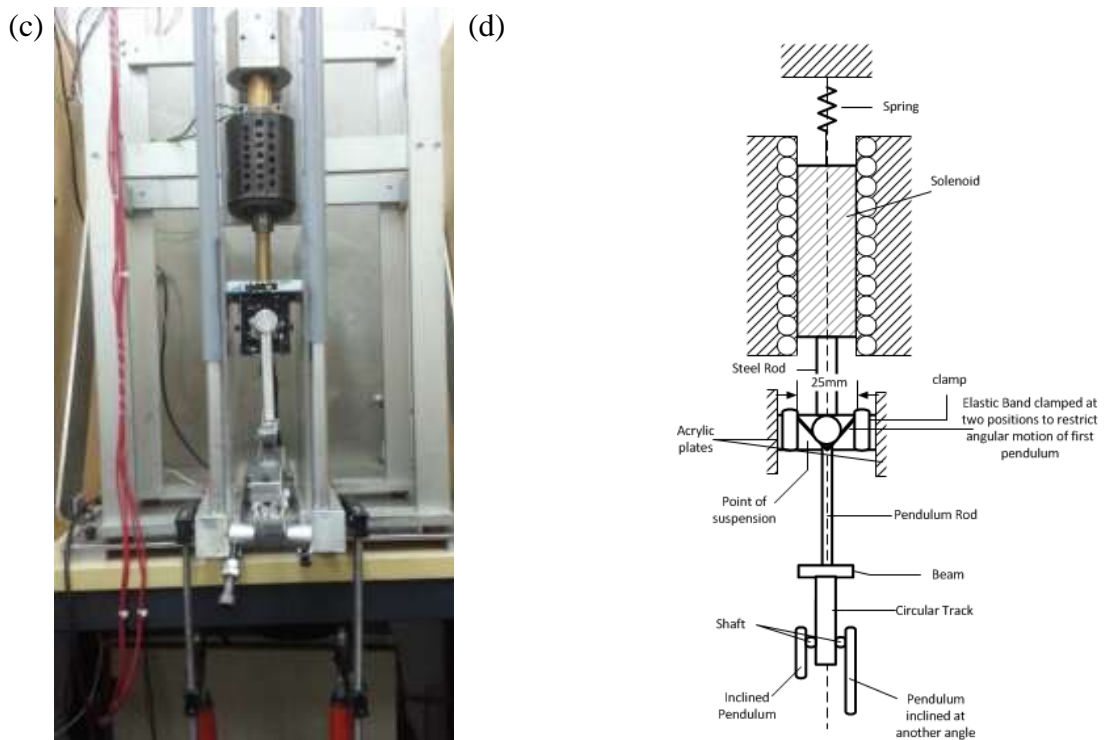(a)   (b)
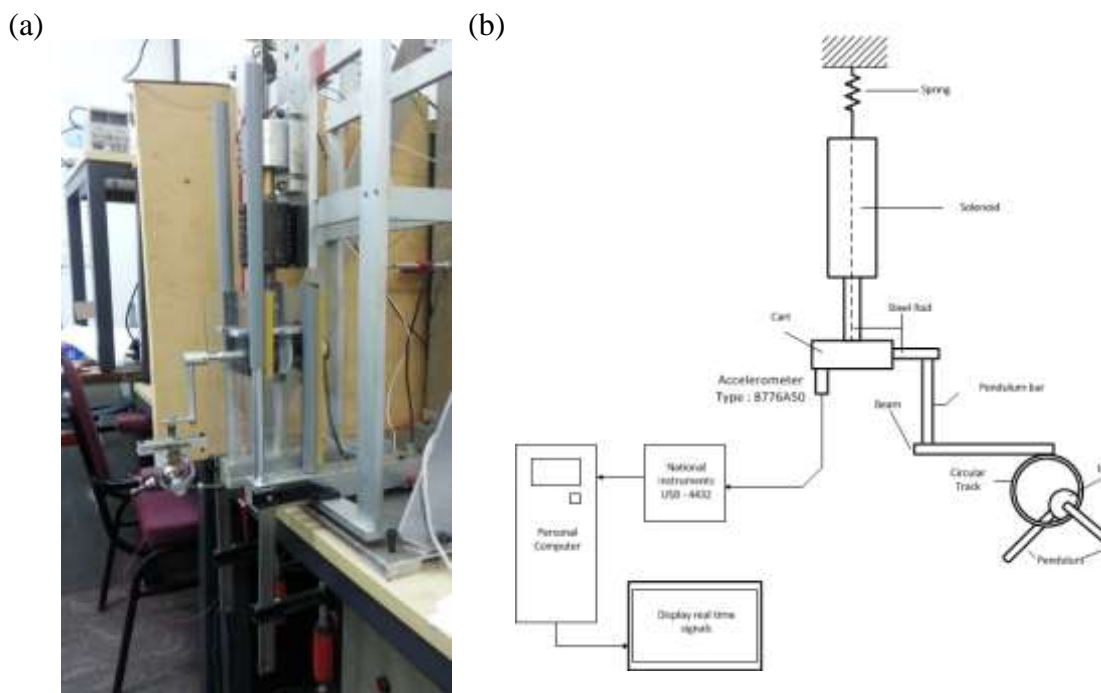
Fig 5. 3: A schematic of the system such that the first pendulum is constrained by an elastic support, side and front views illustrated in (b) and (d) respectively. Corresponding photographs are shown in (a) and (c) also respectively.
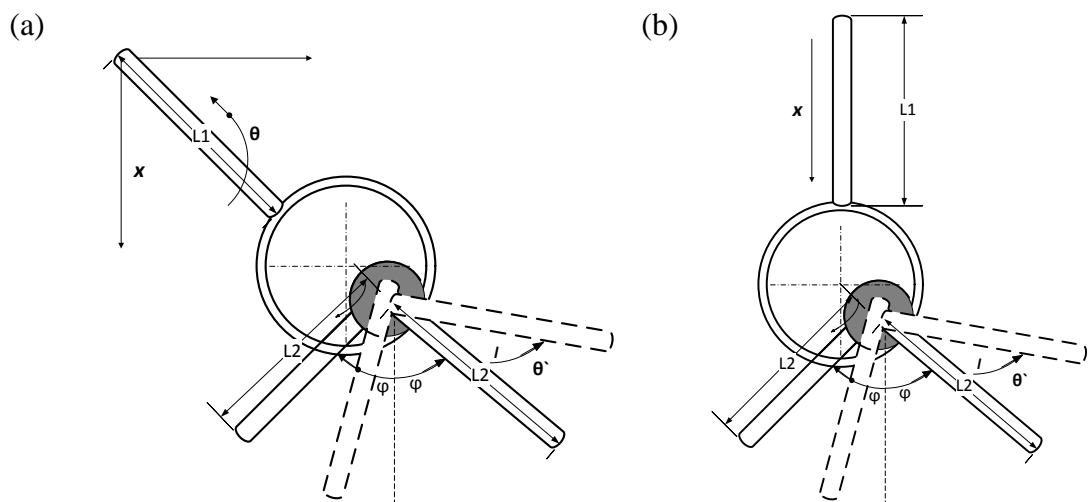

Fig 5. 4 Two pendulum in a circular track (a) shows the pendulum motion from Fig 6.2, and (b) shows the pendulum motion from fig 6.3

Fig 5. 4 shows the movement of the pendulum in all the configurations. Where θ is the angle in which the pendulum oscillates, L1 is the length of the pendulum's arm attached to the cart. Where x is the vertical displacement, L2 is the length of the pendulum's arm attached to the bearing inside the circular track. θ' is the angular displacement in which the pendulum attached to the bearing inside the circular track moves.

There are two configurations, the first of which incorporates a circular track, on which rolling bearings allow a second pendulum to rotate, the configuration can be seen in Fig 5. 2 and the motion of the pendulum is depicted in Fig 5. 4 (a). There are two bolts attached to the bearing shaft at an angle to each other. The reason for this configuration is to perform an experiment to compare with analytical results of Horton *et al* [1] had concluded that a pendulum suspended and moving on an elliptical track rotated more easily than a parametrically excited pendulum. In this experiment, a circular track is used because a circle is a special form of ellipse.

The second configuration limits the motion of the first pendulum using an elastic tape at two positions 25 mm apart each other, as depicted in Fig 5. 3. By means of this configuration, rotations and oscillations are easily reproduced, as it reduces a degree of freedom from excessive travel on the circular track which can be seen from the motion of the pendulum is depicted in Fig 5. 4 (b) where the motion θ is constrained.

The mass of the pendulum itself is 0.26 kg, the shaft carrying the bearings has a total mass of 0.16 kg, and the bolts are of masses 0.028 kg and 0.032 kg respectively. The mass of the inertia acting as point of suspension is 1.4 kg, and the shaft connected to the inertia and suspended by a spring is 0.86 kg in mass. Hence, the total sum of masses adds up to 2.56 kg.

The working frequency ranges between 1.75 Hz to 2.65 Hz. Another frequency of 3.3 Hz has also been identified. The spring stiffness's are 183.1 N/m, 241.2 N/m and 276.3 N/m. These can be interchanged for different operating frequencies. The position of the spring is important to determine the optimal operating frequency. This influences an equilibrium position in determining the variation of electromechanical force when oscillator changes position in relation to a static equilibrium position. The length of the pendulum has a total length of 103 mm, end to end as shown in Fig 5.2 and Fig 5.3 shaft of the pendulum is 72mm, and the spring is suspended at various locations.

Two acrylic plates have been positioned parallel to each other separated by a distance of 73 mm, in order to limit the yaw motion generated from the vertical motion of the system. By wasting less energy in yaw motion, more electromagnetic force could contribute to a larger amplitude of vertical oscillations. As the width of the inertia is 72mm, the use of adhesive tape was sometimes necessary to make up the remaining 1 mm clearance, as well as reduce energy loss due to friction in order to transfer an optimum amount of energy and momentum to the pendulum.

The stiffness in the mechanical spring is 241.2 N/m which is slightly more than that used by Teh *et al* [[2], due to the total mass being slightly heavier compared to the original design. The range of voltages supplied by the variac is also higher between 110 to 130 V, due to requiring a larger amplitude of motion generated from the electromechanical solenoid. Frequency of square waves from the function generator ranges from 1.75 Hz to 2.65 Hz, in particular 2.4 Hz is an optimum operating frequency for both configurations.

The angle between the bolts is most optimum at 135°, such that rotations are continuous and reproducible. , although the angles in this experimental study range from 120° up to 150°.

Data acquisition was performed using National instruments NI- USB − 4432 Microcal hardware and Labview Signal Express software and Origin lab. The Labview Signal Express acceleration signal from the accelerometer at the sampling rate of 2400 Hz. The acquired data using a band pass filter using a lower cutoff frequency of 1.5 Hz and upper cutoff frequency of 5 Hz to minimize noise in the acquire data. Numerical integration algorithms in Originlab software enabled velocity and displacement to be obtained such that phase planes, Poincaré maps as well as amplitude spectra were constructed.

This tumbling chaotic rotational motion is more reproducible in the second configuration i.e. easier to obtain rotations. Beat, period − two and chaotic motion have been observed.

The solenoid has also been switched on and off in a stochastic manner such that the duty cycle is varied in accordance to a random distribution. The particular reason for this investigation is to check if rotations are still possible when forcing is of a stochastic nature. Rotations have been found to be possible for fluctuations up to 30% of the probability distribution.

Fig 5. 2(a) shows a photograph of experimental setup and Fig 5. 2 (b) illustrates the corresponding schematic. A pair of parallel vertical acrylic plates guides the point of suspension to oscillate vertically. A horizontal support bar secures the acrylic plates below them, and is clamped to a rigid table by means of an F-clamp. A solenoid is mechanically fastened to a vertical and rectangular aluminium plate which is clamped

to a frame. A ferrous conductor is made of mild steel. By mechanical connection to a cylindrical brass component, it is suspended from a horizontal bolt by means of a mechanical spring of stiffness 241.2 N/m. This bolt is in turn fastened to the above mentioned aluminium plate by turning it into a tapped screw thread.

Experimental data had been acquired at a sampling rate of 2400 Hz using National Instruments NI- USB − 4432 hardware and Labview software, 10 forcing cycles of data had been omitted as transient and 100 cycles of steady state response were acquired.

The total mass of moving and rotating parts is 2.64 kg, inclusive of a circular track, ferrous conductor, and point of suspension, rotary bearings, bolts and nuts. For testing, the experiment requires an adhesive constraint taped across circular track so that the pendulums do not dislocate from the track due to excessive travel on it. Two clamps securing the rotating point of suspension with the use of an adhesive constraint are secured 25 mm apart edge to edge. The parallel acrylic plates are maintained at 73 mm, due to point of suspension being 72 mm wide. The resulting clearance of 1 mm is filled up with adhesive tape which is sprayed with WD − 40 lubricants to minimize friction. A capacitance of 30 μF was used in the circuit. A multimeter measured the solenoid resistance to be 22 Ω, and collective circuit resistance to be 19.8 kΩ.

Fig 5. 2 (a) describes a first configuration which allows free oscillation of first pendulum. Fig 5. 2 (b) presents some detail with regards to data acquisition. The power is switched on and off in accordance to the frequency of the control waveform, by means of a solid state relay. The control waveform is a square wave generated by a function generator.

Rotational motion, mainly in the form of tumbling chaos, has been possible when point of suspension is actuated as shown in Fig 5. 3. The time series and phase plane has been constructed when frequencies range from 1.75 Hz to 2.25 Hz. This is lower than a frequency of electromechanically excited pendulum [2]. Additional data can be found in the Appendix.
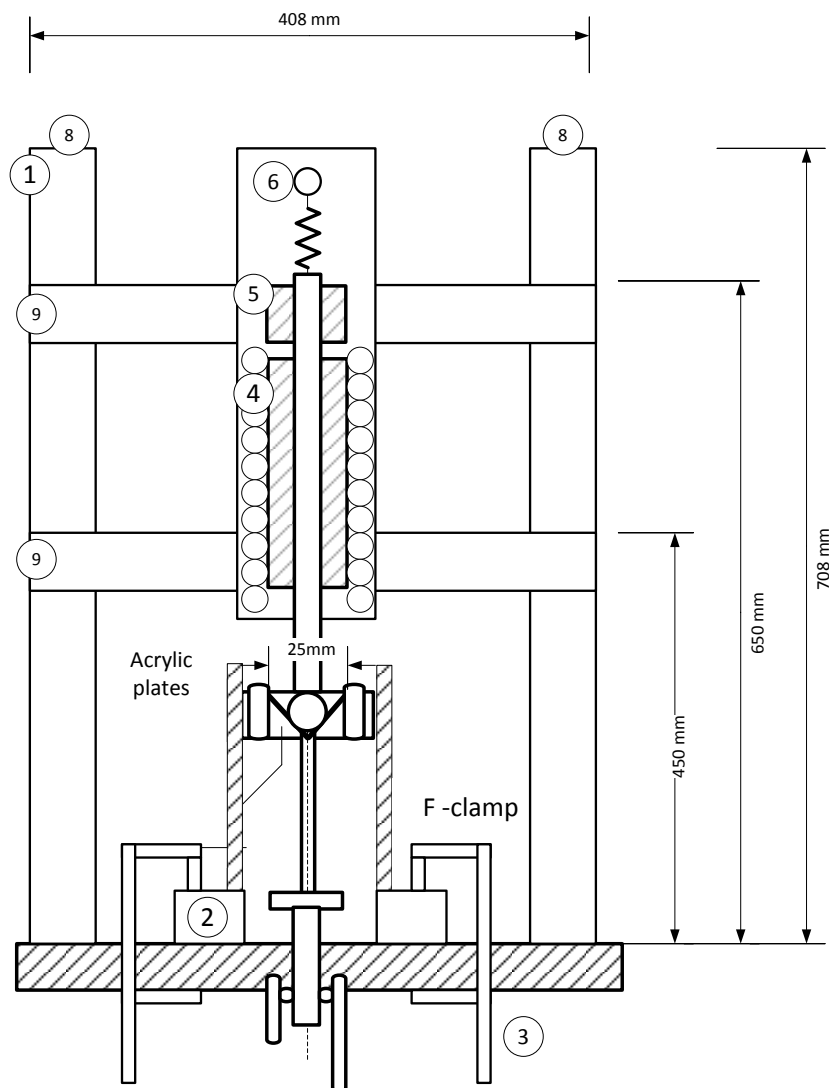
5.3 Experimental rig

Fig 5. 5 Schematic of experimental setup for circular track. 1) Frame, 2) Support bar holding acrylic plates. 3) F- Clamp, clamped onto the table. 4) Solenoid, 5) Linear

Bearing. 6) Bolt holding the spring which carries the conductor, 7) point of suspension. 8) Vertical bar. 9) Horizontal Bar.

As can be seen in Fig 5. 5, a supporting frame of 708 mm height is used in order to allow the configuration to be immobile. The supporting frame includes 4 vertical bars positioned in a square shape (denoted by ⑧ in Fig 5. 5). 4 horizontal bars of 408 mm length (denoted by ⑨ in Figure 4) in addition to the vertical members make up the frame.

A rectangular aluminium plate is fabricated to function as a base plate on which components of this experimental rig are fastened and lined up in a straight line. A row of evenly spaced holes tapped with a 6 mm screw thread, are 10 mm apart each other. A solenoid and linear bearing are attached to the metallic plate, as illustrated by Component ④ of Fig 5. 5, and Component ⑤ in Fig 5. 5.

A conductor, made of brass, connected to a metal rod is inserted into the solenoid and the linear bearing in order to induce electromagnetic interactions. A spring of stiffness 241.2 N/m is suspended as illustrated by the Component ⑥ in Fig 5. 5.

In order to limit yaw motion, two acrylic plates are parallel to each other, 73 mm apart within which inertia oscillates vertically.

5.4 Results and Discussion

An alternating current supplied from a variac actuates point of suspension. The angle between two rotating links is manually adjusted, and a frequency generator switches the solenoid on and off via a solid state relay. For the first configuration, for the frequency ranging between 2.2 Hz to 2.65 Hz, rotations are possible. Period – 2

rotations are observed at a frequency of 2.4 Hz and 110 V input. When the frequency is varied to 2.25 Hz, period 2 oscillations are obtained.

For the frequency ranging between 1.75 Hz to 2.25 Hz, period 2 rotation is possible as seen in. Period – 2 oscillations is observed for a frequency of 1.9 Hz. Period 3 rotations can be created by a frequency of 2.01 Hz. The qualitative response will be discussed later in this section.

(a)
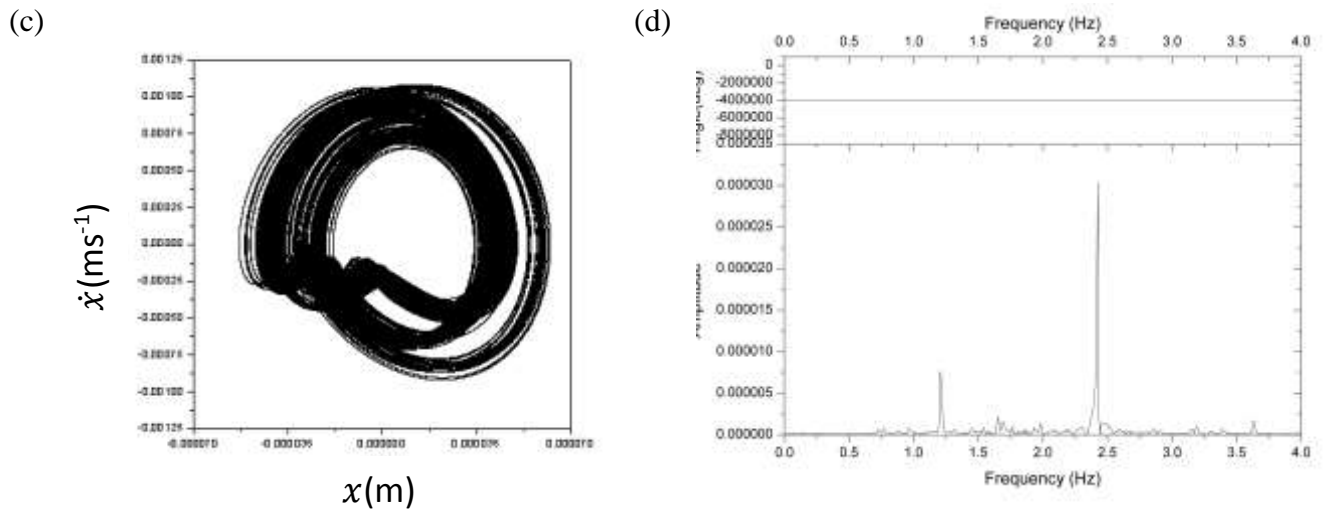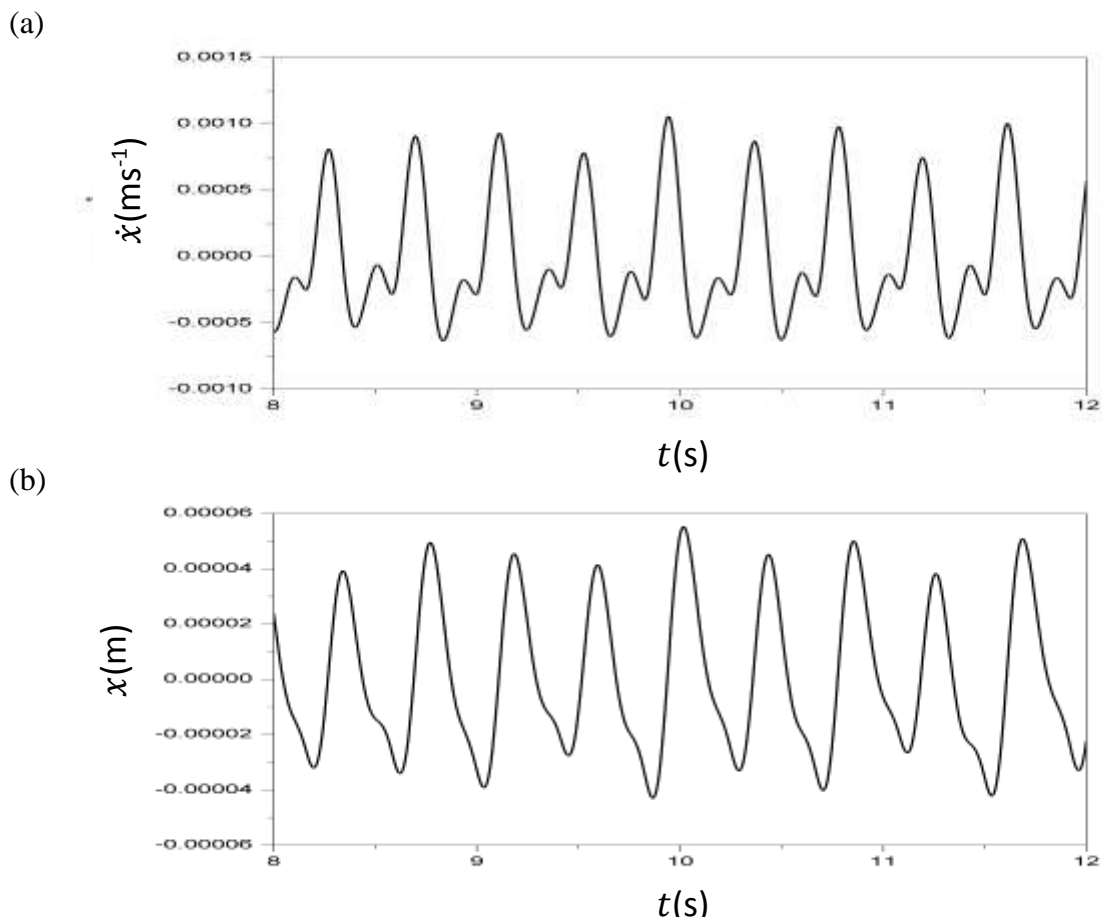

(b)

$\dot{x}(\text{ms}^{-1})$

$x(\text{m})$
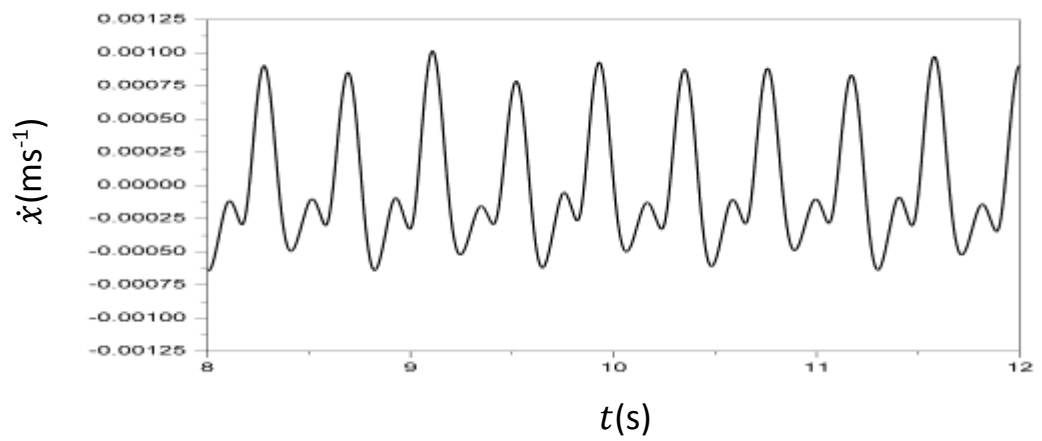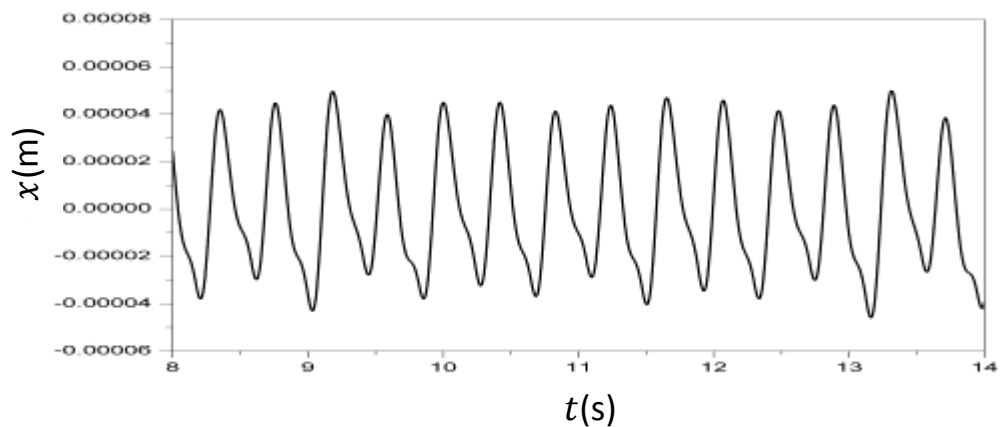
Fig 5. 6: Rotation with free motion of point of suspension, the supplied

voltage is 110 V, and the supplied frequency is 2.4 Hz. Experimental time histories of

point of suspension, in which (a) is that for velocity, (b) represents the displacement,

(c) illustrates phase plane, and (d) is an amplitude spectrum

(a)

$\dot{x}(\text{ms}^{-1})$

$t(\text{s})$

(b)

$x(\text{m})$

$t(\text{s})$

71

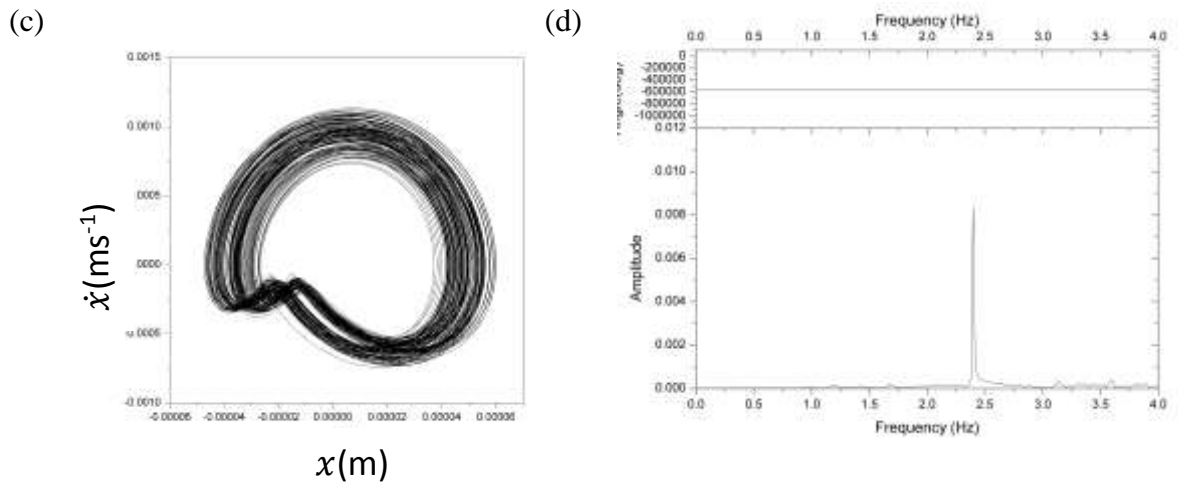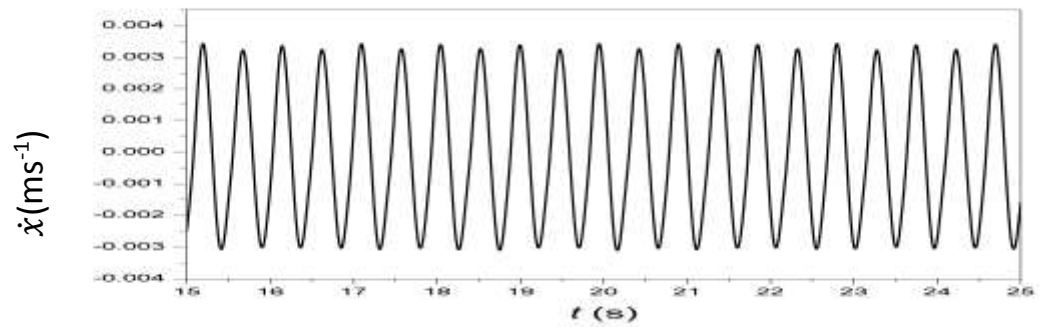(c)   (d)

Fig 5.7 : Oscillation with free motion of point of suspension, the supplied

voltage is 110 V and supplied frequency is 2.25 Hz. Experimental time histories of

point of suspension, in which (a) is that for velocity, (b) represents the phase plane, (c)

illustrates displacement, and (d) is an amplitude spectrum.

The data has been collected after a continuous bifurcation test to measure its

stability and was given the exact initial conditions as presented above. The system begins

to rotate after an external force to initiate a single rotation to the system. After a stable

continuous result, the result is taken and plotted.

Fig 5.7 corresponds to period 2 rotations showing the experimental vertical

displacement – time history. Fig 5.7(c) describes the simultaneous vertical oscillations of

point of suspension. For two periods of vertical excitation, one rotation had been observed

which repeated at equal time intervals. In Fig 5.7, oscillations of bolts had been seen

instead. Phase planes of the steady – state motion were constructed to confirm the nature

of the orbit. It can be seen from Fig 5. 6(b) and Fig 5.7 (b), that there are multiple closed

loops which or tend to appear when the two bolt pendula are rotating. Fig 5.7 (b) consists

of a maximum of two closed loops only. The amplitude spectrum of Fig 5. 6 (d) shows a

spread of frequency components between 1 Hz and 2.6 Hz, whereas Fig 5.7(d) shows
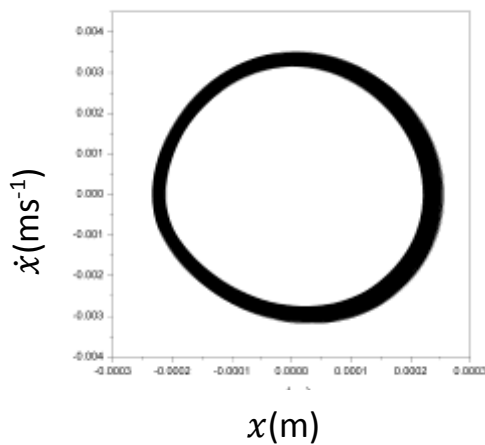
only a distinct frequency peak at 2.25 Hz.

(a)

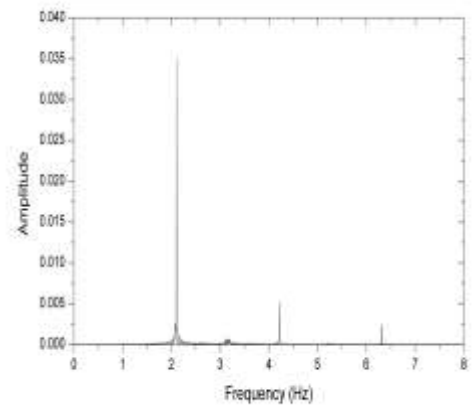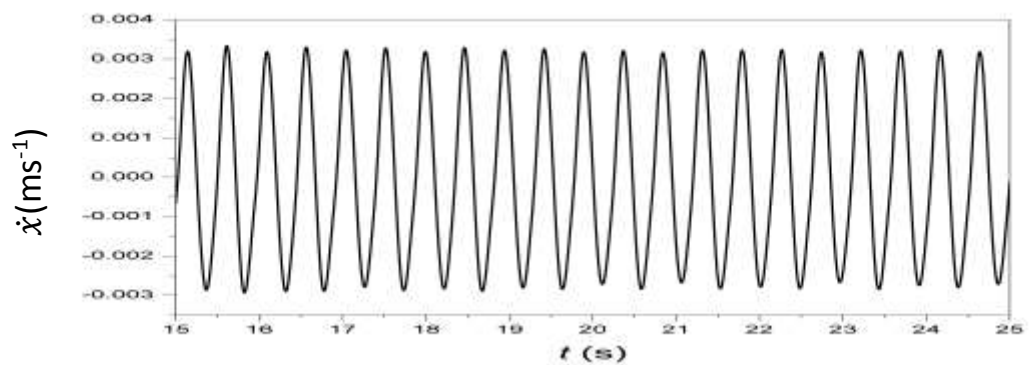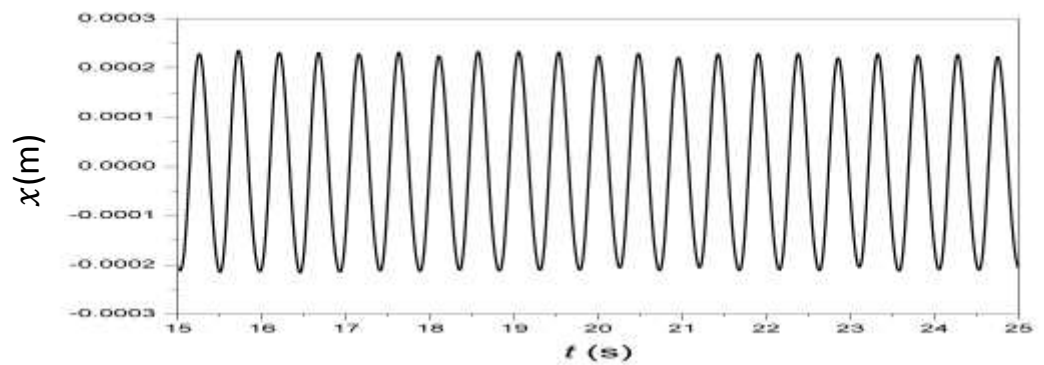
(b)

(c)

x(m)
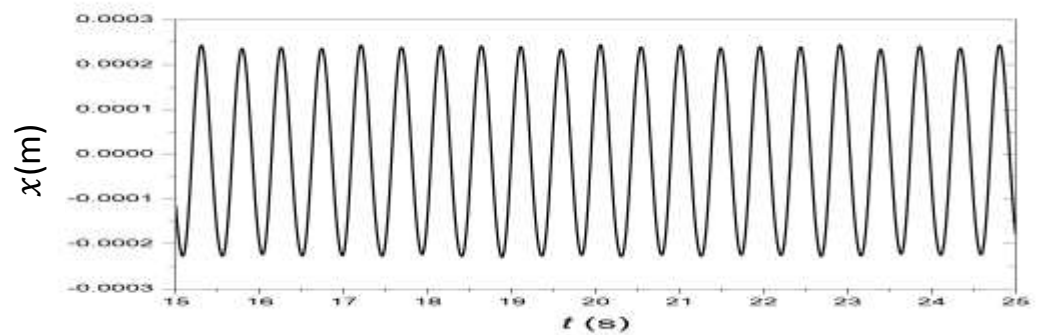
(d)

Fig 5.8: Experimental time histories of point of suspension being restricted by the adhesive constraint where the supplied voltage is 120 V with a supplied frequency of 2.1 Hz. In which (a) is that for velocity, (b) represents the displacement, (c) illustrates phase plane, and (d) is an amplitude spectrum.

In order to obtain the result in the following frequency, amplitude spectra is obtained and adjusted. The system is initiated with external forcing similar to Fig 6.7, as the pendulum begun to rotate continuously, the frequency is re-adjusted in order to locate the range of frequency for the system to maintain the rotational motion, one of the most clear result is shown in Fig 5.8 where the rotational motion seems to bifurcate within a minimum amplitude as shown in Fig 5.8 (c)

(a)
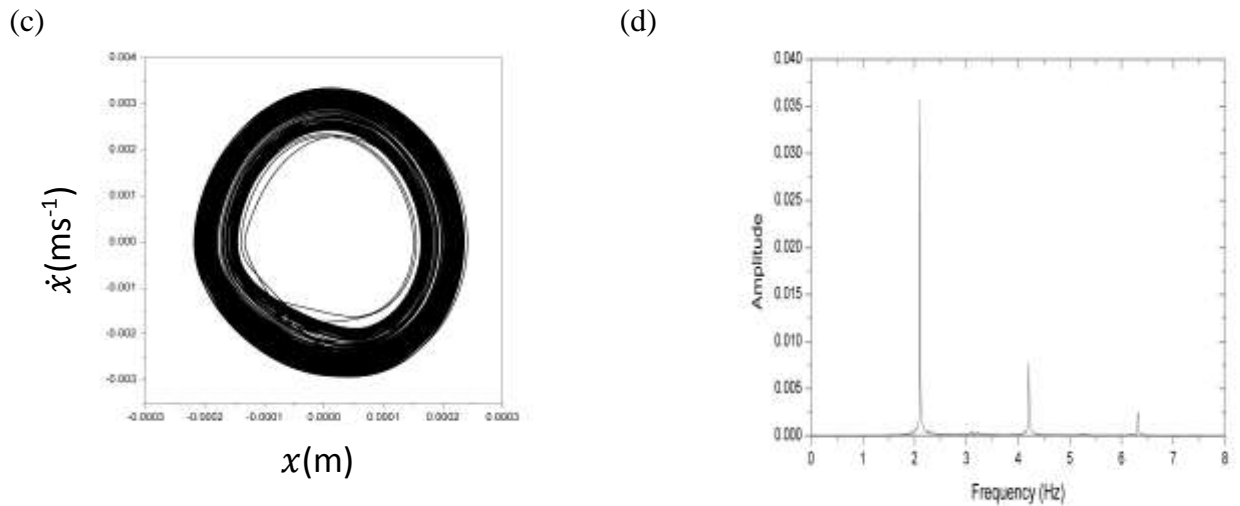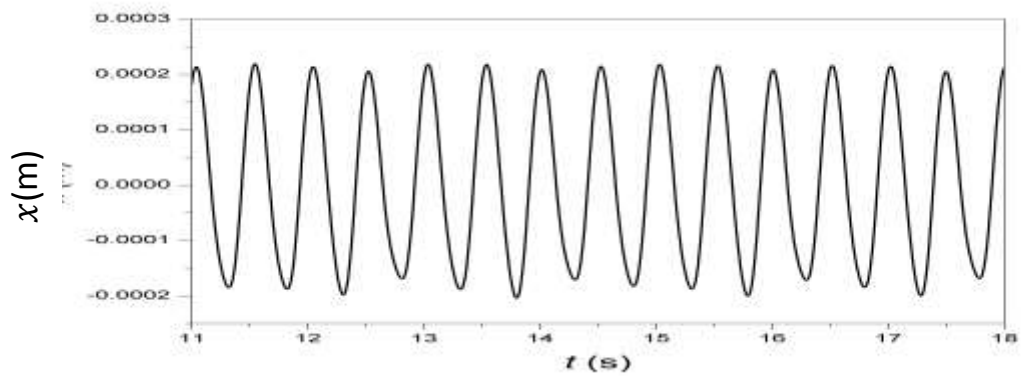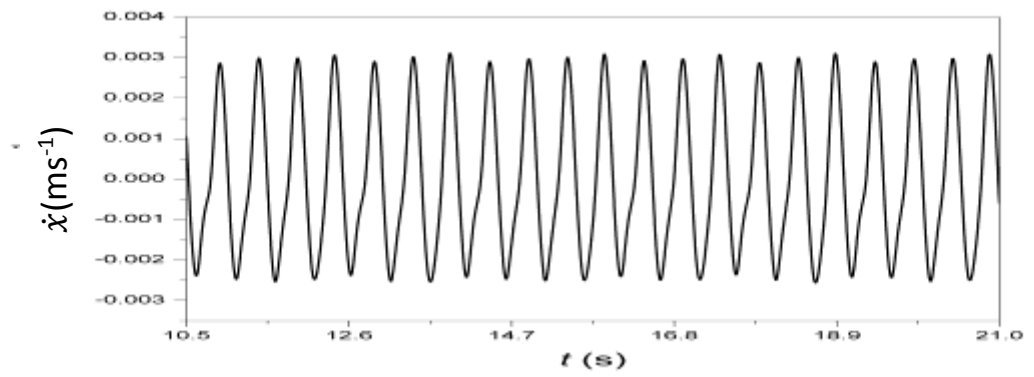

(b)

(c)   (d)

Fig 5.9: Experimental time histories of point of suspension being restricted by the adhesive constraint, where the supplied voltage is 120 V, and the supplied frequency is 2.14 Hz. In which (a) is that for velocity, (b) represents displacement, (c) illustrates phase plane, and (d) is an amplitude spectrum.

Fig 5.8 corresponds to the vertical displacement experiencing period one rotations. Fig 5.8 (c) depicts the time history of the vertical oscillations of suspension point. For this configuration, one period of vertical excitation creates a single rotation, and this repeats itself periodically. In Fig 5.9, oscillations of the pendulum bolts are observed instead.

Phase planes have also been constructed to determine the nature of the orbit. Fig 5.8(b) consists of one distinct closed loop, whereas Fig 5.9(b) is made up of a few loops. The amplitude spectrum exhibits 3 distinct peaks for both cases of rotations, the peaks represent the frequency of the vertical motion, and when there are more peaks the period increases by one for every peak.

The rotations from the second configuration are period one in nature. In comparison, the first configuration mostly induces rotations from beat phenomena, or tumbling chaos. It is also found that the frequency that permits rotations for the first configuration is 2.4 Hz which is slightly higher than 2. 2 Hz in the second configuration.
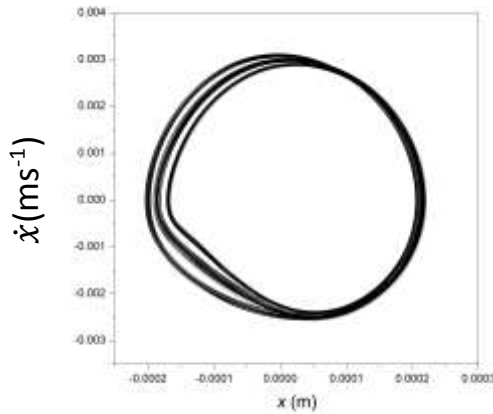
Fig 5. 10 : Experimental time histories of point of suspension being restricted by the adhesive constraint, where the supplied voltage is 120 V, and the supp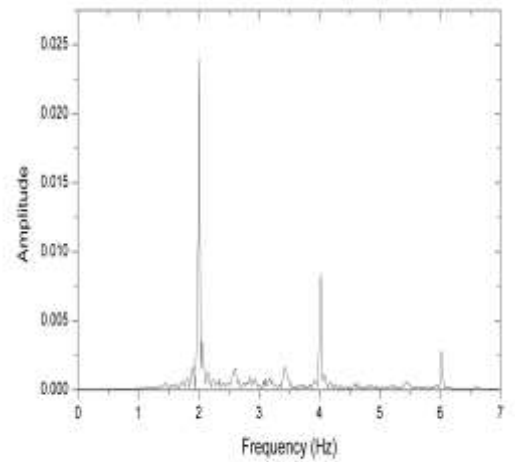lied frequency is 2.01255 Hz. In which (a) is that for velocity, (c) illustrates displacement, and (b) represents the phase plane, (d) represents the amplitude spectra.

When the frequency is 2.012 Hz, aperiodic vertical oscillations are observed. It is thus likely that rotations are chaotic in nature, for a voltage supply of 130 V.

Another configuration is planned in order to achieve rotations by limiting the travelled distance by the inertia to generate rotations. Multiple springs were used in order to constrain the vertical motion of the inertia, as the solenoid RS Stock No. 358-4040 Pull action AC laminated solenoid, such that the maximum distance is 34.2 mm. The frequency allows the system to rotate itself at 3.31 Hz. The bolts have also been replaced, and varied, such that one bolt is 40 mm and the other is 35 mm long. Experimental study indicates that when one of the bolt is slightly shorter, chances of rotation have increased considerably.

5.5 Conclusion

The solution implies that the frequency of the oscillatory response influenced mainly by the frequency of the control waveform, if it is not resonant, as reported by Ho *et al* [71]. The range of frequencies between 1.75 Hz and 2.25 Hz for which a rotational attractor exists indicates a robust nature for the second configuration, which is similar to a double pendulum. The angle between the two rotating arms sharing a common axis is important for rotations to be possible. As for the first configuration, one of the links is constrained to a small angle oscillations, such that the circular track plays a major role in facilitating rotations. The range of frequencies for the first configuration is 2.1 Hz to 2.6 Hz.

Qualitative system response are as follows. For the first configuration, oscillations, rotational tumbling chaos and beat phenomena has been observed. Oscillatory are based upon period two motion.

77

In the second configuration, oscillations and rotations have been identified at 130 V supply and frequency of 2.2 Hz, beat phenomenon has been a precursor to rotational motion. When the power supply was 110 V varying at 2.1 Hz, period one rotations were induced. On adjusting the voltage to 130 V. period two rotations are found. When frequency is at 2.01 Hz, period 3 rotations were found at a range of 2 Hz to 2.1 Hz.

It was sometimes necessary to use an adhesive constraint across the circular track such that the rotating arms do not dislocate. In this case, a range of frequencies for which rotations are stable, is from 1.75 Hz up to 2.25 Hz for the reproducible range. A voltage of at least 110 V using a switched RLC circuit is required to sustain rotational orbits, due to the additional boundary condition. For the first configuration, with adhesive constraint, it is found that the rotational attractor exists from 2.2 Hz up to 2.5 Hz with a standard deviation of 0.1 Hz for a reproducible range. Similarly voltage of at least 110 V is required from an alternating current supply.

With and without adhesive restraint, for similar actuation voltage, the main factor conductive for a rotational response, the frequency range of periodic signal from function generator. As such, it is useful to monitor and measure the current frequency of actuating energy source to ascertain the possibility of rotations. If not possible, the length of rotating links may be altered.

By experimentation, the ideal angle between the rotating disks sharing a common axis is 135°. Although, there are also other angles for which rotations are also possible, 135° yields rotational motion which is most reproducible during the experimentation.

For the rotation in Fig 5. 2, the accelerometer reading measuring vertical motion of suspension constructs a phase plane of period three motion. Suggesting it may be worth investigating and confirming if rotational orbits are always associated with chaotic

vertical oscillations. By using Lyapunov exponent it is found that period three implies chaos. [90]

The rotation for the configuration based on Fig 5. 3, corresponding to configuration based on Fig 5. 2 is likely to exhibit tumbling chaos. Occasionally, rotates in one direction for an extended period of time. The longest duration of observation to date is approximately 53 minutes, the average duration is 30 seconds.

The circular track, have not achieve a robust continuous rotations that can exist in wider range of frequencies. There are also more angle of freedom involved in this configuration. In order to generate continuous rotations, the angle subtended between the pendulums has then been the aim of the experimental work.

Chapter 6

Experimental Work: Pendulum subtending an angle

6.1 Introduction

The experimental work undertaken by Wiercigroch [4] and Teh [2] has improved confidence in using vertical oscillations in generating rotations. The current work seeks to widen the range of frequencies at which pendulum rotations can occur.

Two pendulums rotate about a common shaft such that there is momentum associated with each pendulum. The effect of the angle subtended between these two pendulums is investigated experimentally.

The current configuration also hopes that the physical phenomenon of resonance is beneficial since it exhibits large amplitudes of vibration, with the use of the solenoid, a small voltage input produces a considerable output work which will be explained further later. It has been known that rotations can been generated from a chaotic input forcing [23]. Hence the present work seeks to investigate rotations generated from periodic as well as stochastic (sea waves), vertical excitation.

This chapter documents the data acquired from a new experimental rig in the form of time histories, phase planes and amplitude spectra. The range of the frequencies for which rotations exist will be identified, and ranges for other system qualitative responses will be quantified as well. A description of the experimental configuration was made, so as to introduce experimental methodology and system dynamic responses. The experimental results will be discussed in relation to varied system parameters such as the angle subtended between the two pendulums, frequency and voltage.

6.2 Experimental Setup

The configuration using a circular track, which can be seen in Fig 6.1 was fabricated. Although rotations were found to exist, the configuration and acquired data have limitation that continuous rotations were not reproducible. This was discussed in Chapter 4. However, it was found from this experiment that two pendulum subtended by an angle connected to each other by a common shaft, has increased the chances of generating continuous rotations, which laid the basis for the configuration that will be discussed in this chapter.
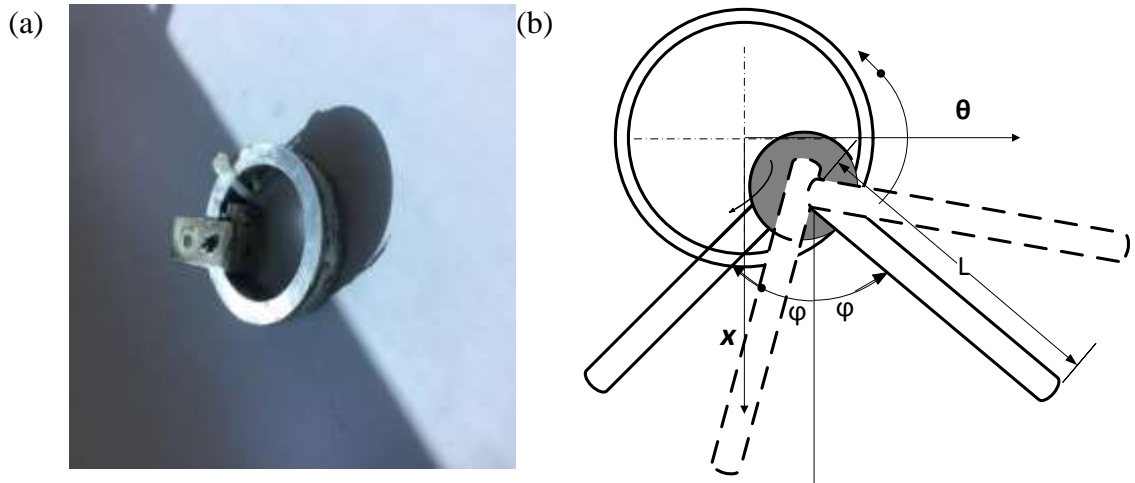
Fig 6.1 Fabricated Circular Track

Fig 6.1 shows the fabricated circular track such that it is as light as possible. It is made from three main components, two of which are made from plates and the circular track is made from a cylinder. A bearing (SKS 626-2Z) which acts as the roller for the pendulum. These three components are attached to each other using an epoxy glue. This assembly guides the bearing to move on the track, while acting as a pivot for the pendulum to oscillate or rotate. When the vertical oscillatory excitation exceeds a threshold value, impacts occur and rotations are rare. When the bearing moves along a semicircular track, some rotations are observed, albeit not necessarily continuous.

Fig 6.2 The configuration investigated with the use of a tape, in order to constrain the motion for the bearing, instead of using the circular track. Rotations are currently ongoing.

Fig 6.2 reveals the configuration that generates reproducible rotations. The pivot is subjected only to a vertical excitation without other degrees-of-freedom, and rotations were observed. Increasing the frequency of periodic excitation still facilitates rotations of pendulums, and thus, this configuration was further modified keeping the constrain pendulum on tact; Fig 6.3 also reveals a rotational motion at a higher frequency, and to indicate the presence of the pendulum.

Fig 6.3 Rotations currently ongoing, the system is viewed from the front view but the figure was not captured directly before disassembling. Rotations achieved at 9.8 Hz and a voltage supplied of 17 V.

6.2.1 Experimental Configuration

Fig 6.4 shows the current experimental rig for facilitating the experiments of two pendulums with a subtending angle. The experimental rig utilizes a pull type linear solenoid (Model: RS 358-4040) to actuate the pivot of two pendulums. The linear solenoid is mounted on an aluminum base plate, which is clamped against a rigid frame. Inside the linear solenoid is a steel bar, and the pendulum support is mounted at the bottom end of the steel bar. The pendulum assembly houses a shaft that pivots the two pendulums with adjustable angle and a magnetic encoder, which is mounted in series with the pendulum axis. Three tension springs are used to enable the pendulum assembly to oscillate in vertical direction. Two of them are placed at both sides of the solenoid. The pendulum assembly is connected to the lower ends of those tension springs by means of a rod which is held inside a dedicated hole at the pendulum assembly. On the other hand, the upper ends of those tension springs are suspended onto another rod which is held inside an aluminum block that is mounted firmly above the linear solenoid. The third spring connects the bottom part of the pendulum assembly to a horizontal plate, which is an extension of the rigid frame, by means of a pair of mechanical hooks. Also, a laser sensor is positioned at 40 mm below the static equilibrium position of the vertical oscillator, as shown in Fig 6.4 (c).
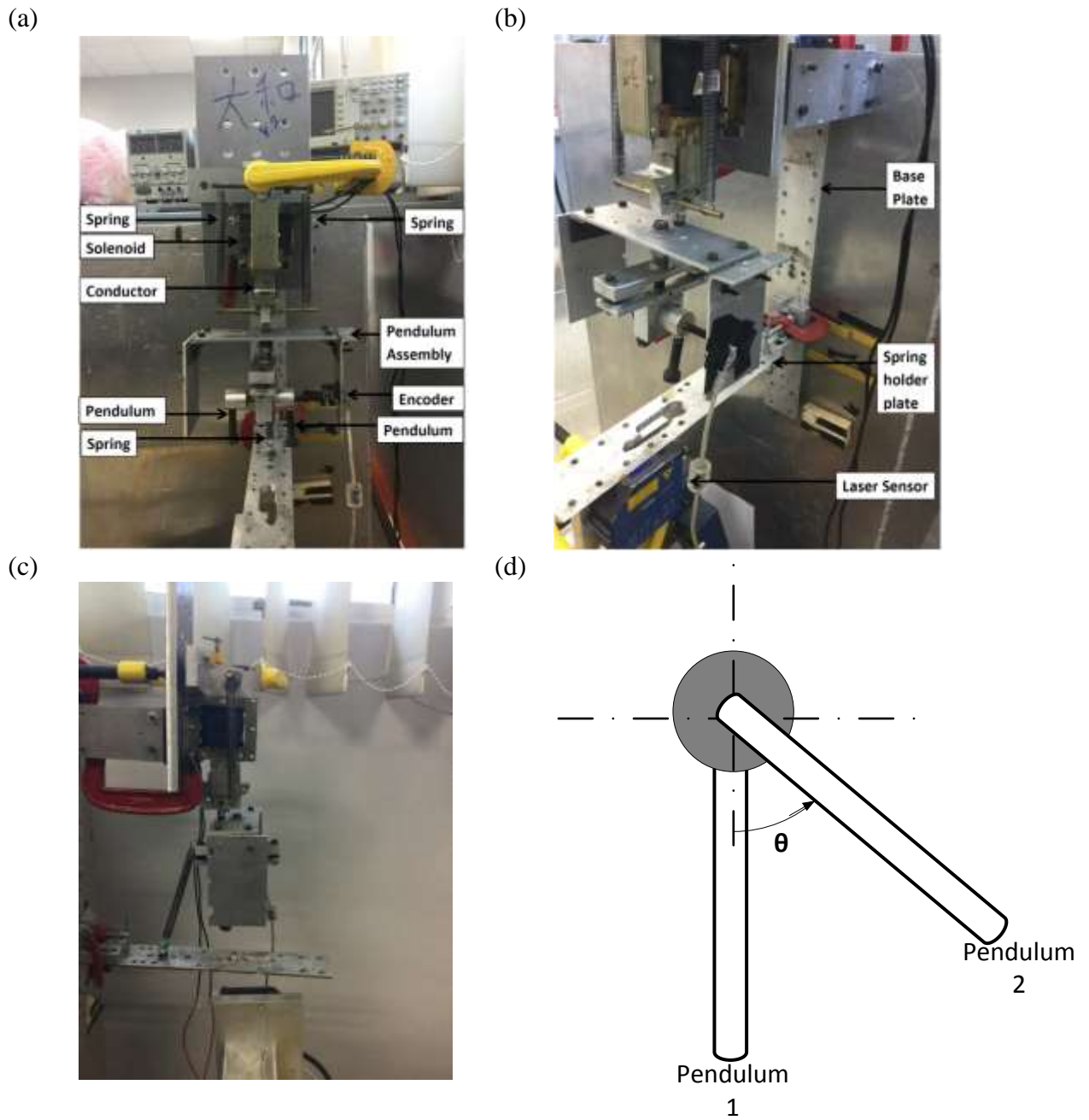
Fig 6.4 Experimental rig for vertical excitation of two pendulums subtended by an angle (a) represents the laser sensor view from the front where it is below an aluminium bar, with a hole that allows the laser to identify parameter. (b) Represents the side view and the position of the laser's position. (c) Represent the side view of how the system is clamped. (d) The subtended angles
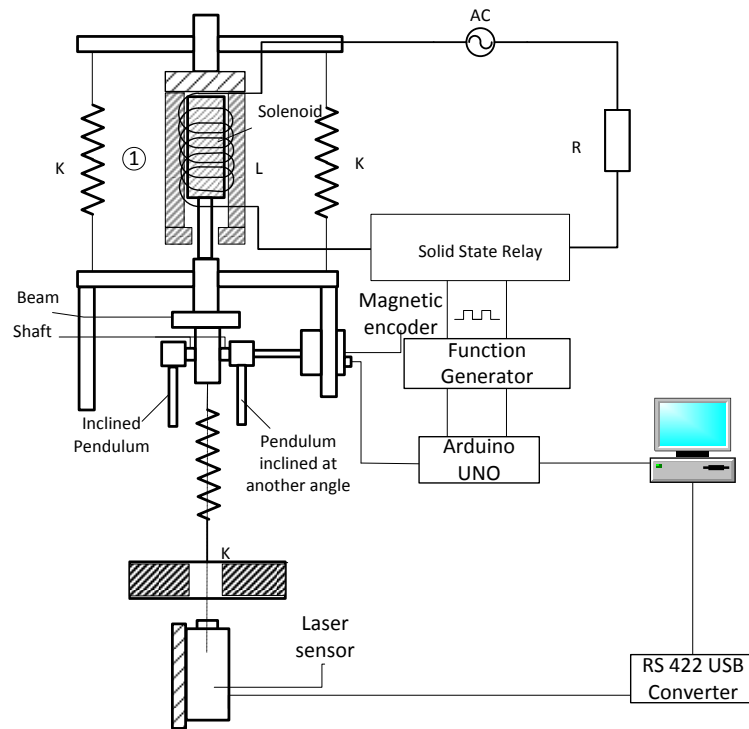
Fig 6.5 Full schematic of the working experimental product including the sensors

The schematic of the pendulum setup of present work is illustrated in Fig 6.5. Electromagnetic force is affected on a steel bar within the linear solenoid to actuate the pendulum assembly in vertical direction as depicted in Fig 6.5. The linear solenoid is connected in series to an AC power supply and a solid-state relay. An external circuit is used to switch the circuit of the linear solenoid on and off accordingly via the solid-state relay, and the voltage of the external circuit is generated from an arbitrary waveform generator (model: Wavetek 75). By switching the solenoid on and off repeatedly, it produces intermittent forcing effect on the pendulum assembly. The working principle of the proposed experimental setup is similar to that reported in [2], where the pendulum assembly oscillates as it is electromechanically-excited by a solenoid. The difference is that the steel bar of the linear solenoid in present work has limited vertical displacement. The linear solenoid used in this work has a closed end at the top of the solenoid, as depicted in Fig 6.5. This displacement constraint causes the

steel bar to collide with the top end of the solenoid as it travels upwards, thus it produces

the impacting effect for pendulum experiments at certain operating conditions.
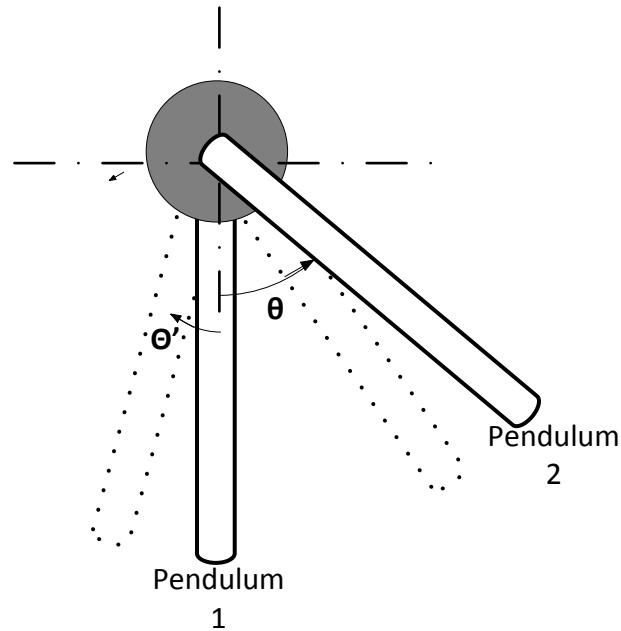

Fig 6.6 The motion of the pendulum of the angle.

The angle differences can be shown from Fig 6.6 in which θ is the angle

difference between Pendulum 1 and Pendulum 2. For most of the experimental cases

the pendulum begins rotating in the direction shown by θ'. This is due to the initial

tumbling given by the external force most of the time, Fig 6.7 illustrates the motion

on how the pendulum generates its excitation with the help of an initial perturbation.
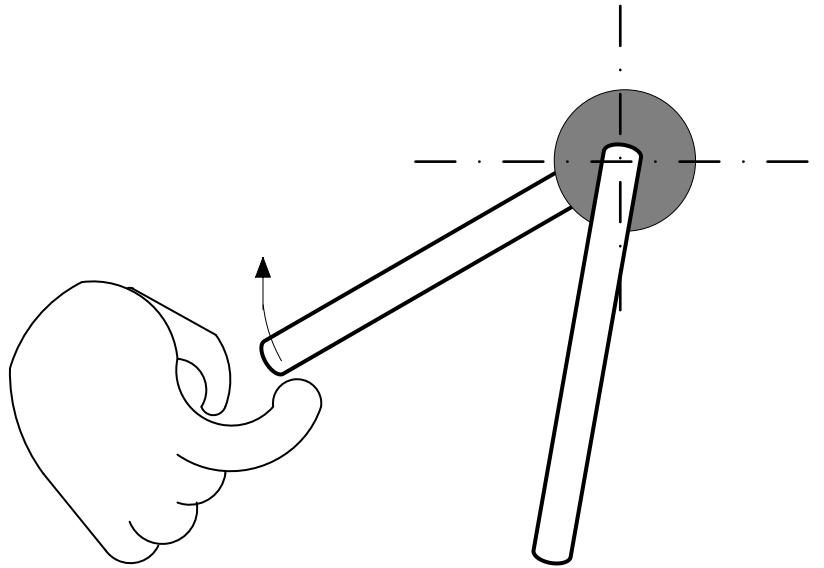
Fig 6.7 Initial perturbation caused by flicking the pendulum

The Pendulum is given an initial perturbation as it can be seen from Fig 6.7 , the reason for the initial perturbation is due to generate an initial momentum for the pendulum to generate rotations. This is because when the solenoid pulls the conductor vertically, there is no momentum to build up the pendulum rotation in the horizontal direction, nor is there any momentum to actuate the pendulum. After confirming that it is capable of having continuous rotations for at least 10 seconds, the results can be recorded.

The results that will be recorded for the experiment are vertical displacement, and the angular displacement. The vertical displacement is recorded in order to analyze the vertical oscillation of the conductor, and the angular displacement is to record the motion of the pendulum so that it is possible to determine the attractor of the pendulum.

The vertical displacement of the pendulum assembly is measured using an Opto laser sensor (model: NCDT-1700), and the signal is fed to the computer system via the RS 442 USB converter. The laser sensor is installed at a separated frame for minimizing

the effect of vibration to ensure accurate measurement. The angular displacement of the pendulum pivot is measured using a magnetic encoder (model: RS 714-2693, AEAT – 6012A Absolute magnetic encoder) which is powered by an Arduino Uno microcontroller board. The microcontroller board also functions as a data acquisition device to acquire signals from the magnetic encoder as well as the input signals generated by a signal generator to the solid-state relay and feed these signals to the computer system via a USB connection. The Arduino software is installed in the computer system to allow the communication between the computer system and the RS 442 USB converter (software: ILD 1700 Multichannel Tool) as well as the Arduino Uno microcontroller board (software: Arduino 1.6.8) for controlling the hardware interfaces while manipulating the acquired signals in real time.

4.2.2 RL Circuit
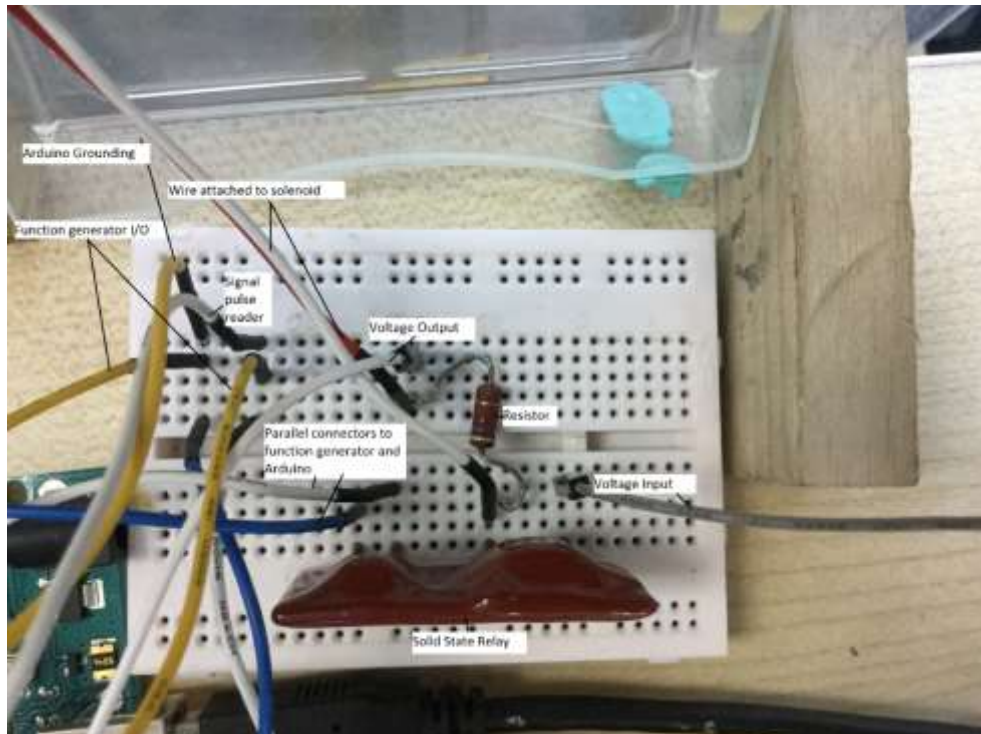
Fig 6.8 RL circuit connection

The RL circuit was constructed based on [11]. However, as the solenoid used require lesser voltage. The capacitor was removed as the capacitance do not permit low voltages to pass through obstructing any excitation for the conductor. After the capacitance was removed, the circuit has a high chance of getting high current when running for a long duration. Causing some of the wires to burn. In order to avoid the heat problem, the solenoid is allowed to rest after every 15 minutes for about 10 minutes, or until the SSR(Solid State Relay) has cool down.

6.2.2 Frictional Analysis

The masses of the pendulum support, the pendulum, and conductor are measured using an electronic digital balance as 1612 g, 17.8 g, 19.26 g, and 376 g respectively. The full length of both the pendulum was measured using Vernier caliper as 34 mm and 38 mm respectively. The resistance of the circuit was measured using the multimeter which is 4980 Ω, These parameters will be determined with the use direct measurement. Based on the acquired results of the masses, the moments of inertia of pendulums can be calculated as 1.6314×10^{-5} kg m^2 and 1.8073×10^{-5} kg m^2 respectively.

In order to determine the stiffness of the spring's tension, a static test is used. The initial distance between the suspension point and the loading point of the spring is measured before loading twenty two masses in stages to the tension spring. For each stage the distance between both ends of the tension spring is measured and the extension of the spring is calculated by deducting the initial distance measured between both ends from the measured distance. Linear curve fitting is obtained for the measured data as

shown in the Fig 3.1. It can be seen from Fig 3.1 that the calculated tension spring has a stiffness constant of 92.6 N/m and a loading of 4.5 N is required for the extension of spring to occur. By combining this result with the mass information, static calculation can be performed using equation (5.6) by removing the input and derivative terms to obtain the equilibrium extension of the spring when the pendulum assembly is loaded onto the spring. It is calculated as -0.0021m which is similar to the experimental initial displacement.

The non-linear variation of inductance as the metal conductor travels within the solenoid can be determined by measuring the inductance along the displacement of the metal conductor within the solenoid. Fluke PM6304(Fig A. 2) is the device used to measure the inductance of the coil inside the solenoid. The position of the conductor is progressively varied from upper or lower extreme end of the solenoid towards its center. The measurement of inductance is taken for smaller interval of displacement of metal conductor until it cannot be moved further.

Free fall responses of pendulum are used to determine the coefficients of linear damping and coulomb friction of angular coefficients of linear damping and coulomb friction of angular axis. The experimental configuration is restricted to one degree of freedom by means of a F-Clamp, which can be seen in Fig 6. 9 (Left). The pendulum is released from an angle of 135° and it's free fall response is measured using absolute magnetic rotary encoder and recorded with the use of Arduino. Equation (4.11) is simplified for the simulation of free fall response using Simulink by eliminating the terms related to vertical axis. Origin lab is used to determine the friction coefficients in Equation (3.3) by minimizing the following objective function, which describes the discrepancies between the measured responses and the simulated responses of pendulum free fall.

$$E_\theta = \frac{1}{m} \sum_{h=1}^{m} \sum_{j=1}^{n} (\theta_j - \theta_j^d)_h^2 \qquad (6.1)$$

Where m is the total sets of experimentally obtained responses, θ_j is the vector of discretized angular response simulated using the simplified version of Equation (4.11), and θ_j^d is the vector of discretized angular responses obtained from experiment. This numerical identification procedure is a form of decrement method similar to that of work reported in [7]. For this purpose, free fall responses of pendulum are recorded for a nine sets of the same condition. The extracted initial conditions are used to simulate the response and the coefficients C_θ and σ_θ are found based on the average of the nine sets of results as 0.902 x 10^{-5} N m s/rad and 1.8 x 10^{-3} N m.

A similar approach for vertical axis is used to determine the coefficients of linear damping and Coulomb friction for vertical axis. The pendulum is dismounted from the pendulum support to eliminate its coupling influence on the vertical axis which can be seen in Fig 6. 9 (Right). The pendulum support is released from the highest vertical displacement and its free vibration response is measured using the laser sensor and recorded using Micro-epsilon software for NLD1700. Equation (4.6) is simplified for the simulation of free vibration response using Simulink by eliminating the terms related to angular axis. The coefficients in Equation (4.17) have been determined by minimizing the following objective equation:

$$E_y = \frac{1}{m} \sum_{h=1}^{m} \sum_{j=1}^{n} (y_j - y_j^d)_h^2 \qquad (6.2)$$

Where y_j is the vector of discretized vertical response, simulated using the simplified version of Equation (4.10) and y_j^d is the vector of discretized vertical responses obtained from the experiment. Free vibration responses of pendulum support

are recorded for two sets of initial conditions, and coefficients C_y and σ_y are optimized based on these two sets of data as 0.2793 Nsm^{-1} and 0.195 N, respectively.
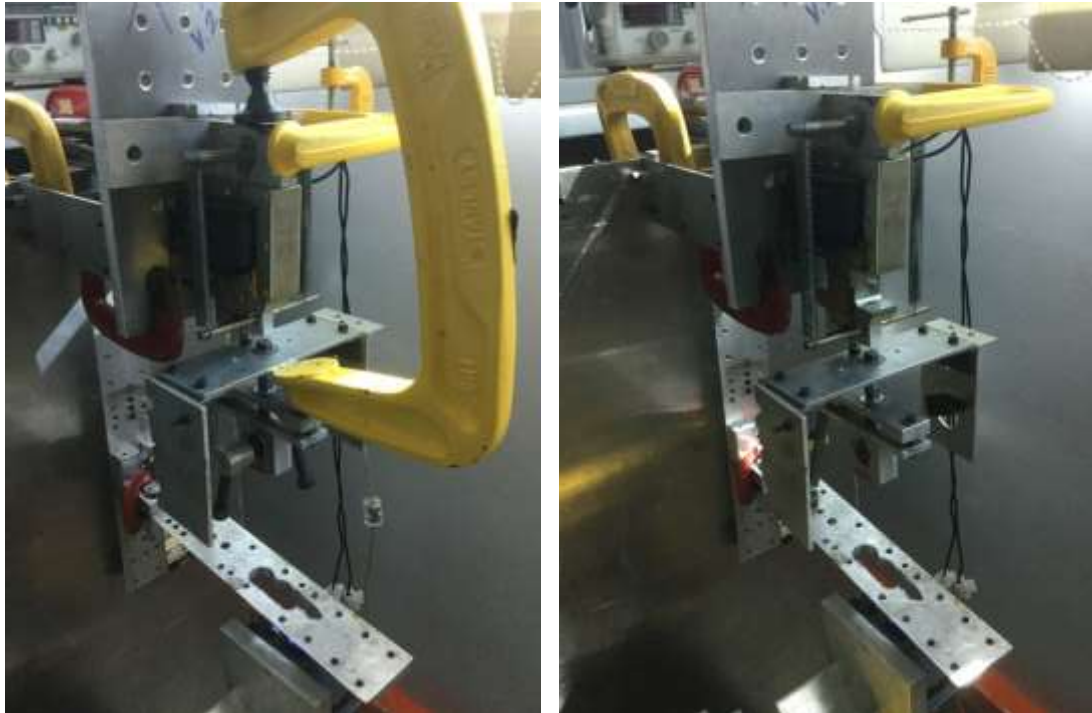

Fig 6. 9 (Left) Pendulum assembly is restricted by means of an F- clamp to identify the angular damping and coulomb friction. (Right) Pendulum dismounted from the pendulum support to identify the vertical damping and coulomb friction.

In order to completely analyze the damping and coulomb friction, the degree of freedom that can effect the results are restrained leaving only the degree of freedom of the wanted results. Fig 6. 9 shows how the configuration is restrained to acquire angular damping and vertical damping respectively.

(a)   (b)   (c)

(d)   (e)   (f)

$\theta(°)$

(g)   (h)   (i)

time (s)
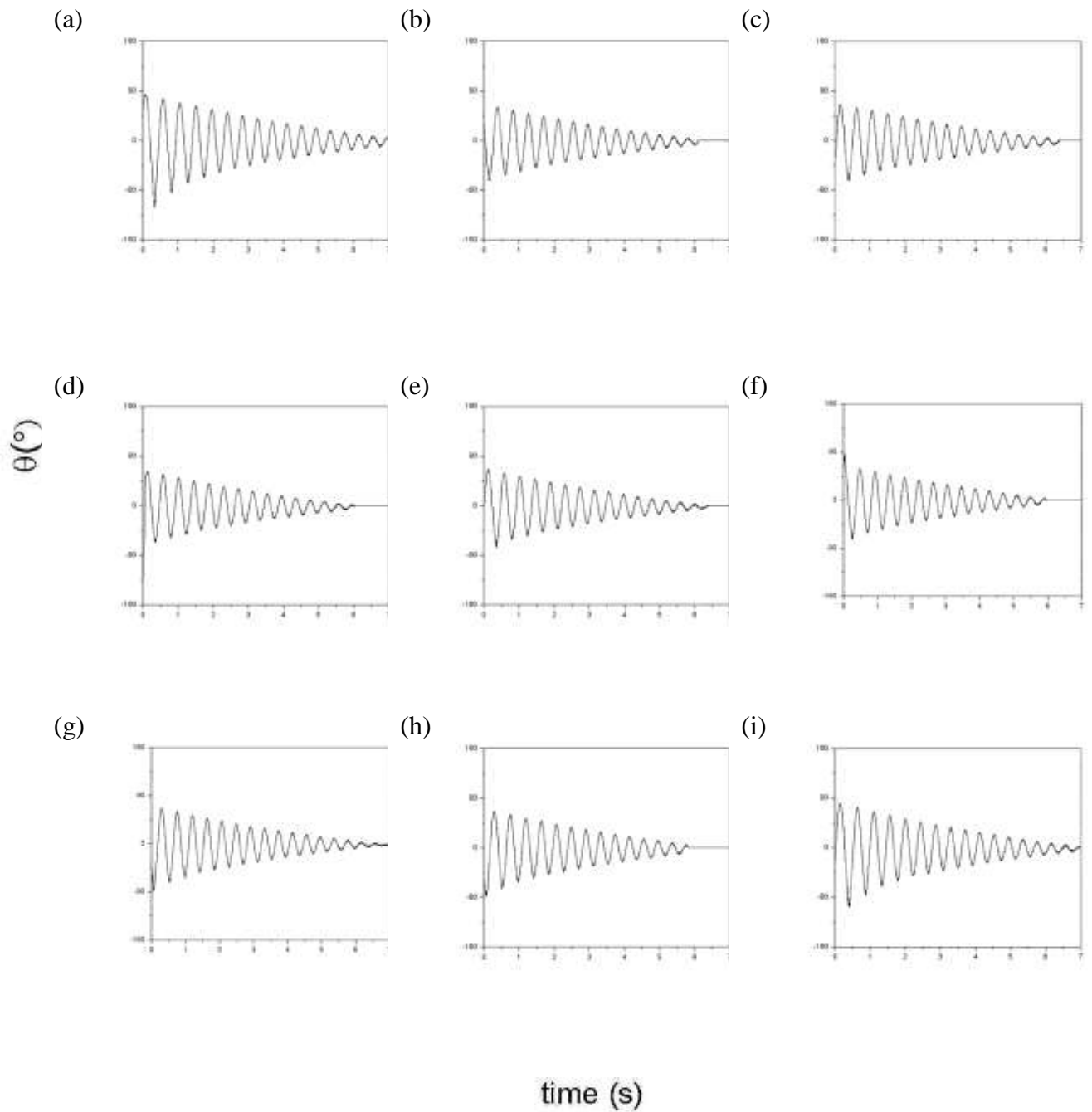
Fig 6.10 A zero initial velocity and non – zero initial angular displacement precedes
each time history to estimate damping characteristics.

Fig 6.10 shows the position of the pendulum, when the vertical motion is
restrained. The pendulum is given a push from the same position to identify the
damping characteristics of the pendulum.

94

(a)
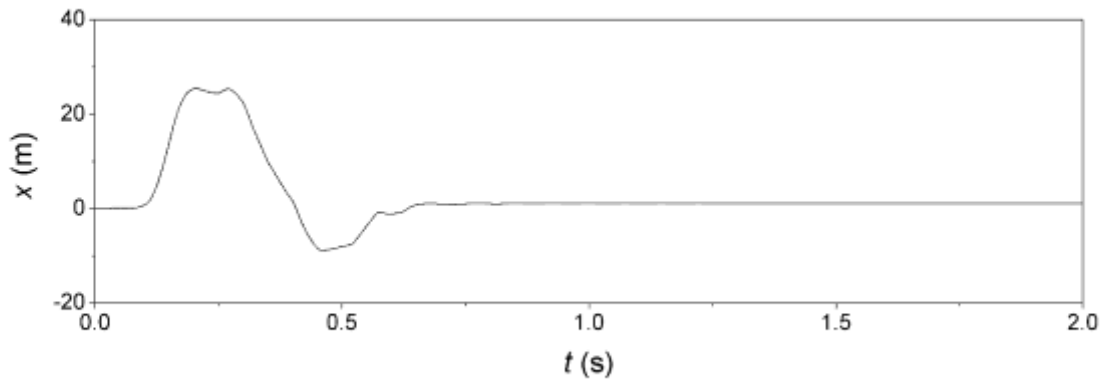
(b)
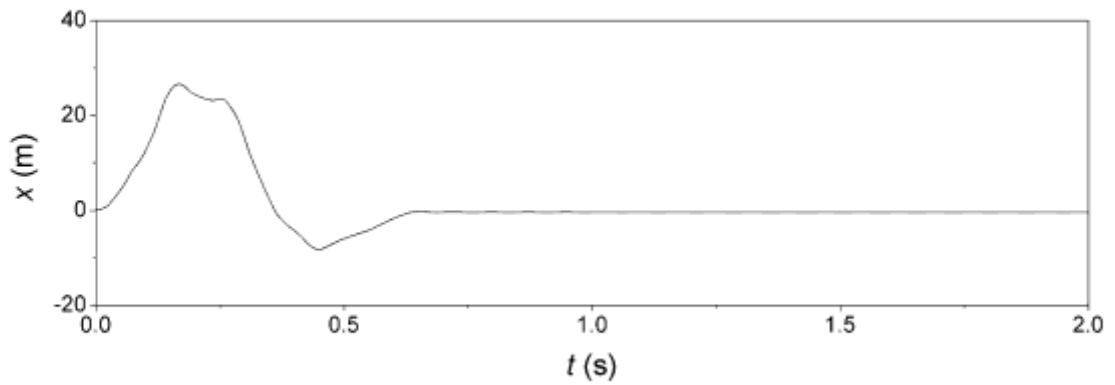
Fig 6.11 Determining damping characteristics for vertical displacement

6.2.3 Identifying Lyapunov Exponent

Calculation of the largest Lyapunov exponent is an indication of the nature of qualitative system response, especially as to whether it is chaotic.

An algorithm in Lagspace 3.0 software [51] is composed of formulas dedicated to solve Lyapunov exponents and have been used.

Experimental data of the time history is saved as a data (.dat) file and imported to Lagspace 3.0 software to calculate the largest Lyapunov exponent. The exponent pertaining to the time series shows when the values are negative, the system is periodic whereas the latter shows chaotic. The responses made by the experimental time series for period one rotations, oscillations were found to be negative. Stochastic and chaotic oscillation causes the experimental time history response to be positive.

The largest Lyapunov exponent is an indication of the nature of the qualitative system response, in particular to find out whether it is chaotic. The calculation of this Lyapunov exponent was done through an algorithm in Lagspace 3.0 software [51] based on the formula provided directly from the software. Experimental data of the time history was saved as a data (.dat) file and imported to Lagspace 3.0 software where the largest Lyapunov exponent can be calculated. The exponent pertaining to the time series shows when the values are negative, the system is periodic whereas the latter shows chaotic. The responses made by the experimental time series for period one rotations, oscillations were found to be negative. Stochastic and chaotic oscillation causes the experimental time history response to be positive.

6.3 Results and Discussion

The configurations are tested accordingly with different sets of input. The results are explained and shown respectively.

The rotations were investigated with different parameters of angles to investigate the optimum angular distance between the two pendulums. The investigated angles are 25°, 45°, and 90° which are chosen due to continuous ease of actuating

rotations, which can be seen at Fig 6. **12**. At a switching frequency of 3.884 Hz and supply voltage of 15 V, (a) and (b) corresponds to an angle of 25°, (c) and (d) represents 45°, and (e) and (f) represents 90°. The difference between these 3 time histories is the sustainability of rotations and its duration. Reproducibility of the time histories for the subtended angles 25° and 45° is more robust when compared to the subtended angle of 90°. 5 tries are required to obtain figures (e) and (f) whereas every try for figures (a) to (d) is successful. However, the angle 90° is also capable of generating rotations with impacts unlike the rest. Many other angles have been experienced with such as Fig 6.13 where the angle is at 0° and the pendulum are only capable to actuate continuous oscillations. Optimum angles are found within the range of 25° to 45°. Other angles larger than 60° have been found to not facilitate rotations, except for 90°.

The objective of this experiment is to obtain rotations from different types of forcing, three types of forcing was periodic forcing, stochastic forcing, and chaotic forcing.

Periodic forcing is when the movement of the solenoid is given a consistent frequency to actuate the activation of the solenoid. The solenoid then causes the conductor to have consistent periodic vertical oscillation.

Stochastic forcing is when the solenoid has a phenomena and a controlled activation, hence the solenoid causes the conductor to oscillate vertically but at a controlled manner that is not a consistent frequency.

Chaotic forcing is when the solenoid is activated without any controlled frequency or even if there are any consistent frequency causes the conductor to move vertically without any particular trend, different factors such as impacts or inconsistent

motions causes the system to tumble inconsistently and thus the best resultant when the

pendulum is capable of rotating in such scenario.
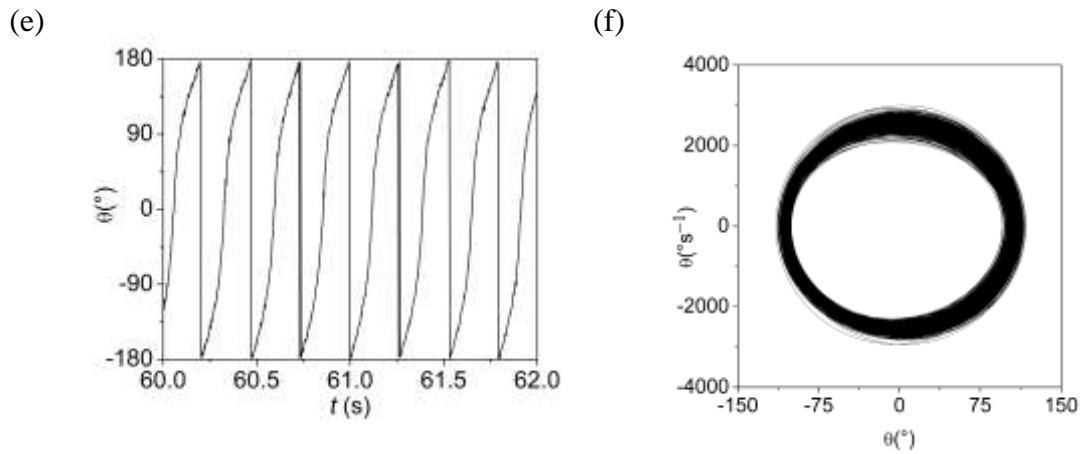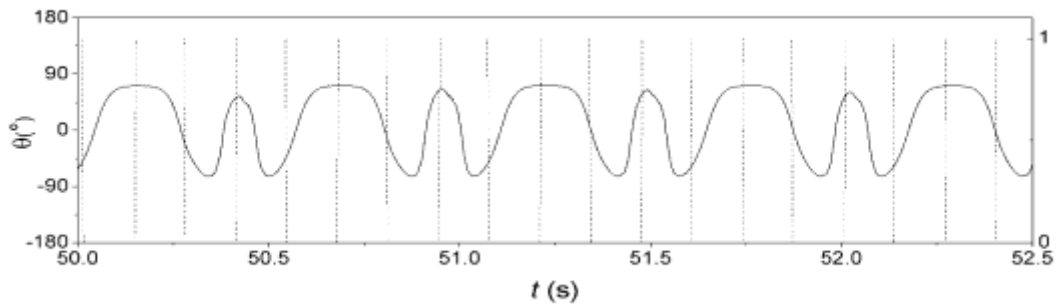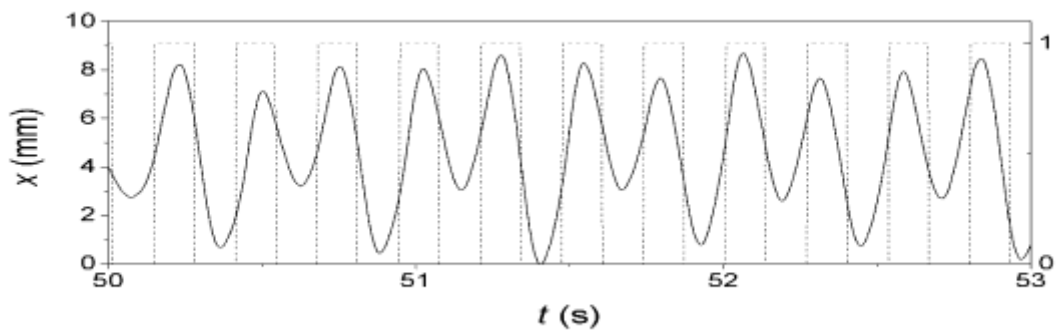
(a)

(b)

(c)

(d)

(e)

(f)
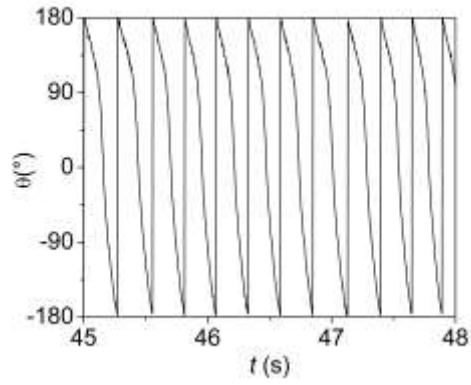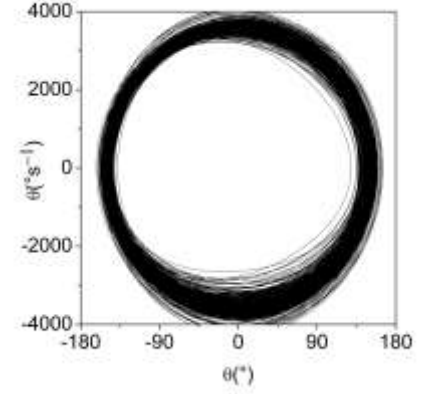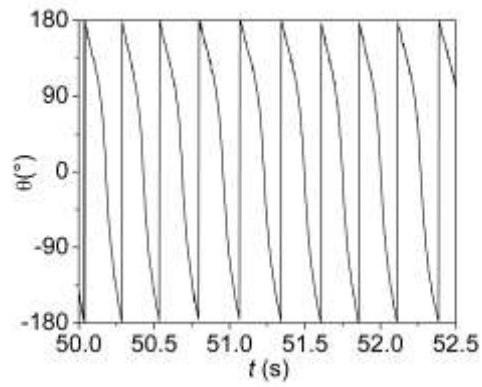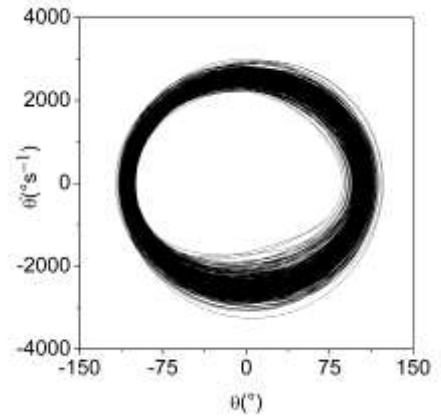
Fig 6. 12 The time history and phase planes for the same angles are paired, (a) and (b) corresponds to the rotation when the angle between the pendulums are 25°, (c) and (d) corresponds to when the angle between the pendulums are 45°, (e) and (f) corresponds to the angle between the pendulums at 90°
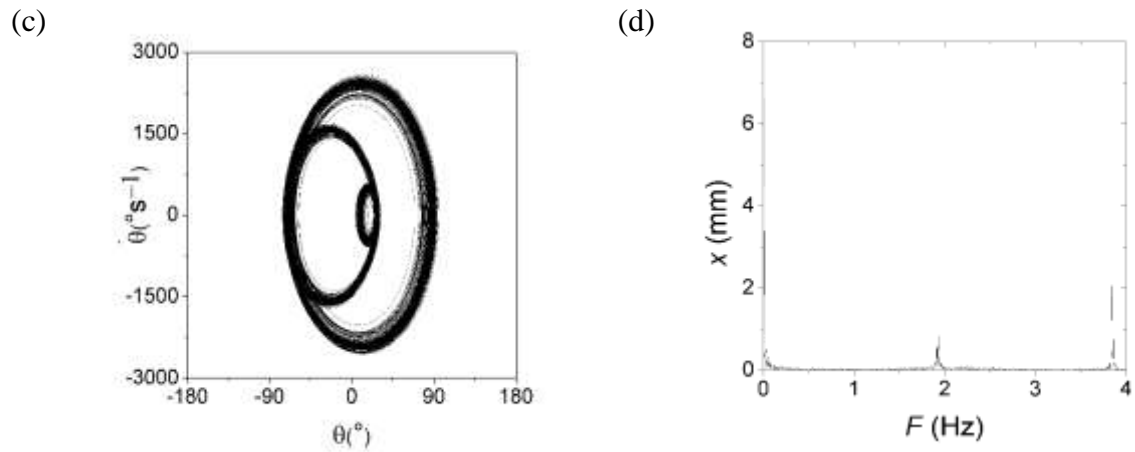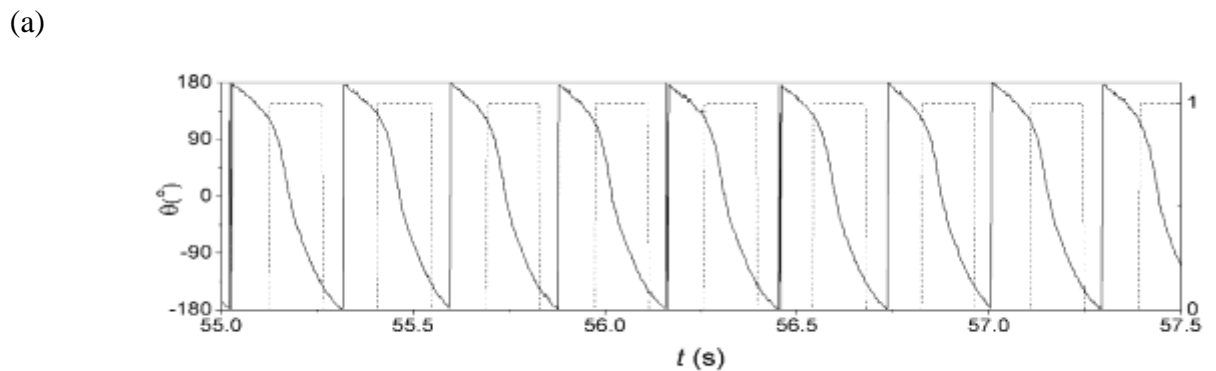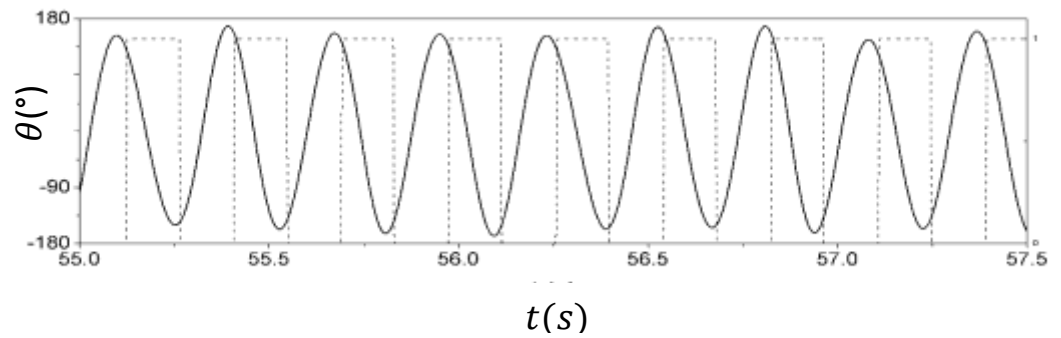
(a)

(b)

(c)

(d)

Fig 6.13 (a) Time history of angular displacement, **θ**, when the angle is kept at 0° and the frequency of 3.84 Hz. Dashed lines describe a random switching on and off of solenoid, and (b) represents the time history of vertical oscillations. The corresponding (c) phase plane and (d) amplitude spectrum of vertical displacement; The phase plane and amplitude spectrum was measured for of 500 forcing cycles.

6.3.1 Angles subtended at $2\varphi = 25°$

The results of the pendulum due to changing the angle for 25°

(a)

(b)

$t(s)$

(c)

$\theta(°)$

(d)

F (Hz)
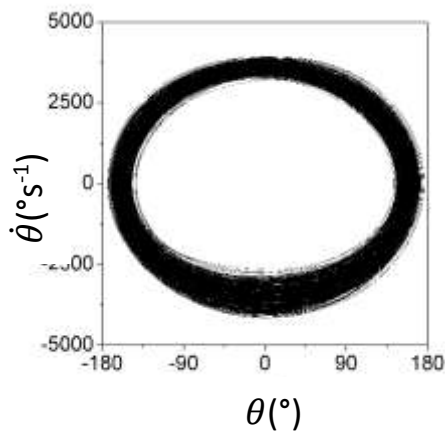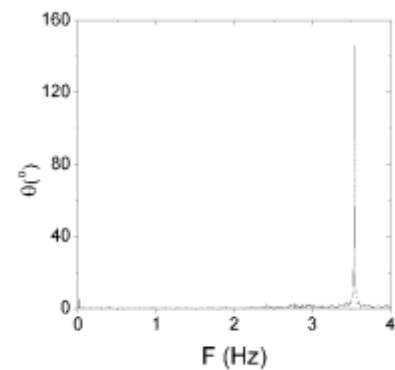
Fig 6.14 (a) Experimental time history of angular displacement, $\boldsymbol{\theta}$, when the angle in between is kept at 25° and the frequency of 3.6 Hz. (b) filtered experimental time history. (c) phase plane and (d) amplitude spectrum of angular displacement.

Fig 6.14 shows the experimental time history of the rotating pendulum when the angle is kept at 25° and the frequency of 3.6 Hz. Dashed lines describe a random switching on and off of solenoid. The phase plane and amplitude spectrum was measured for of 500 forcing cycles.

Table 6. 1 : Distribution table of Voltage supply against Frequency for the angle 25°

Angle = 25°	Voltage (V) →	14 V	18 V	22 V
Frequency (Hz) ↓	1.5 Hz -	OI		OI
	2 Hz -	OI	OI	OI
	2.5 Hz -	OI	OI / OII	OI
	3 Hz -	OII / RI	OII / TC	OII / TC
	3.5 Hz -	OII / RI / TC	OII / TC	OII / TC
	4 Hz -	RI	OII / TC	OII / TC
	4.5 Hz -	RI	OII / TC	OII / TC
	5 Hz -	RI	TC	OII / TC
	5.5 Hz -	RI	TC	OII / TC
	6 Hz -	RI	RI (6.2) / TC	TC
	6.5 Hz -	RI	TC	TC
	7 Hz -	RI		TC

Legend : OI = Period 1 Oscillation , OII = Period 2 Oscillation, RI = Period 1
Rotation, TC = Tumbling Chaos
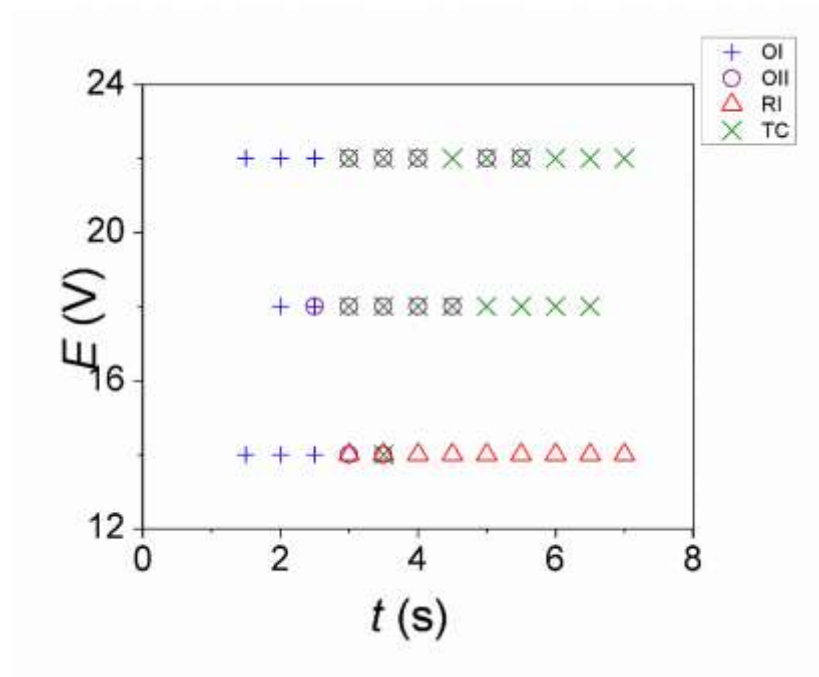
Fig 6. 15. Distribution Diagram for the pendulum for the angle 25°

Legend : OI = Period 1 Oscillation , OII = Period 2 Oscillation, RI = Period 1 Rotation, TC = Tumbling Chaos

The concentration on this graph shows similar result when compared to any other angles, and rotations were achievable hence the results shown for this angle is emphasized on the distribution diagram.
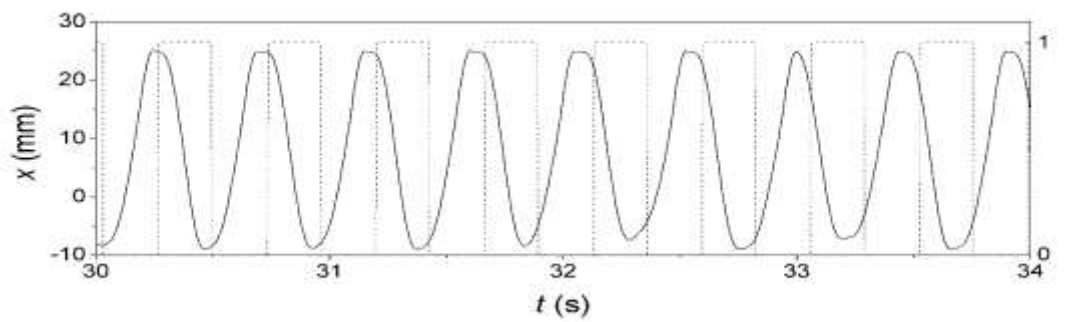
6.3.2 Angles subtended at $2\varphi = 45°$

Period-one oscillations can be found when the configuration is supplied with low frequencies. Fig 6. 16 (a) shows an excitation with a frequency of 2.2 Hz. Impact occurs at these frequencies due to the sensitivity of the solenoid. The phase plane was drawn to identify the periodic motion.

(a)
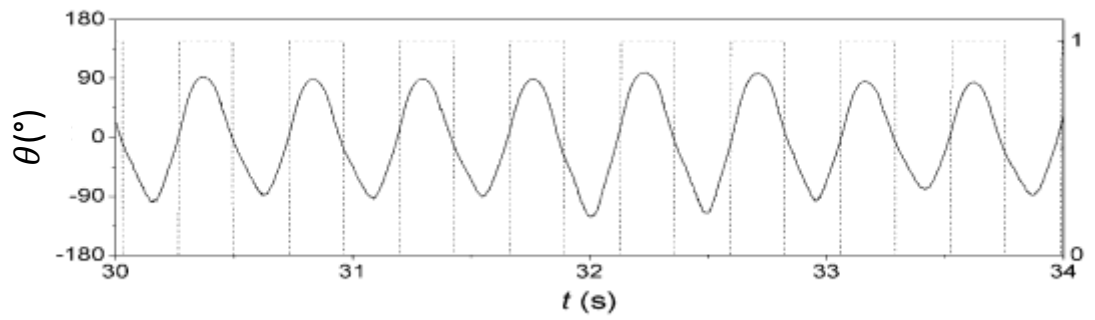
(b)
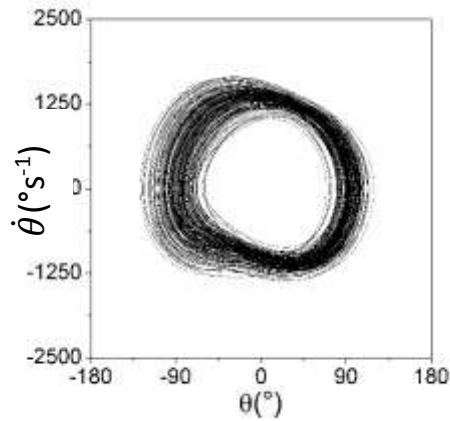
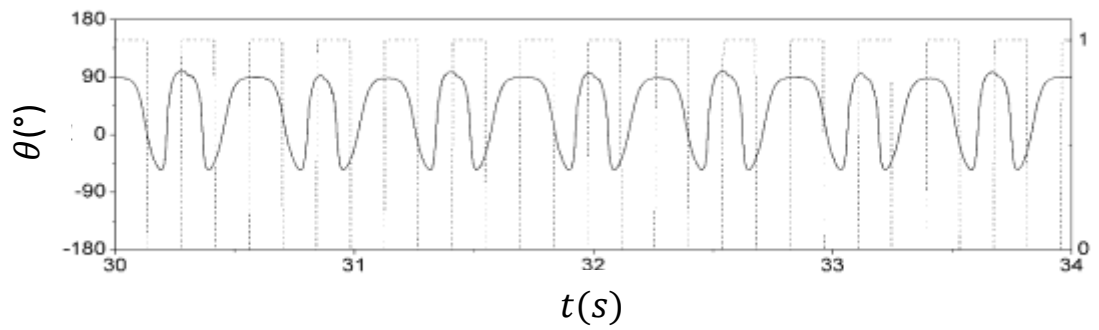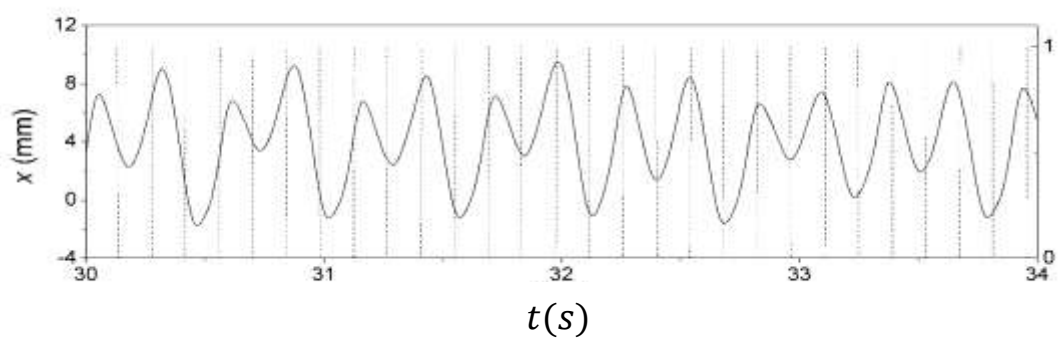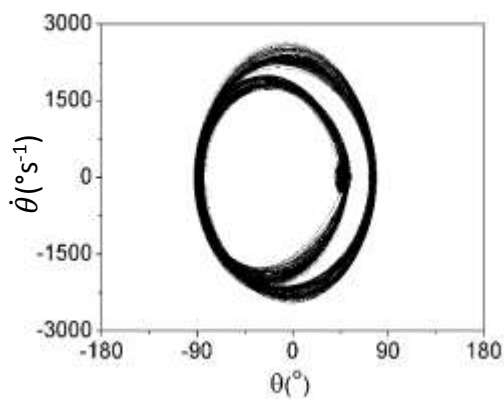(c)   (d)
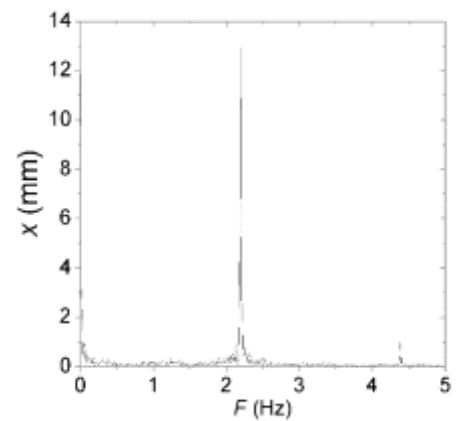
Fig 6. 16 (a) Experimental time history of the angular displacement of pendulum suggesting period 1 oscillations at 2.2 Hz, and voltage of 12 V; (b) Experimental time history of vertical oscillation; (c) Phase plane and (d) Amplitude spectrum of angular displacement.

Experimental time history of the angular displacement of pendulum suggesting period 1 oscillations when solenoid is switched on and off at 2.2 Hz, and the voltage supply is set at 12 V. The phase plane was measured for of 500 forcing cycles.

(a)

(b)
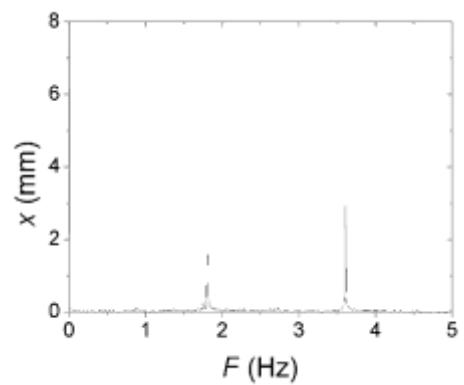

(c)   (d)

Fig 6. 17 (a) Experimental time history of the angular displacement of pendulum

suggesting period 2 oscillations 3.61 Hz, 14 V; (b) Time history of vertical

oscillation; (c) phase plane and (d) amplitude spectrum of angular displacement;

The result from Fig 6. 17 indicates a period – two oscillation with a frequency

of 3.61 Hz and a voltage supply of 14 V. The time history shows how one forcing cycle

requires double the amount of time to respond as compared to period-one oscillation.

The phase plane indicates a period two oscillation. The phase plane and amplitude

spectrum was measured for of 500 forcing cycles.
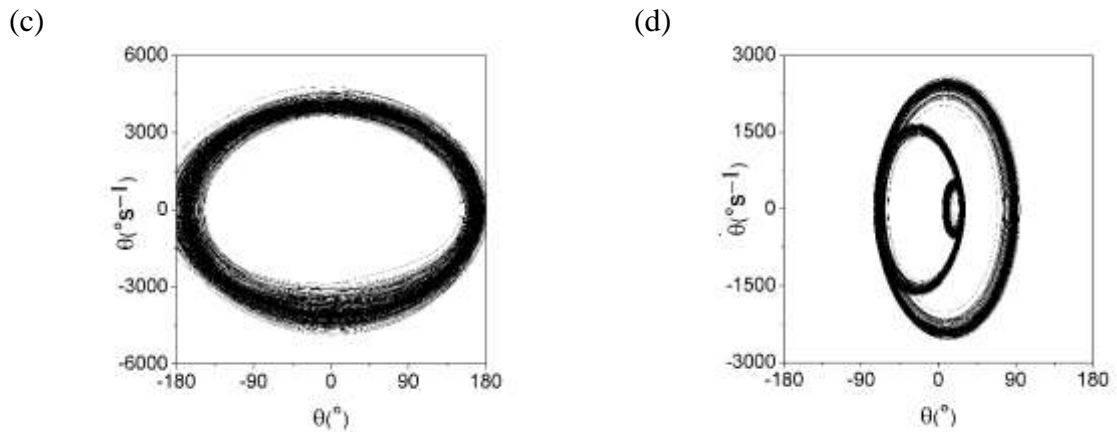
(a)

(b)

(c) (d)
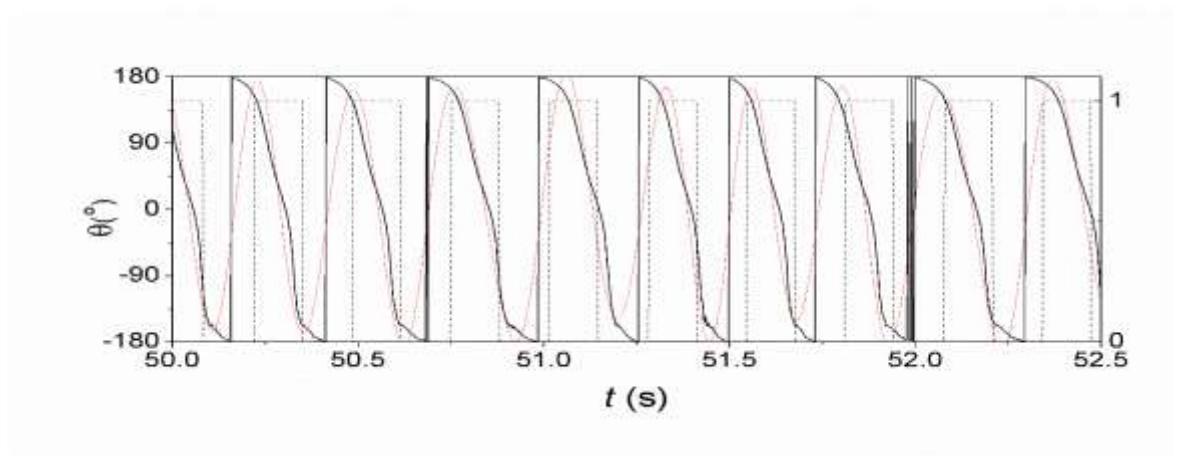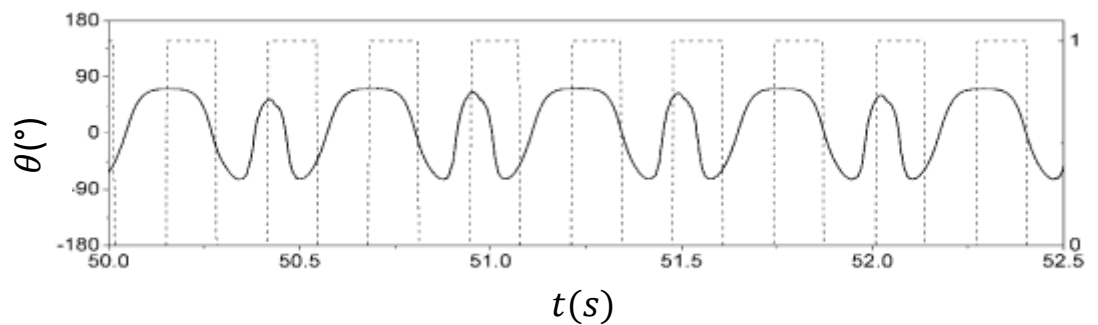
Fig 6. 18 Coexisting attractors. (a) Experimental time history depicting rotations when solenoid is switched on and off at a frequency of 3.84 Hz. Input voltage 16 V. (b) phase plane (c) Experimental time history depicting period two oscillations with same input (d) phase plane of (c).

Coexisting attractors exist in the configuration, this is observed in Fig 6. 18. Where (a) represents the experimental time history depicting rotations and (c) represents the experimental time history depicting period two oscillations. The voltage supplied to the solenoid was 16 V and a frequency of 3.84 Hz. An initial perturbation was required to achieve both rotations and oscillations. For the phase plane 50 transient cycle elapsed before 500 steady state cycles were plotted.   As oscillations and rotations can be found in the same frequency. Rotations are found to be more reproducible as compared to oscillations, the difference of the results are due to the perturbation supplied to the pendulum.
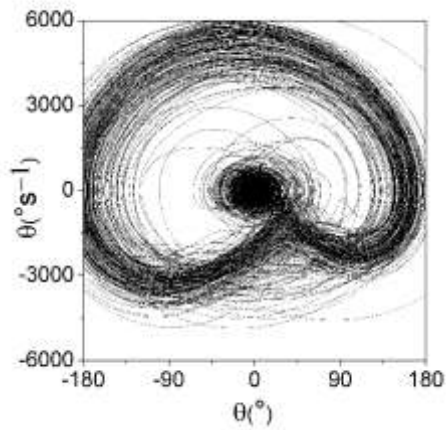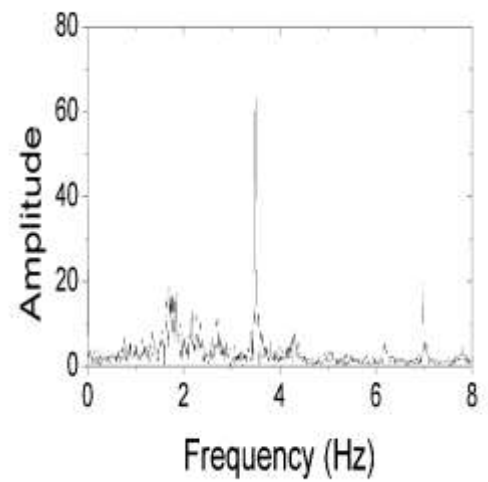
(a)
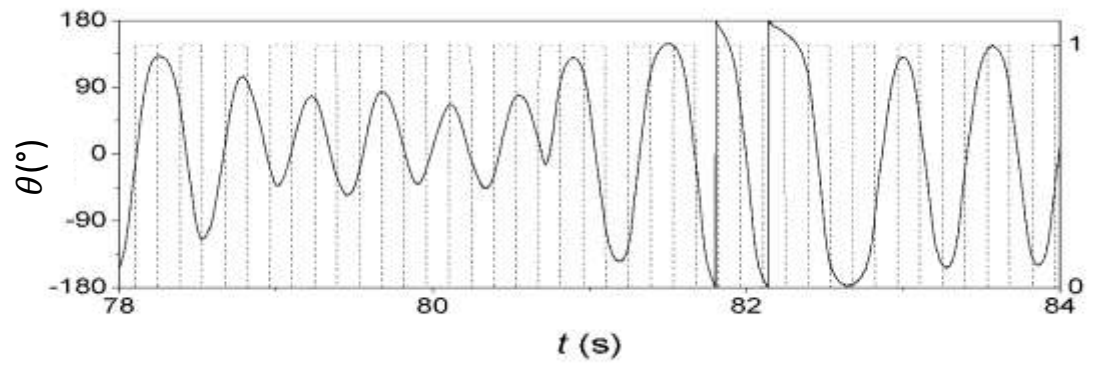
(b)
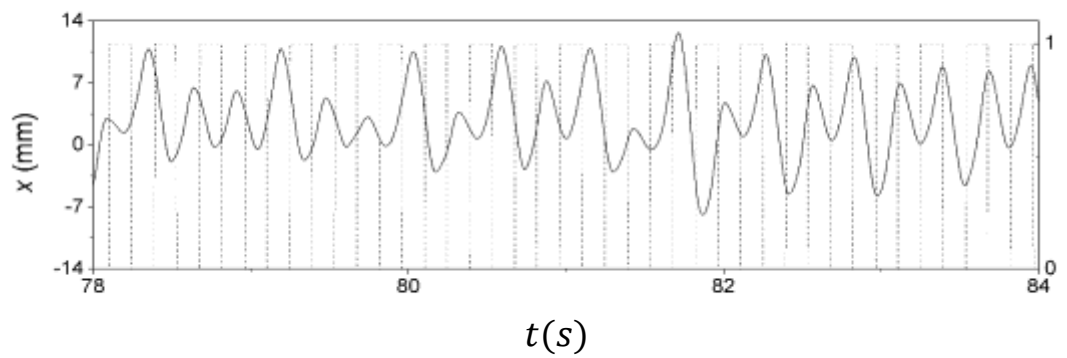
(c)

(d)

Fig 6.19 (a) Experimental time history of the angular displacement of pendulum

suggesting tumbling chaos with an input of 3.57 Hz, and 14 V; (b) Time history of

vertical oscillation; The corresponding (c) phase plane and (d) amplitude spectrum of

angular displacement;

Tumbling chaos is indicated which is presented in Fig 6.19 With a frequency of 3.57 Hz and voltage input of 14 V, at this point the data is observed to have oscillations as well as rotations. The occurrence takes place even when impacts were not induced. The phase plane and amplitude spectrum was measured for of 500 forcing cycles.
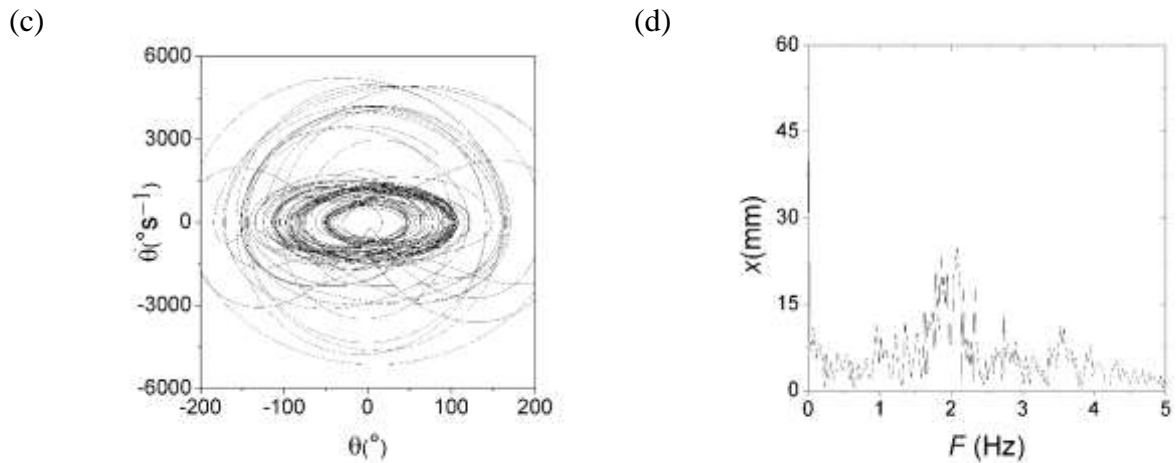
(a)

(b)

(c)

(d)
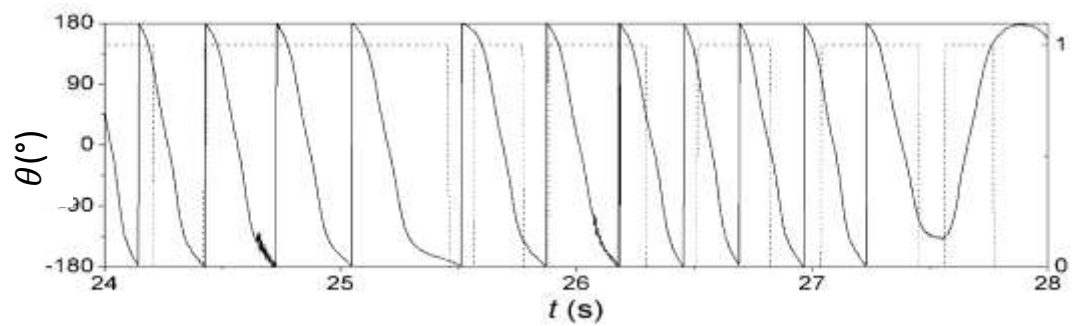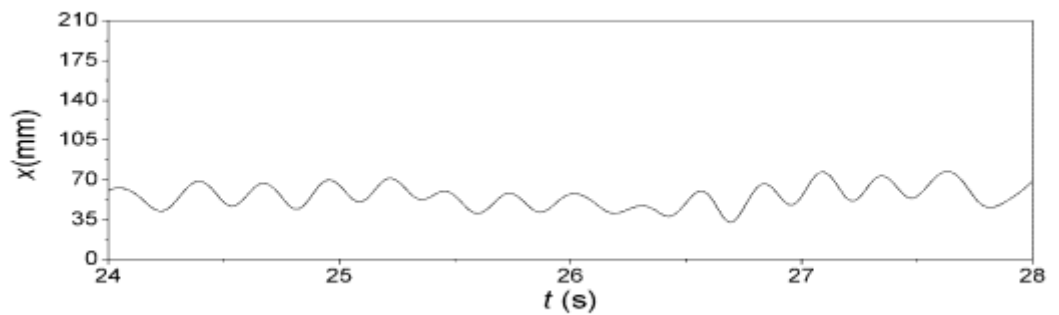
Fig 6.20 (a) Experimental time history of angular displacement, $\boldsymbol{\theta}$, when solenoid is switched on and off in a random manner. (b) represents the time history of vertical oscillations. The corresponding (c) phase plane and (d) amplitude spectrum of angular displacement;

Fig 6.20 shows the pendulum's behviour when the function generator is switched on and off in a random, and the dashed lines describe the signals sent to the function generator. . The stochastic random number is generated with the use of MATLAB as stated previously in the pulse generated reveals a chance of rotations as well as tumbling. The vertical displacement in Fig 6.20 (b) is observed and it can be found that within a scale on which it oscillates within 25 s to 27.5 s shows that the pendulum is capable in generating rotations, however when the displacement travels randomly at a larger oscillation, the pendulum switches to oscillations. The phase plane and amplitude spectrum was measured for of 500 forcing cycles.

(a)
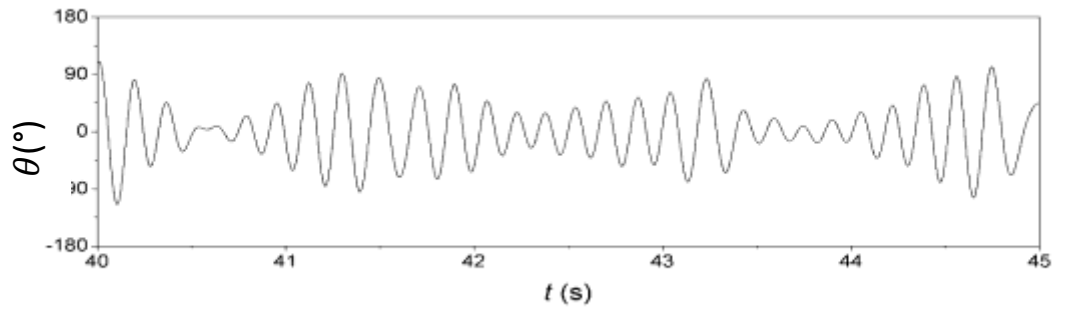
(b)
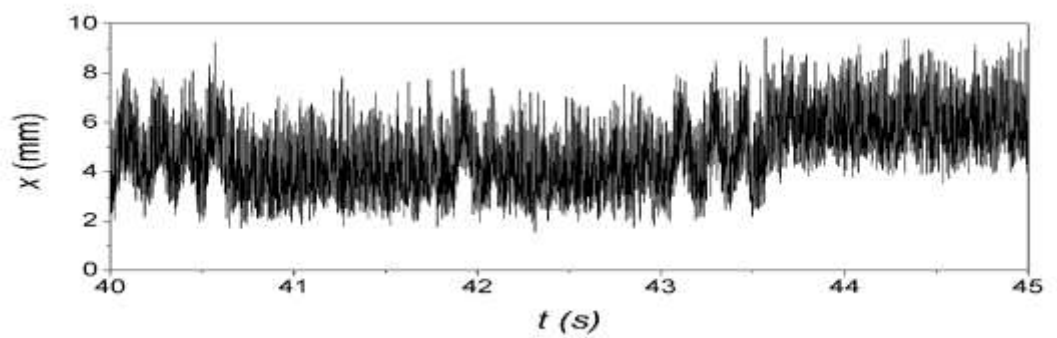
(c)
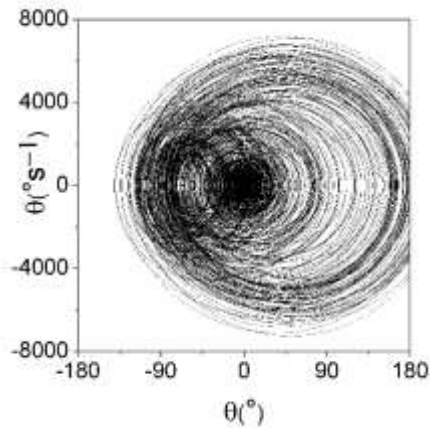
(d)
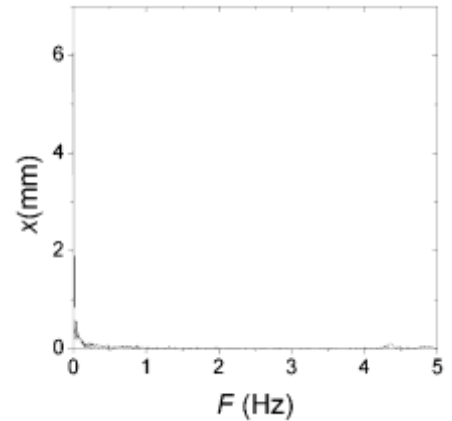
Fig 6.21   Chaotic waveform suggesting both oscillations and impacts. The voltage supplied to the solenoid was 14 V and the solenoid is switched on and off in a chaotic manner. (a) Time history of angular displacement, $\boldsymbol{\theta}$ (b) Time history of the vertical displacement (c) The phase plane (d) Amplitude spectrum of angular displacement.

A chaotic waveform was tested using the duffing's equation which can be observed in Fig 6.21, the voltage supplied to the solenoid is 14 V and an initial perturbation was

required to achieve rotations, the dashed lines describe the signals sent to the function generator.   .generating data in which the value is determined by the change of the previous value, the graphical data was generated with oscillations occurring for a set period of time with no rotations occurring. The phase plane (d) is made after 50 transient cycles have elapsed before 500 steady state cycles were plotted.

(a)

(b)

(c)　　　　　　　　　　　　　　　　　　　　　(d)
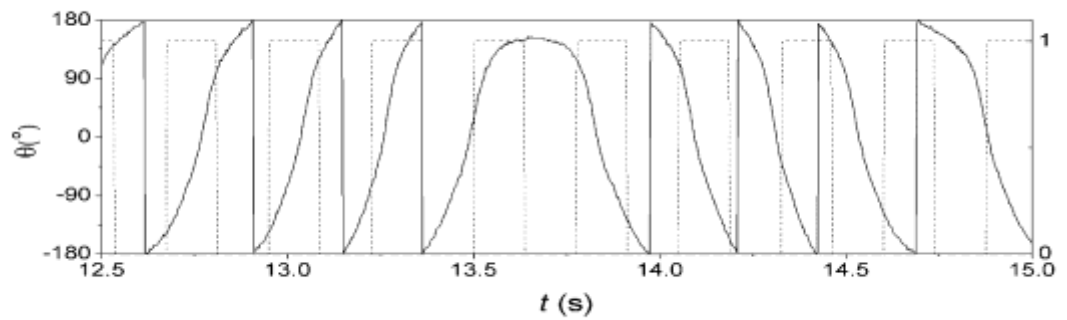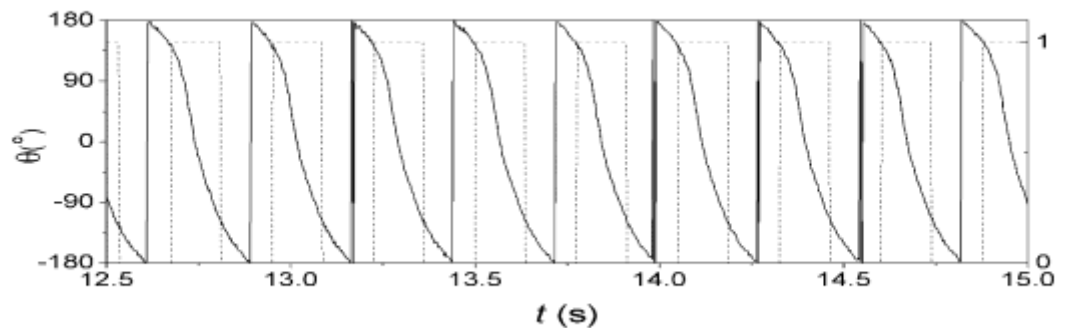
Fig 6. 22 Comparison of time responses for different sets of voltage (a) Experimental time history depicting rotations with an input of 3.71 Hz and 20 V. (b) Experimental time history depicting rotations with an input of 3.71 Hz and 14 V. (c) Phase plane for (a). (d) Phase plane for (b).

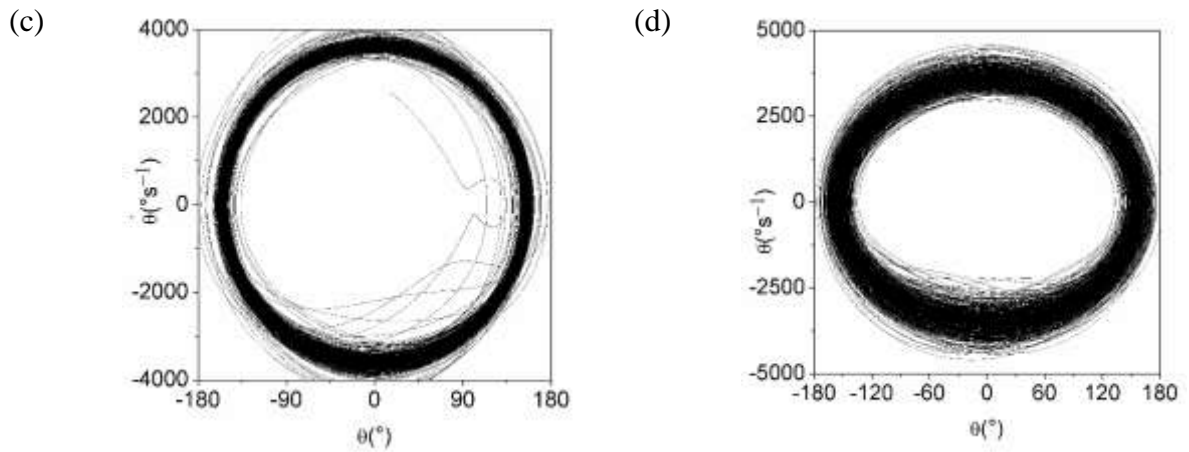In Fig 6.22 The voltage was altered to identify how the configuration would work when impacts were present, with an initial perturbation that was given to achieve rotations in Fig 6. 22. Two sets of graph was used to compare the observation. Fig 6. 22 (a) shows tumbling chaos when the voltage supplied was 20 V which is sufficient to cause impacts. Fig 6. 22 (b) shows rotation occurring without impacts at a supplied voltage of 14 V. For phase plane (c) 50 transient cycle elapsed before 500 steady state cycles were plotted. For this graph, impacts were present.

Table 6. 2 : Distribution table of Voltage supply against Frequency for the angle 45°

Angle = 45°	Voltage (V) →	14 V	18 V	22 V
Frequency (Hz) ↓	1.5 Hz -			OI
	2 Hz -	OI	OI	OI
	2.5 Hz -	OI	OI / OII	OI
	3 Hz -	OII	OII / TC	OII / TC
	3.5 Hz -	OII / RI / TC	OII / TC	OII / TC
	4 Hz -	OII / RI	OII / TC	OII / TC
	4.5 Hz -	OII / RI	OII / TC	OII / TC
	5 Hz -	RI	TC	OII / TC
	5.5 Hz -	RI	TC	OII / TC
	6 Hz -	RI	TC	TC
	6.5 Hz -	RI	TC	TC
	7 Hz -			TC

Legend : OI = Period 1 Oscillation , OII = Period 2 Oscillation, RI = Period 1
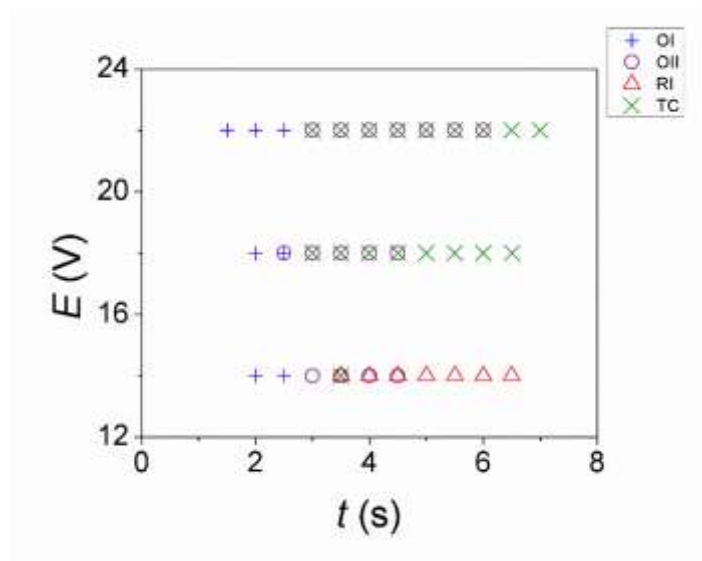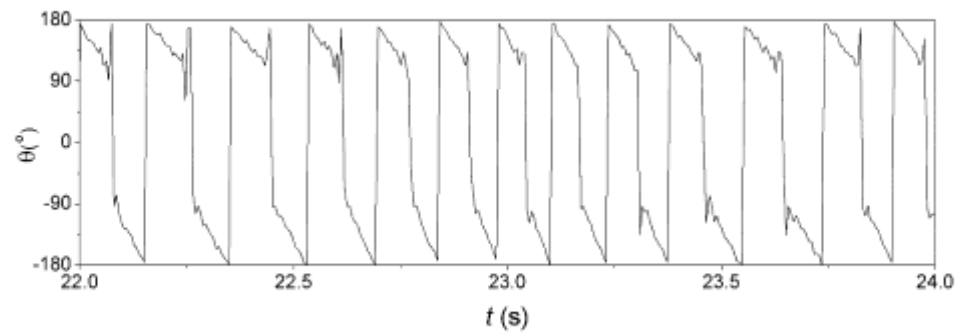
Rotation, TC = Tumbling Chaos

Fig 6. 23 Distribution Diagram for the pendulum for the angle 45°

Legend : OI = Period 1 Oscillation , OII = Period 2 Oscillation, RI = Period 1 Rotation, TC = Tumbling Chaos

6.3.3 Angles subtended at $2\varphi = 90°$

(a)

(b)

(c)

(d)
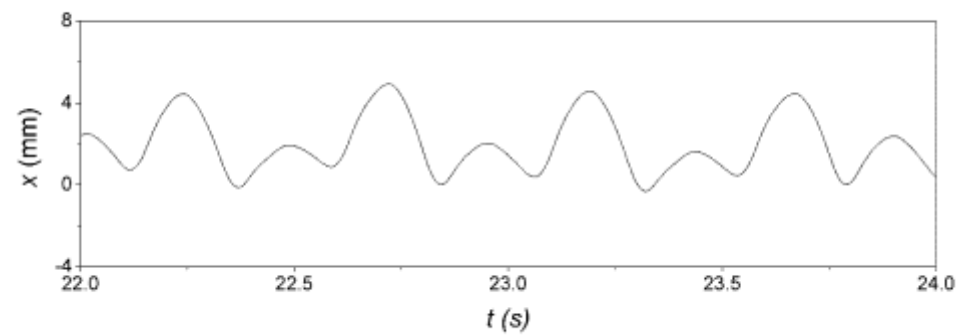
Fig 6. 24 (a) Time history of the angular displacement of pendulum suggesting period 1 rotations with an input of 6.5 Hz , angle between two pendulums is 90°, and voltage supply at 14 V; (b) Time history of vertical oscillation; The corresponding (c) phase plane and (d) amplitude spectrum of angular displacement;

In Fig 6.24 the angle between the two pendulums is fixed at 90°, with a voltage supply of 14 V and frequency at which the solenoid is switched on and off is at 6.5 Hz. The rotations of the pendulum is found to exist in range above 6 Hz, when the observed vertical displacement travels at a much more smaller amplitude compared to the average vertical displacement. The phase plane and amplitude spectrum was measured for of 500 forcing cycles.

(a)

(b)

(c)

(d)
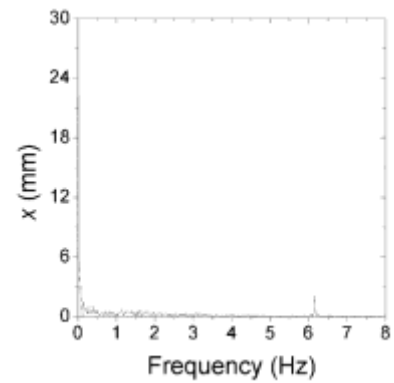
(e)
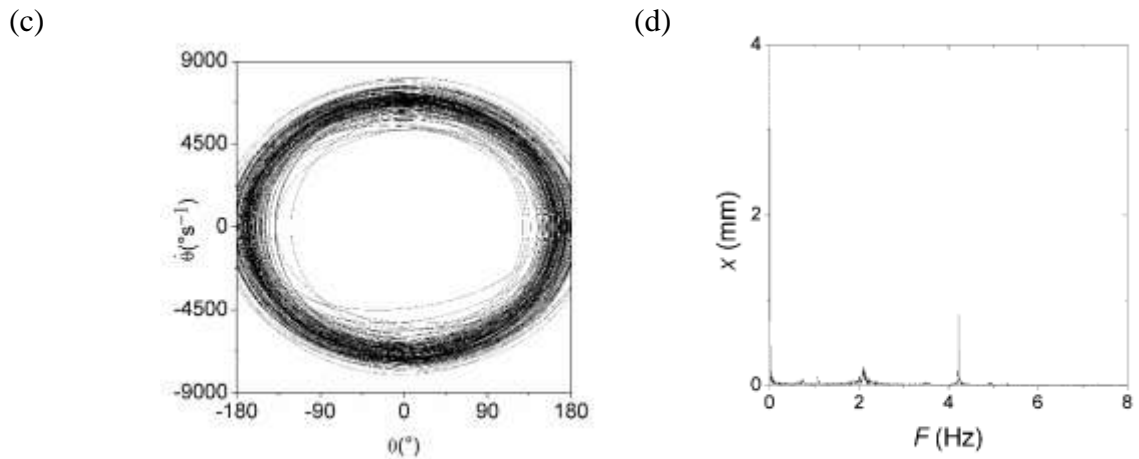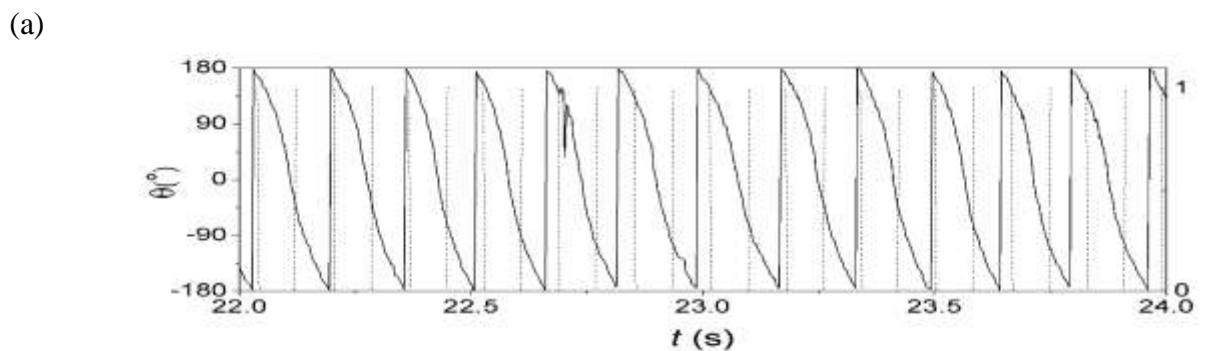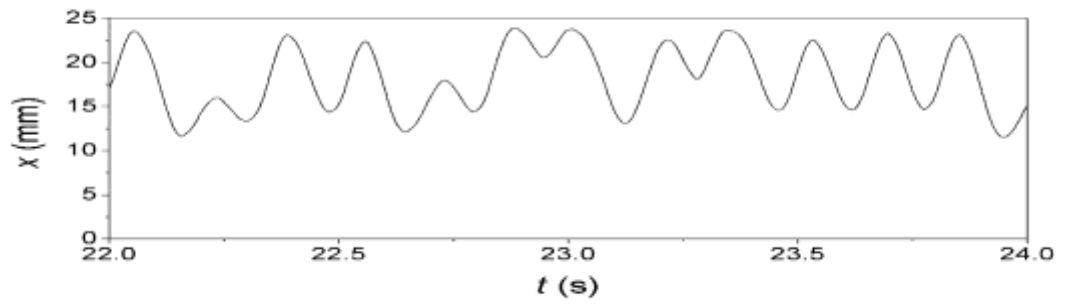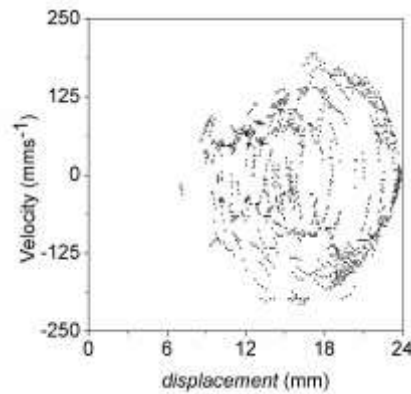

Fig 6. 25 (a) Time history of the angular displacement of pendulum suggesting period 1 rotations with an input of 6.15 Hz and voltage of 22 V which causes impacts; (b) Time history of vertical oscillation; The corresponding (c) phase plane and (d) amplitude spectrum of angular displacement; (e) Poincare map of the vertical displacement taken for every 0.16s.
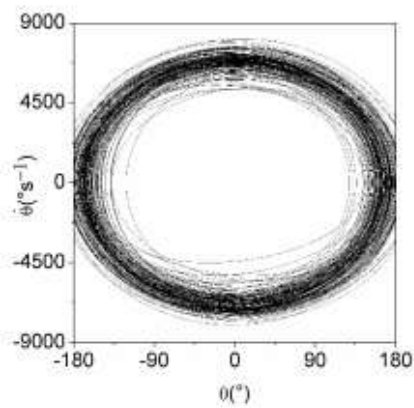
In Fig 6.25 the angle between the two pendulums is fixed at 90°, with a voltage supply of 22 V which causes impacts, and frequency at which the solenoid is switched

on and off is at 6.15 Hz. The results shown previously are all similar approaches of the system but at a different angle, the graphs are all displayed in the same format where (a) is the time history of the system at the indicated frequency, (b) reveals the time history after it is filtered using bandpass within 2 Hz to 6.5 Hz, (c) reveals the angular velocity of the system after it is differentiated with the use of Originlab function. (d) is the phase plane of the behavior and (e) is the FFT plot for the configuration. For graphs (d) and (e) only 500 forcing cycles were used to plot, with the first 50 cycles removed in order to remove the initial bifurcations.

With the angle positioned at 90°, the pendulum is found to facilitate rotations when the vertical oscillation moves with a frequency of 6.15 Hz, and it is undergoing inconsistent vertical oscillations. However, the highlighted findings for this result is that despite the system undergoing inconsistent movement, it is also undergoing impacts. Impacts originally is an unwanted effect to any systems, however the pendulum is capable of rotating in such case, and is capable of exploiting the impacts. Thus making energy harvesting possible even at an irregular and impact motions.

Table 6. 3 : Distribution table of Voltage supply against Frequency for the angle 90°

Angle = 90°	Voltage (V) →	14 V	18 V	22 V
Frequency (Hz) ↓	1.5 Hz -			OI
	2 Hz -	OI	OI	OI
	2.5 Hz -	OI / RI	OI / OII	OI
	3 Hz -	OII / RI	OII / TC	OII / TC
	3.5 Hz -	OII / TC / RI	OII / TC	OII / TC
	4 Hz -	OII / RI	OII / TC	OII / TC
	4.5 Hz -	OII / RI	OII / TC	OII / TC
	5 Hz -	RI	TC	OII / TC
	5.5 Hz -	RI	TC	OII / TC
	6 Hz -	RI	TC	RI / TC
	6.5 Hz -	RI	TC	TC
	7 Hz -			TC

Legend : OI = Period 1 Oscillation , OII = Period 2 Oscillation, RI = Period 1
Rotation, TC = Tumbling Chaos
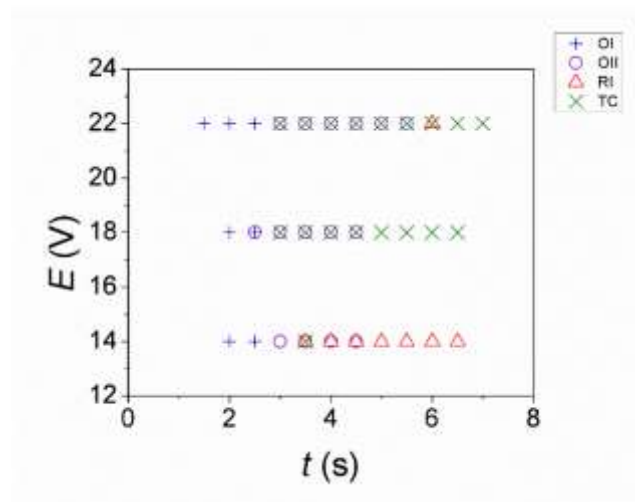
Fig 4. 26 Distribution Diagram for the pendulum for the angle 90°

Legend : OI = Period 1 Oscillation , OII = Period 2 Oscillation, RI = Period 1

Rotation, TC = Tumbling Chaos

6.4 Angles and bifurcation analysis

In this sub chapter, an identification of what angles can be used and their topologies.

A set of time series is taken in order to deduce the topology of the configuration. It was analyzed in this manner as by using Arduino UNO, the results are found to have a buffer within a small range and has affected the accuracy of the results. This factor thus was taken to an account to identify the changes of the pendulum within a small area of frequency where it transcends to rotations.

Bifurcation table was deduced however, as indicated from the above statement. The analysis of the bifurcation table's accuracy was far from the ideal bifurcation table and can be found in Fig A. 22

Multiple angles were used in order to find the closest range of changes.

(a)
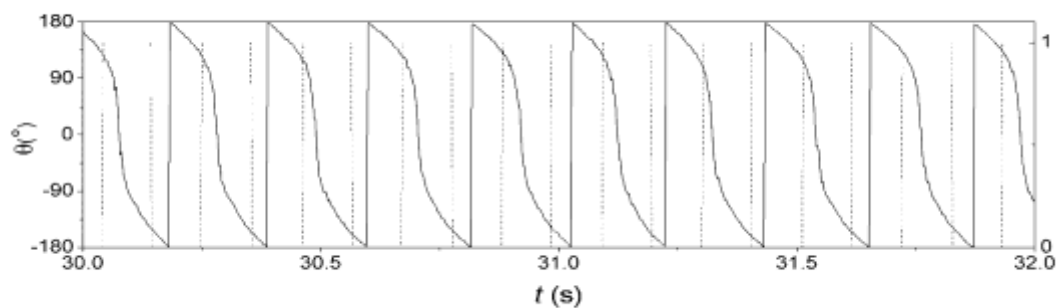
4 Hz $2\varphi = 10°$ angle

(b)
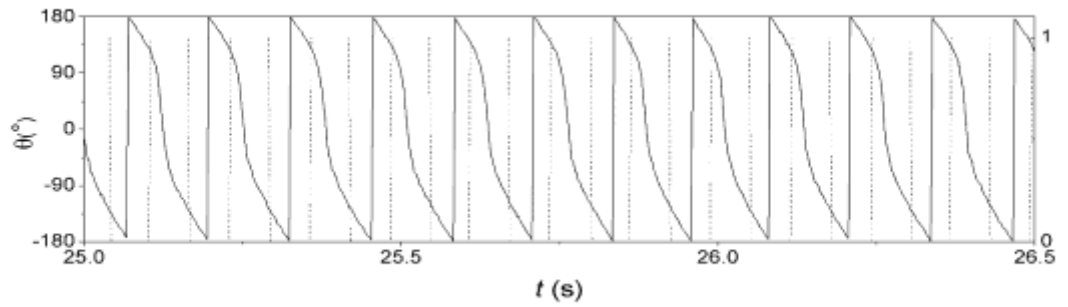
6.75 Hz $2\varphi = 10°$ angle

Fig 6. 27 10° angle was tested to determine whether it is capable of rotating at smaller angles.

The angle 10° was approached in order to determine the range of angular differences and how much can it is capable of rotating up to, these two experimental time histories determine the average rotational angles and was used to identify the rotating capabilities.

(a)
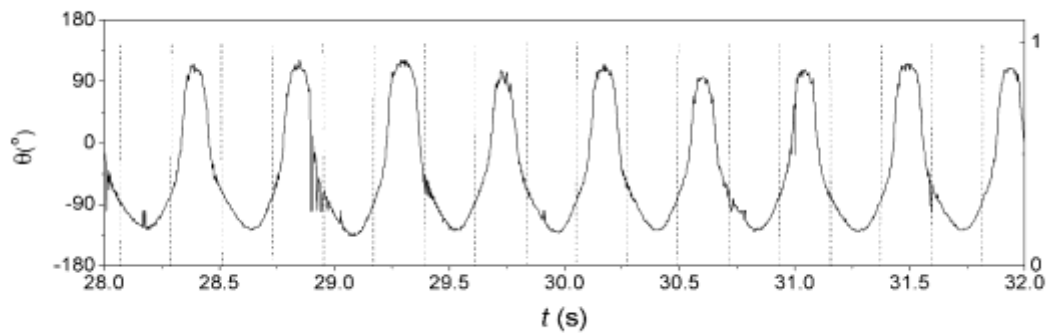
2.25 Hz $2\varphi = 25°$ angle
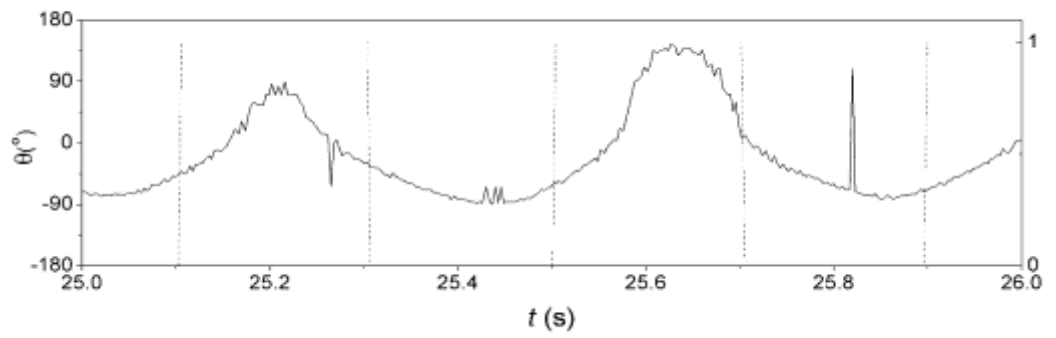
2.5 Hz $2\varphi = 25°$ angle

(c)
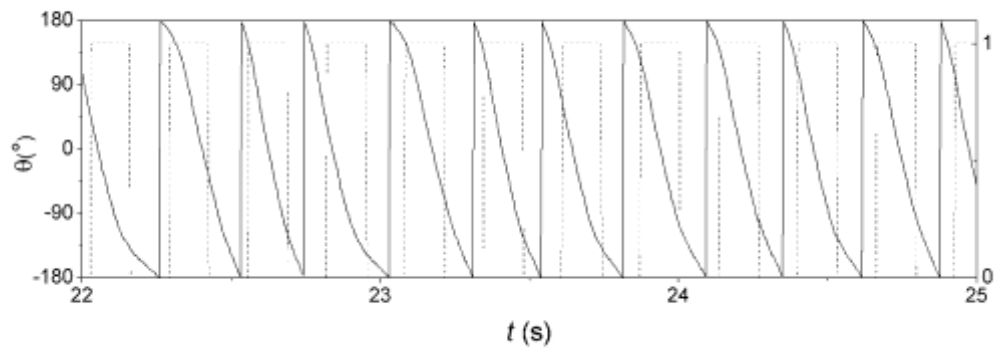
3.8 Hz $2\varphi = 25°$ angle

(d)
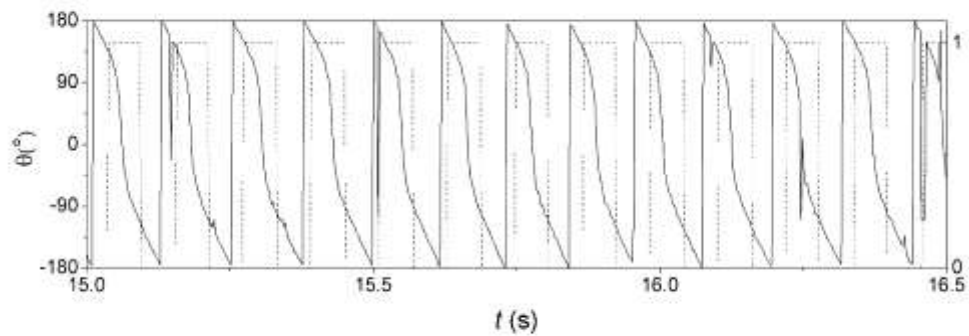
7.25 Hz $2\varphi = 25°$ angle

Fig 6. 28 25° was used to determine the topology and understanding of angles range between 0° to 30°.

The angle 25° between the two pendulums is used to determine the bifurcation analysis of the pendulum. When using small angles, it is not capable of generating rotations at frequencies below 3.5 Hz and it also found that the range can reach up to 7.25 Hz as can be seen from Fig 6. 28 (d). It is capable of generating continuous rotations at frequencies higher than 7.25 Hz. However, when applying that frequency the solenoid requires a slightly larger voltage, and when that amount of voltage is applied. The conductor gets attracted more closer to the solenoid and cause the conductor to hit the casing of the solenoid. The impacts then causes losses of momentum in the pendulum, causing it to lose rotations.

When the angle is kept below 30°, at frequencies around 2.5 Hz, it is currently undergoing oscillations. This allows an idea that when the angle is kept below 30°, the transition of attractors from oscillation to rotations are not around within this frequency.

(a)
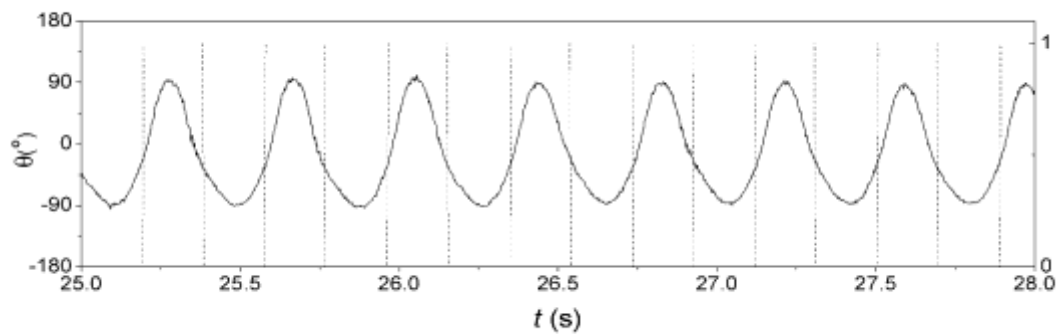
2.2 Hz $2\varphi = 60°$ angle

(b)
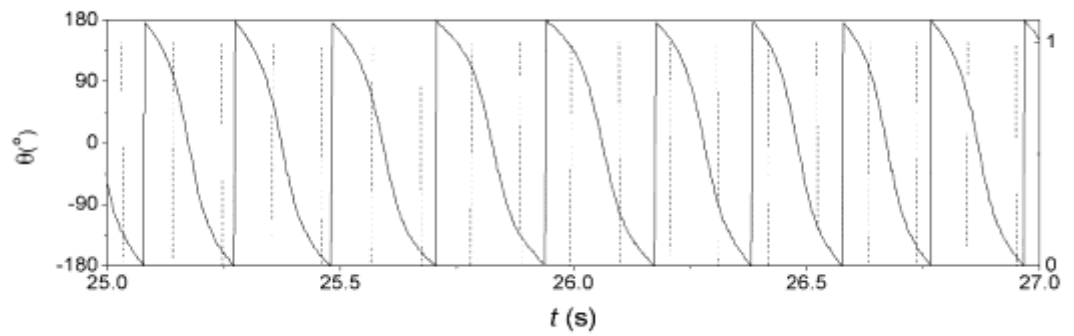
4.3 Hz $2\varphi = 60°$ angle

(c)
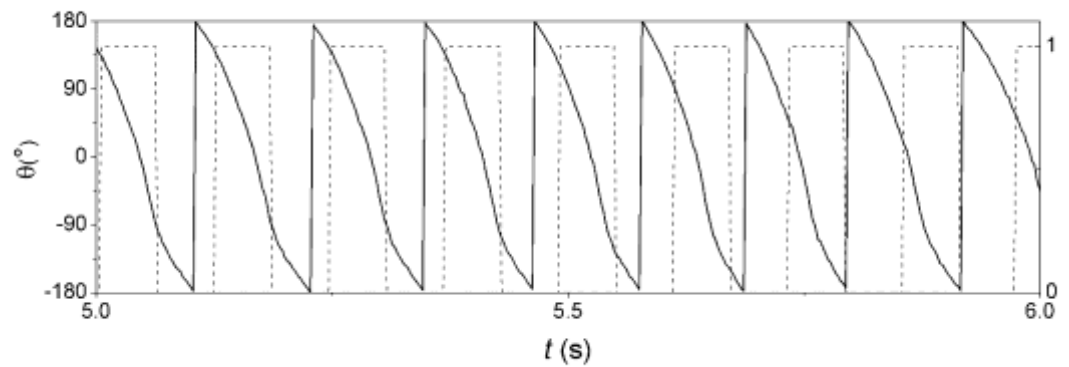
7 Hz $2\varphi = 60°$ angle

A study when the angle is subtended at 60° is identified. It is found to facilitate rotations at frequencies similar to 45° as well as 90°. However, the parameter did not find any chance of rotating when the conductor is undergoing impacts.

(a)
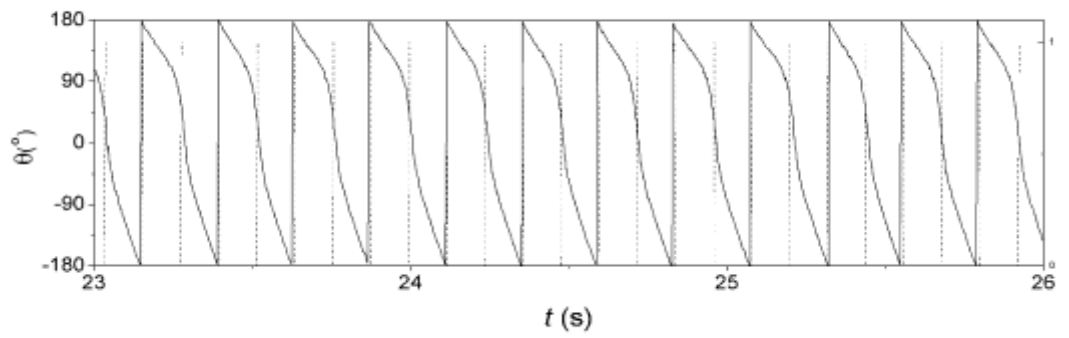
3.5 Hz $2\varphi = 80°$ angle

(b)
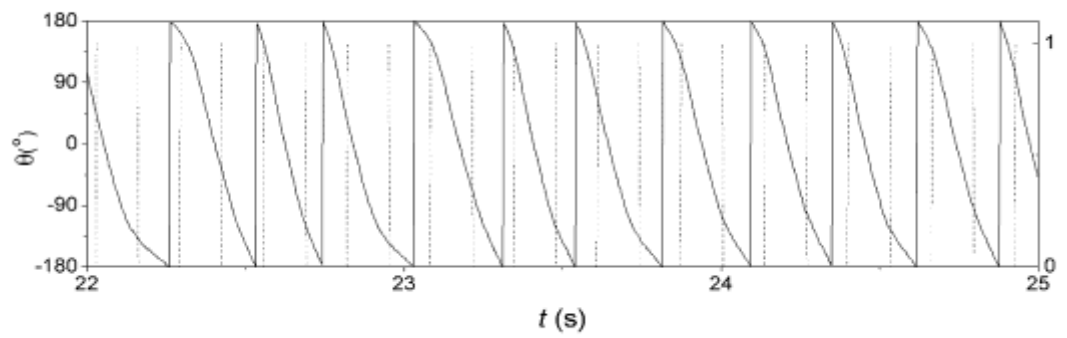
3.8 Hz $2\varphi = 80°$ angle

(c)
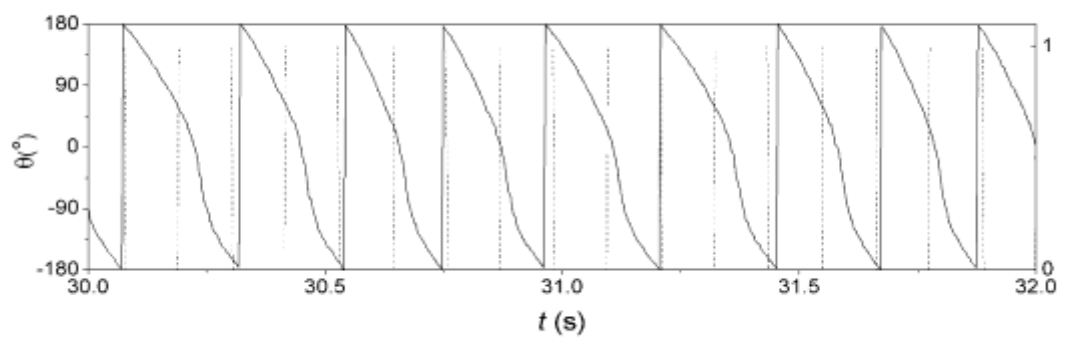
4.5 Hz $2\varphi = 80°$ angle

(d)
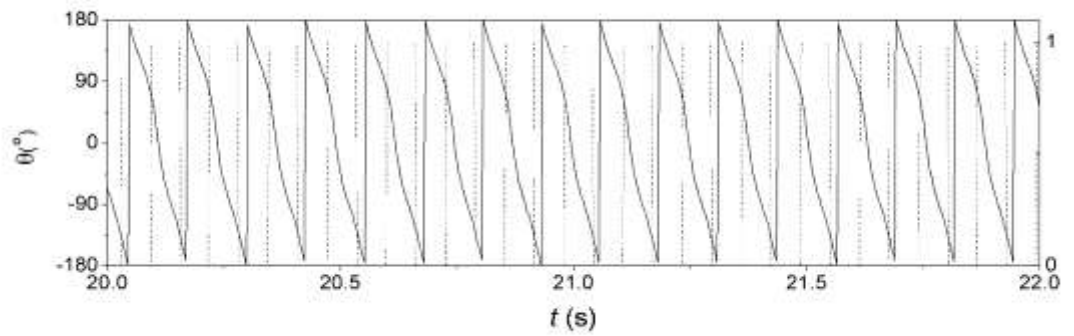
6.8 Hz $2\varphi = 80°$ angle

A study when the angle is subtended at 80° is identified. It is found to facilitate rotations at frequencies similar to 45° as well as 90°. This angle have been found to be able to facilitate rotations with impacts. This might be possible since it shares a close range with 90°.

(a)

2.4 Hz $2\varphi = 110°$ angle

(b)

126
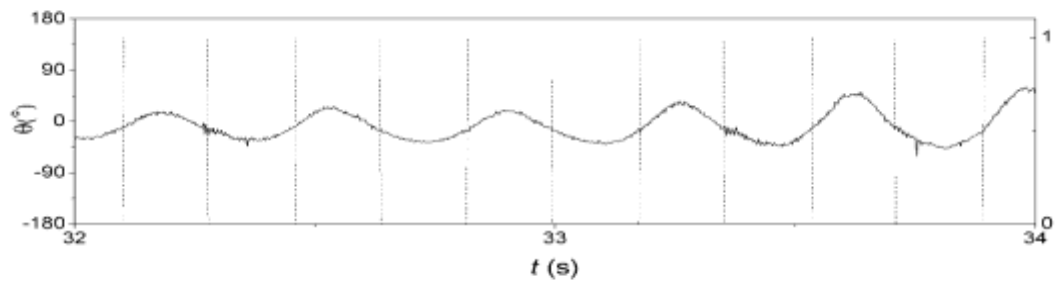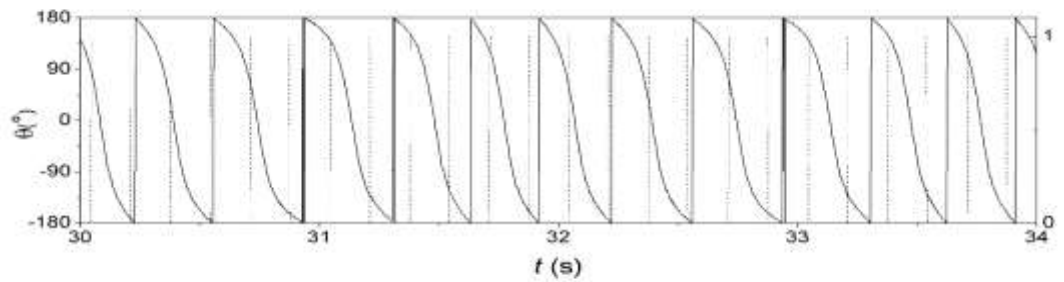
2.5 Hz $2\varphi = 110°$ angle

(c)
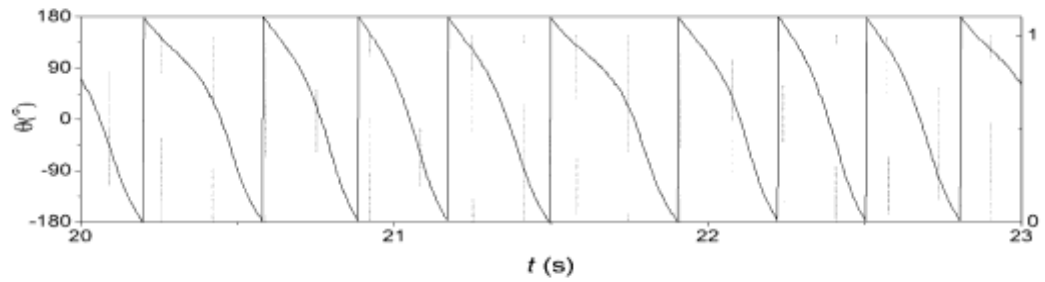
3 Hz $2\varphi = 110°$ angle

(d)
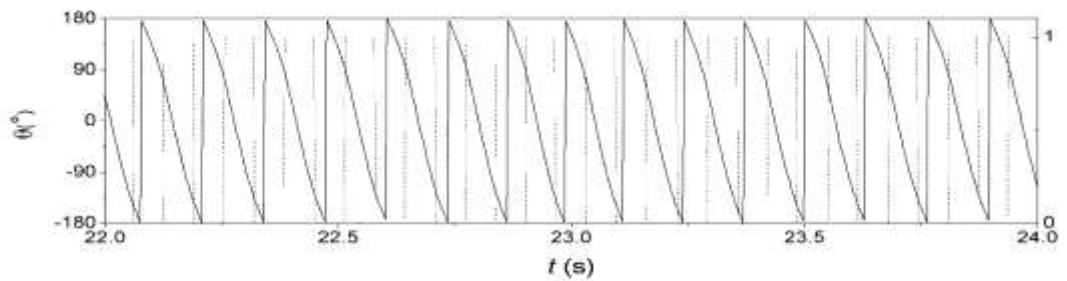
6.8 Hz $2\varphi = 110°$ angle

A study when the angle is subtended at 110° is identified. It is found to facilitate rotations at frequencies similar to 45° as well as 90°.It is also found that when the frequency is raised to 2.5 Hz from 2.4 Hz, the topology of the pendulum changed from oscillation to rotation. When the angle is subtended at 110° between the two pendulums, it is found that it is capable of facilitating rotations at an earlier frequency compared to when the angle is subtended at 25°.

(a)
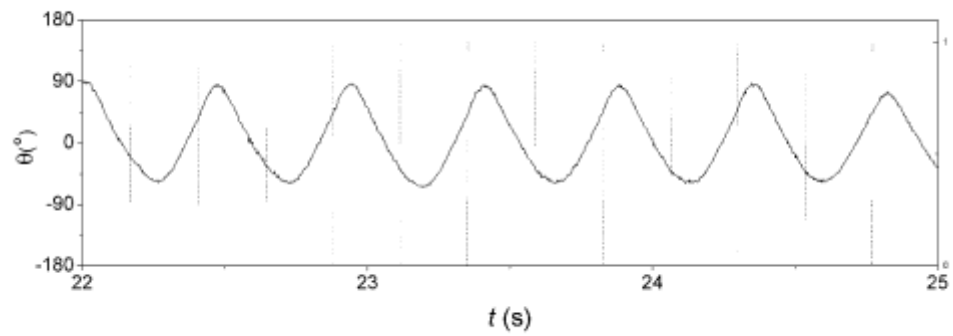
2.5 Hz $2\varphi = 90°$ angle

(b)
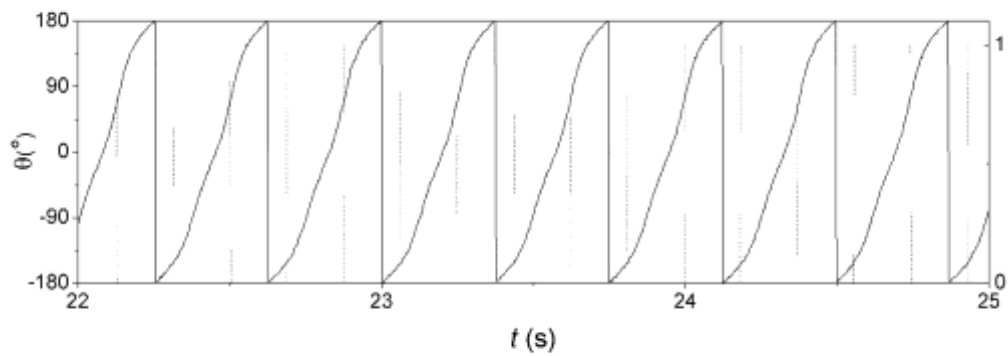
2.65 Hz $2\varphi = 90°$ angle

Fig 6. 29 The angle 90° was used to determine the topology differences to determine the transition from oscillation to rotation.

The angle 25°, 45°, 90° and 110° was used to determine the topology differences. It is found that when the angle is below 45° the range of rotations occur from 3.5 Hz to 7.25 Hz, and when the angle is kept above 45° the range of rotations occur from 2.55 Hz to 6.8 Hz. This may be due to a resultant force of subtended angles between the two pendulums that causes the pendulum to rotate at a different potential well.

(a)
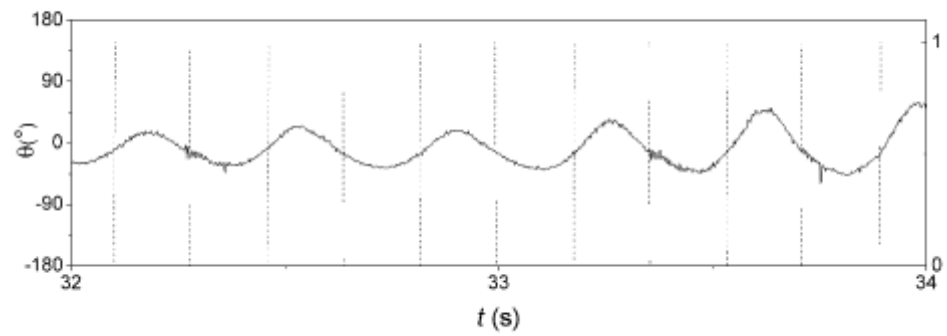
2.4 Hz $2\varphi = 110°$ angle

(b)
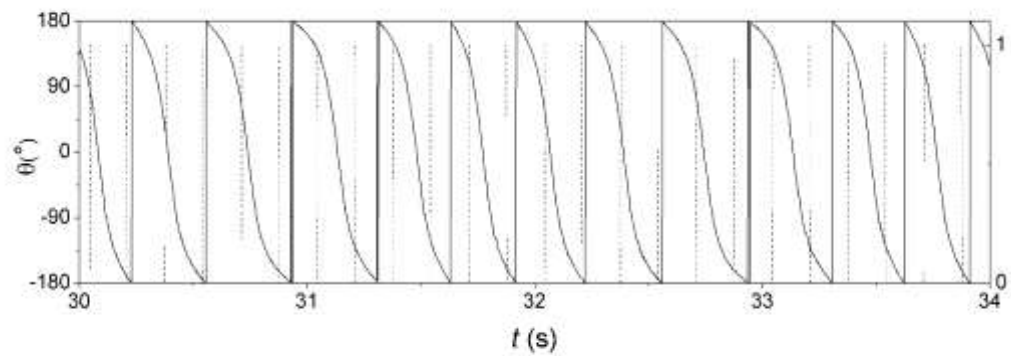
2.55 Hz $2\varphi = 110°$ angle

Fig 6. 30 The angle 110° was used to determine the topology differences to determine the transition from oscillation to rotation.

From the two angles 90° and 110° from the figures above it can be seen that the frequency differences between them shows a difference of approximately 0.15 Hz. This indicates that the transition from oscillation to rotation is within the two points.

The selected angles above were used due to the initial selection and the first angles that have been determined to allow continuous rotations to occur initially.

6.5 Rotations of Pendulum with an attached generator.

In order to convert kinetic energy into electrical, a generator is required. The pendulum generating rotations will be used in order to provide such kinetic energy to a generator. In this case, the rotations will be transmitted to the generator with the use of a gear which then transfers rotational kinetic energy to the synchronous moving motor.

The method however, requires a similar gear or a gear that syncs the motion of the initial gear to reduce energy losses. With this said an elementary experimental test is conducted in order to investigate such function.

When the rotations occur, the results will be captured and analyzed in order to determine the energy generated to investigate the efficiency of the pendulum and whether it can function as a generator.

6.5.1 Experimental Configuration
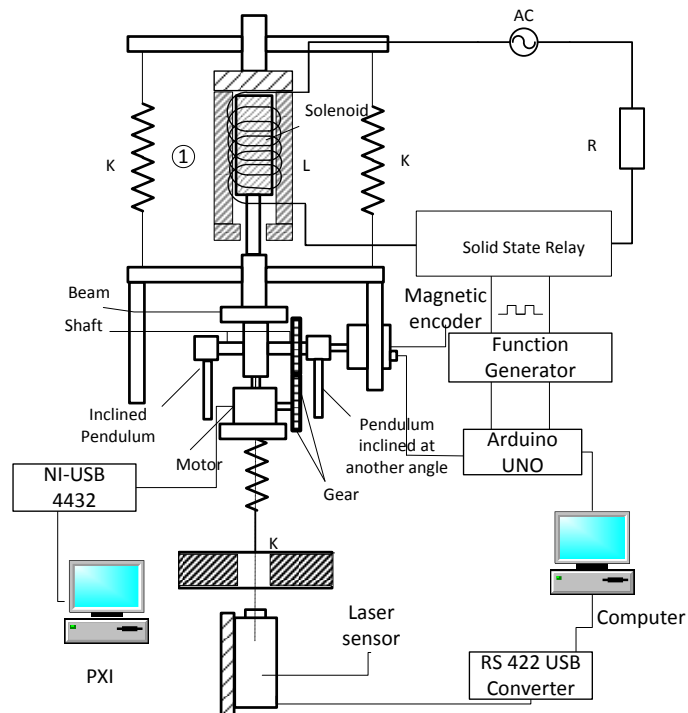
Fig 6. 31 Generator is attached below the pendulum support.

In this configuration, the Generator is attached which is currently labeled as motor in

Fig 6.31. In this chapter, all labels with motor is also known as the acting generator.

Fig 6. 32 the photograph on the left shows the generator attached to the pendulum, on the right shows the view of how the motor is held by a plate that is attached to the pendulum support.

In this chapter a Generator is introduced to function as a generator for the mechanism. The generator used is FA 130 Tamiya Motor of 2 V DC. The resistance was determined by Fluke PM6304 Programmable Automatic RCL Meter, and while rotating the generator, it can be seen that the values of the resistance fluctuate from 1.28 Ω to 2.77 Ω. When stationary, the motor resistance is at 1.37 Ω.
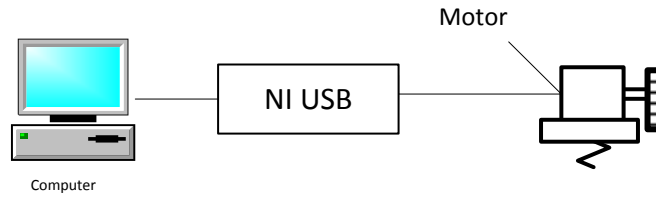
Fig 6. 33 Connection of the Motor to the receivers.

The generator is attached to a plate and the signal junctions are connected to the receivers which can be seen in Fig 6. 32. The NI USB (Appendix) acts as a port to obtain the voltage from the Motor, which then transmit it to the computer using the software LabVIEW signal express.

The gear used for the generator is a 2 mm bore diameter shaft, 24 Teeth Spur Gear, of 12.6 mm Pitch Diameter. The plastic gear (RS − 5217398) used for the pendulum shaft which can be viewed on the right side of Fig 6. 32, is 56 Teeth Spur Gear, 44.8mm Pitch Diameter , 6mm Bore Diameter.

The results are transmitted by means of two gears which are connected to the pendulum shaft, as well as the generator. The rotations of the pendulums are transmitted to the gear on the shaft and thus actuates the gear attached to the generator. When the rotations occur, the results are captured by the NI USB which was discussed above, and the captured results can be seen in Fig 6. 34.
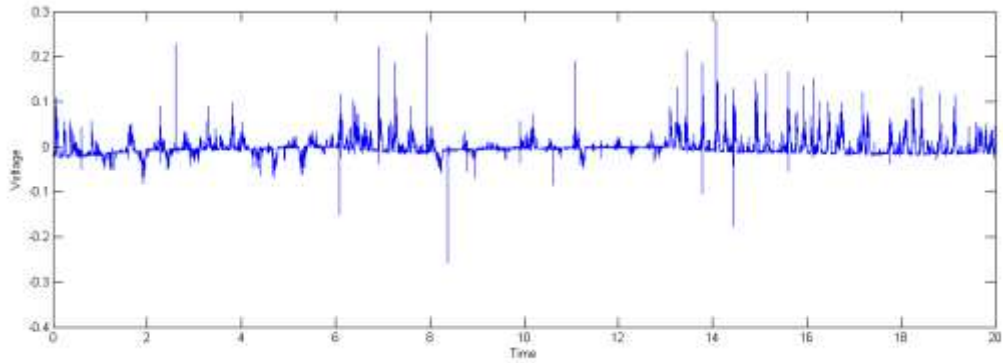
Fig 6. 34 Tumbling rotations at 6 Hz.

Fig 6. 34 shows the rotations of the gear of the generator that was actuated by the shaft. The rising spikes imply rotations occurring. The voltage acquired with the use of the motor is capable of generating voltage up to 0.3 V.

The frequency used for the result is 6 Hz, and it undergo tumbling chaos. Different sets of frequencies were tested in order to achieve results. However, the gear spurs may plays a major role in terms of energy efficiency transmission. Some energy are loss due to sounds and unwanted frictions causing the rotations to be unstable.

The gear was then modified to gears that was given from a children's toy in order to solve the above problem. The schematic was then modified to have two equivalent gears as can be seen in Fig 6. 35

Fig 6. 35 Generator gears were changed to one that are taken from toys.

In Fig 6.35 2 similar gears from the same pack were used in order to assemble this. The efficiency has increased and the friction and losses were minimize allowing more kinematic rotational energy to be induced.

(a)

(b)
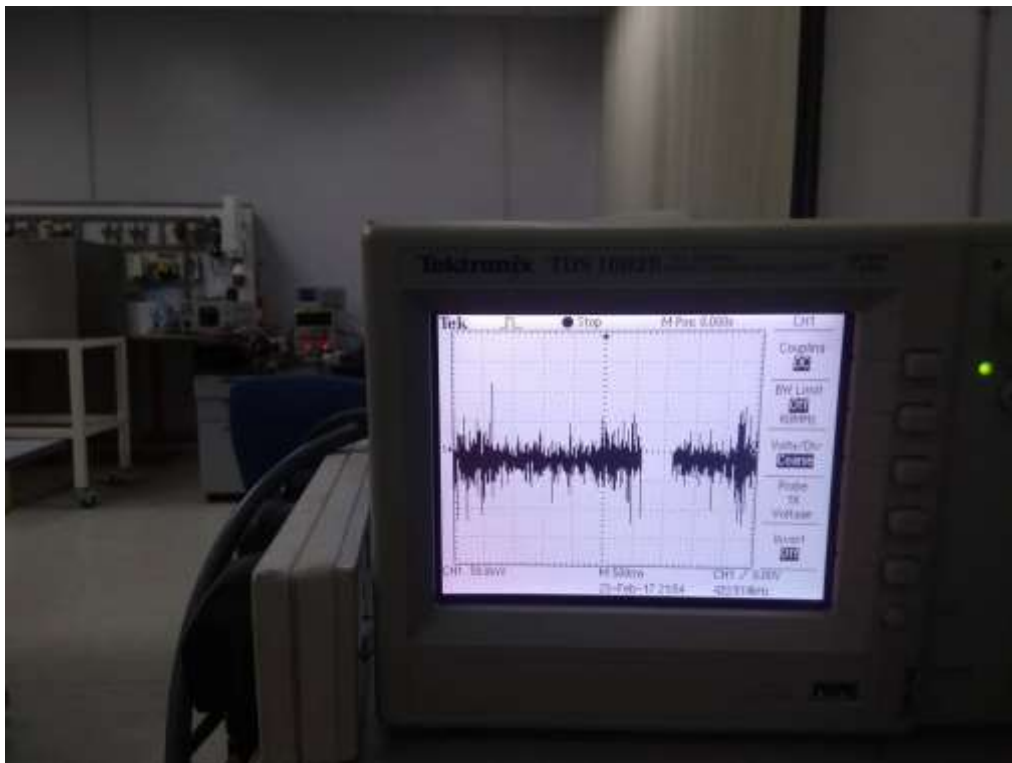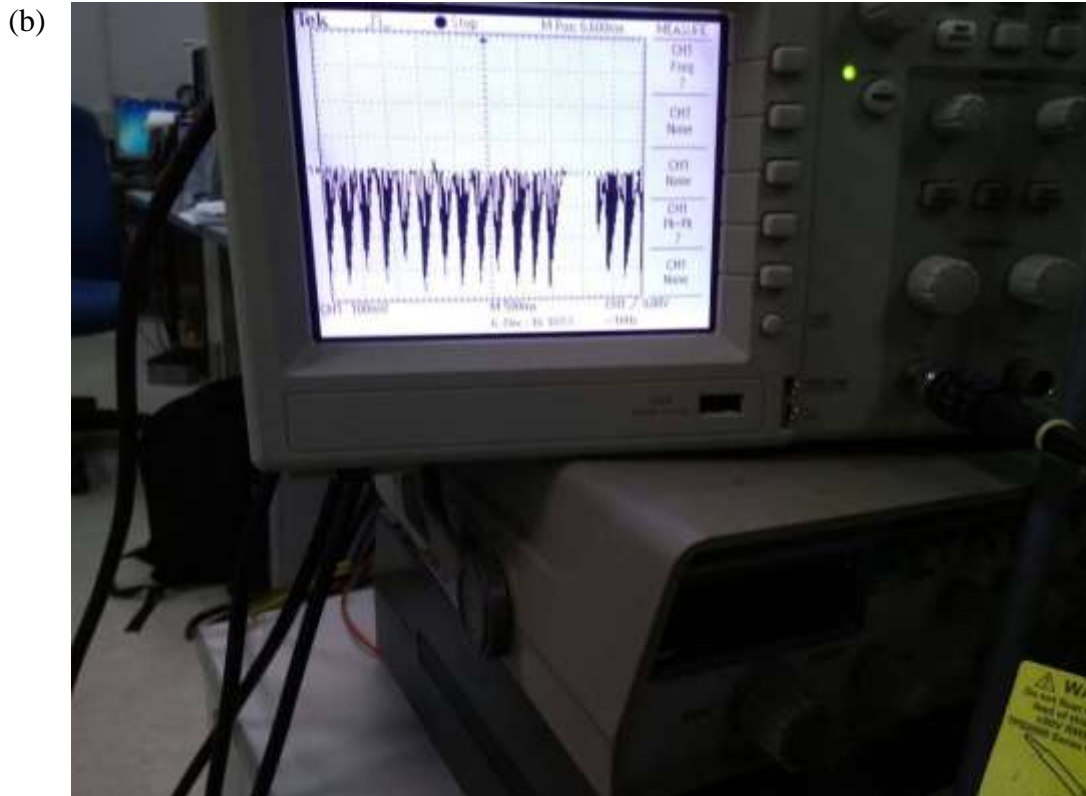
Fig 6. 36 The reading of the oscilloscope when rotation is occurring. (a) and (b)

shows a different graphical interface despite having the same initial conditions.

When the gears were changed, the pendulums move smoother and is capable of

generating continuous rotations as compared to the previous gear set. The data was then

accumulated with the same method as discussed previously and the sampling rate was

changed to 2kHz.

6.5.2 Power conversion

The energy output was then calculated using the equation derived below

$$P_{out} = \int V(t)I(t)dt \qquad (6.3)$$

$$P_{out} = \int \frac{V^2(t)}{R} dt \qquad (6.4)$$

$$P_{out} = \frac{1}{R} \int V^2(t) dt \qquad (6.5)$$

P_{out} can be determined by identifying the area under the curve. In this case the equation was tested by MATLAB. The code will be provided in the appendix.

The motor used has the power to generate 0.25 V at maximum, and it was used because the size of the motor is small enough to fit in between the two pendulums.
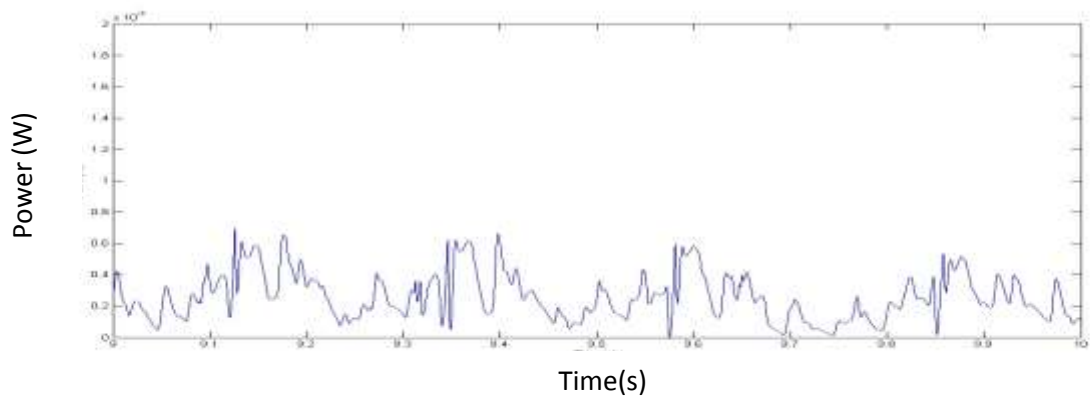
Fig 6. 37 The power output running at 4.13 Hz, when filter is applied to remove the noise
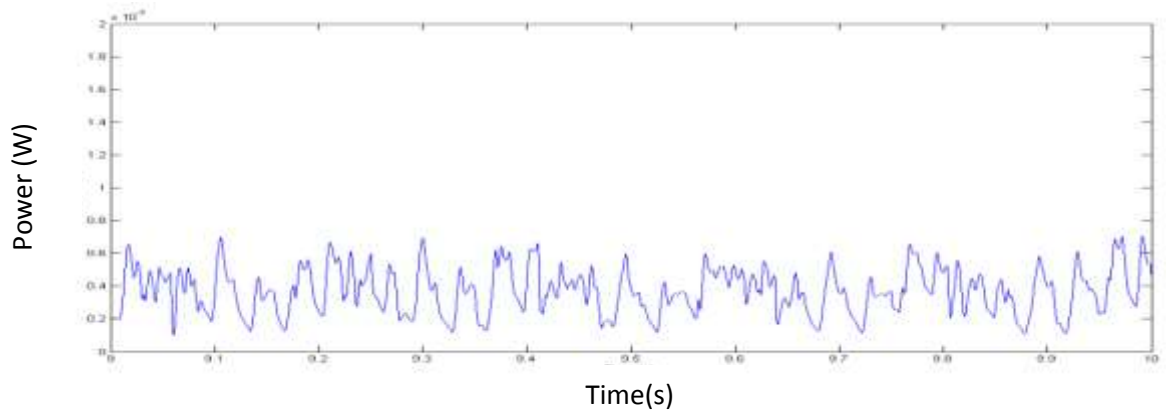
Fig 6. 38 The power output running at 5.3 Hz, when filter is applied to remove the
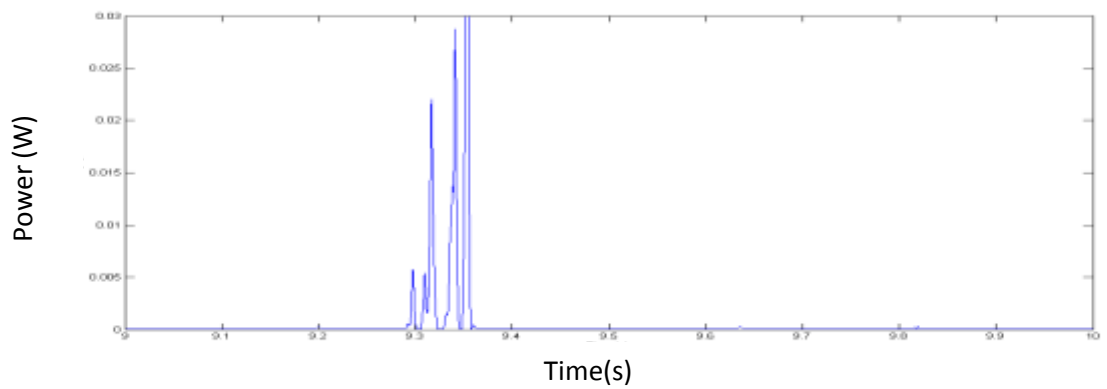
noise

Fig 6. 39 The power output running with a stochastic input to the solenoid, when filter

is applied to remove the noise.
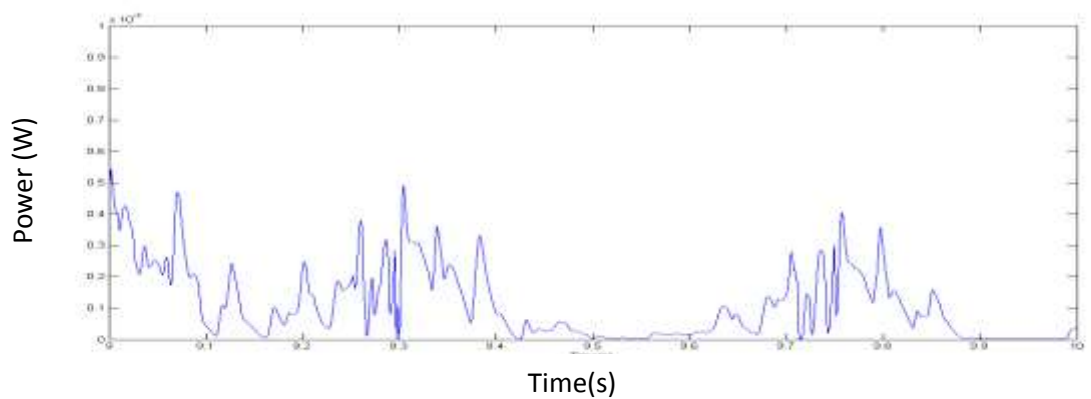
Fig 6. 40 The power output running with a chaotic input to the solenoid, when filter is

applied to remove the noise.

The power generated for each graphs is obtained using the equation above the power generated is .4091 W per second. The Power is generated using the equation applied to MATLAB. When the frequency is 5.3 Hz the power generated is at 0.5341 W. When stochastic waves were supplied to the solenoid, the motor functioned differently and the reading then showed that the power generated is at 0.8114 W. While when the solenoid is undergoing chaotic magnetic attraction, the power generated by the pendulum is 0.408 W. While the voltage input is 14 V to 22 V.

6.6 Conclusion

Periodic signals were found to contribute to rotations generation whereas Stochastic and Chaotic signals were found to contribute to coexisting attractors such as Period-one and period-two oscillations, and tumbling chaos. Rotations were also found to occur when Stochastic signals were used, when impacts were present. The observed data showed that the range of frequency where rotations can be generated have been widened from the previously known 2.5 Hz to the current 7.25 Hz. Expanding the frequency further may deem to be possible, however due to the solenoid allowing a maximum motion, the rotations during 7.5 Hz has caused the conductor to hit and create impacts. This causes the pendulum to lose it's rotating capabilities at this state.

Angles within 30° to 60° were capable of facilitating rotations. When the angle subtended between the two pendulums were set to 0°, the pendulums were positioned side by side and were only capable of maintaining period-two oscillations.

The subtended angle has been the biggest contribution to the configuration, Fig 6.2, and Fig 6.3 have shown how efficient the model when vertical oscillations are able to allow rotations to take place. When configured with the recording devices the range of frequencies are reduced, and concludes the results, the observed frequencies are found to be much lesser as compared to when it was initially observed from the identification of the model. The results were analyzed and found to have investigated that the range of frequency of the system

The range of attractors for period one oscillations exist between 1.5 and 2.9 Hz, A power supply of 15 V is sufficient to initiate the solenoid. Impacts occur within this range.

The increment of frequency allows period two oscillation to occur, without impacts. The period two oscillations are found within the range of 3 Hz and 5.4 Hz.

The range of tumbling chaos can be found within 3.2 Hz and 3.5 Hz, where within this range rotations, and oscillations are co − existing attractors. Initial conditions determine the resultant attractor.

The range of continuous rotations occur within the range of 3.5 and 5.4 Hz, without impacts, the range is similar to that of period two oscillations because both attractors co-exist within this range. However, rotations are easily produced within this range. After continuous rotations, the frequency can be ramped up and is found to be able to maintain rotations up to 9 Hz. However, the data is unfortunately not reproducible.

An initial perturbation, resulting in an initial velocity may tend towards two possible attractors either oscillatory or rotational. In order to identify oscillations, a

gentle touch is given but, it requires a slightly larger force to keep it continuous. An even larger force will cause rotations, and is useful to perturb trajectories.

As observed from the results, a subtended angle of 45° has resulted in the dynamic responses. By inspection of time histories and phase planes, qualitative system response is found to be a period two oscillation. Tumbling chaos has also been observed in Fig 6. 22 (a).

The power output resulted with the use of the motor indicates that it is not an efficient energy extraction device. This case only occurs due to the used motor as well as the spur gear used. Multiple factors are taken into an account and the proceeding solutions are factors such as, adapters for the motor in order to deploy or use larger gears that reduce unwanted friction and noise. A longer shaft to hold the pendulum as well as the gear.

Chapter 7

Conclusions

7.1 Mathematical analysis of the experimental configuration

In Chapter 4, the mathematical modeling has been found to have a correlation with experimental data, and hence can be further developed as a numerical tool to optimize the mechanism when it is deployed in a vibrating system. The dynamics of the system requires a more thorough understanding of it, as it was found to not correspond to the experimental results.

The mathematical model was configured with the derivation of the equation. However, the model could not be simulated despite using two different types of software – Dynamics software [54] and Simulink.

The dynamic response of the vertical oscillation is highly affected by the electromagnetic forces induced by the solenoid. The motion equation derived from the dynamics equation of the oscillating conductor was modelled as a discontinuous system. Hence the mathematical equation and model would have to be further investigated. The

idea and approach of the mathematical model of the system dynamics are presented. For the equation, Dynamics software was used in order to simulate the equation to create a loop, when the simulation was running, due to the discontinuity. The loop was found to be cancelled at 0.02 seconds from the initial point.

7.2   Pivot on a circular track

The usage of the circular track was tested and while it was found to be possible to have rotations, there are some limitations that are found to exist, hence inhibiting rotations.

The configuration made use of a large solenoid and a vertically-oscillated pivot to actuate a pendulum to travel on a circular track. It was found in the experiment discussed in Chapter 6 that the circular track did not appear improve the reproducibility of rotations.

One of them being that pendulum "jumps" when the vertical oscillations occur. A more robust body is required to hold down the pendulums in such a way that the degree of freedom in motion is limited.

The rotations of the pendulum are to allow free motions of the pendulum to move in the circular track, and gain horizontal momentum when the first pendulum oscillates. This occurrence is similar to how monkey's jump from one rope to another. The momentum produced was hypothesized to assist in the pendulum motion, and

perhaps is capable to generate rotations. However having too much degree of freedom caused the pendulum to be incapable of generating rotations.

7.3 Experimental studies on subtended angles

Two pendulums have been deployed and studied to identify whether it is possible to widen the range of the frequency compared to a single pendulum, in order to allow wider range of usage in real life occurrences. It also identifies more ways on how to harvest energy in many different unpredictable conditions such as sea waves, storms and earthquake.

The study of the two pendulums connected by a common shaft, can also be used in vertical oscillating devices such as automotive parts, and vibro-impact drillers in order to harvest wasted energy, and increase their efficiency as well as making the battery life span longer.

Waves provide constant and powerful energy, unlike wind energy. Therefore by increasing the range of frequencies where rotations can occur in such situations will expand the possibilities of extracting energy.

The experimental findings have proved that the frequency range for generating pendulum rotations have been increased from within 1.5 Hz to 2.3 Hz and is modified to 2.55 Hz to 7.25 Hz. The angle differences between the two pendulums also played a large part in expanding the range of frequencies that allow rotations to exist. Frequencies between 60° and 110° can generate rotations at frequencies from 2.55 Hz to 6.5 Hz. Angles between 10° to 60° generate rotations from 3.5 Hz to 7.25 Hz.

The rate of voltage changes indicate the power of vertical oscillations generated by the solenoid, and in such case. The solenoid was utilized to generate vertical oscillations with a low frequency of 1.5 Hz. A small voltage is applied until it reaches a minimum amount of 12 V, enough to generate oscillations with impacts for that frequency. While the frequency of the solenoid is increased, the initial voltage of 12 V became insufficient to generate vertical oscillations. As such, at 3.5 Hz when provided with a power supply of 12 V, the conductor inside the solenoid was capable of oscillating with an offset of 5 mm in each direction from its original position. When the voltage supply reaches an amount enough to not have a rigorous vertical oscillation, rotations can be found. Thus it had been identified and proven in the experimental work in Chapter 4 that the vertical oscillations is sufficient to generate rotations are within a range of 20 mm for the pendulums subtended by an angle.

7.4 **Recommendations for future work**

Further Analysis using a different data recording device:

Further parametric study still needs to be undertaken to understand the system. Bifurcation analysis needs to be performed to quantify all system responses and the parameter values at which rotational motion exist and cease with the help of a more accurate and precise data acquisition device.

As the Arduino UNO has a lot of noise in the data itself, it did not manage to get an accurate bifurcation diagram which can be seen in the Appendix.

Solenoids of a different inductance characteristic could be used.
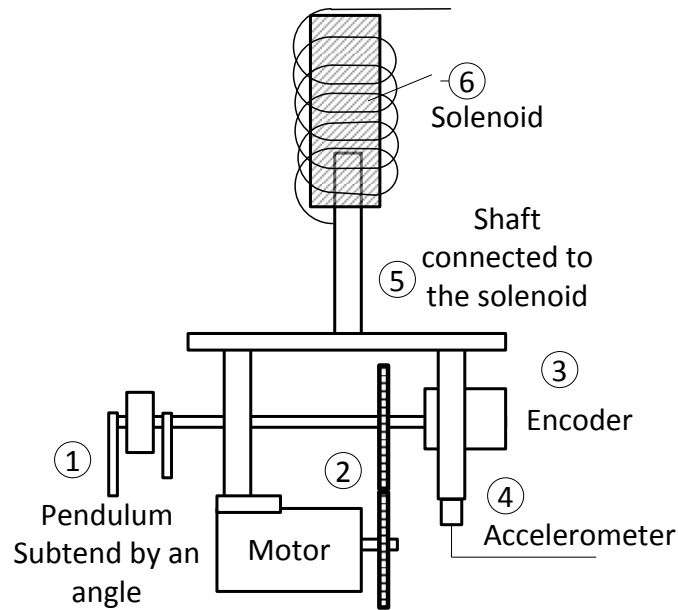
Fig 7. 1 Design of the pendulum attached to the cart from Fig 5. 2

The pendulum support similar to the one provided by Teh [2]. With the pendulum positioned in such method, there is a possibility to allow the configuration to work as if it is similar to the configured experimental system.

Each component's advantages of the outcome presented in Fig 7. 1 is listed down below for the future analysis:

(1) The pendulum is connected to a long shaft where, the outer pendulum can be adjusted to subtend an angle. The inner pendulum will be completely locked in one position of the pendulum so that it cannot be adjusted and will not loosen.

(2) The motor is attached to the cart, where the gears are adjustable and motors are interchangeable since there will be no restriction in which motor should be used, as well as which gears will be used. As the configuration reported in Chapter 4 only allows a limited choice of both gears and motors. The power output after the motor has been modified may allow more energy to be harvested.

(3) As the encoder is directly fixed to the shaft, there will be a more stable point and ease of data acquisition in the angular position of the pendulum, allowing for a more accurate sets of data and a more analytical understanding.

(4) The accelerometer will be used for the vertical displacement reading, which is more accurate as compared to using laser sensor. This will also make the data acquisition system more robust, since the laser sensor will detect the position of the pendulum support only within a certain range.

(5) The shaft which acts as the conductor for the solenoid should have a larger range of vertical oscillations, as there are no restrictions of displacement for the shaft. This is because the restriction of displacement of the shaft will lead to Impacts and hence limiting the range of frequencies.

(6) The solenoid should have a higher power rating, and thus the variation of power supply will have a smaller effect on solenoids reaction for example in Chapter 4 when increasing the voltage supplied to the solenoid by 1 V, it shows a tremendous change causing impacts to occur easily and limiting analysis. It also allows capacitor to be included for a safer analysis that minimizes the chance of the circuit breaking due to heat loss.

Energy Harvest

Upon achieving possibilities of rotations for the configuration, possible equipments can be included in order to harvest the energy as well giving a feedback to the system to allow it to initiate rotations by itself after an initial input. A stator or an energy harvesting device can be connected to the system to generate electricity.

Harvesting through motions of sea wave similar to what Yurchenko [100] has suggested. The configuration can be further improved to harvest energy from the waves

by using the water wave as the vertical oscillation and convert rotations from the pendulums.

<u>Application ideas</u>

The configuration can be further applied in systems that uses vertical oscillations and make the system more efficient as well as long lasting since it is capable of generating its own electricity through vibrations.

The configuration also seeks to provide further efficiency, hence motorized equipment that involves vertical oscillations or continuous pumping action such as a vehicle engine, can further improve the efficiency of the petrol usage, as well as extending the lives of the motor.

The system configuration can also be implemented in such a way that it can relate to the Ark reactor analysis, where the rotational concept is used using two electrons positioned in the same configuration as the pendulum and allows it to continuously rotate at a certain arc and generate electricity.

References

[1]   B. Horton, J. Sieber, Thompson and M. Wiercigroch, "Dynamics of the nearly parametric pendulum," *International Journal of Non linear Mechanics* **46***,* pp. 436 - 442, 2011.

[2]   S. H-. Teh, K. H-. Chan, K. C. Woo, H. Demrdash, "Rotating a pendulum with an electromechanical excitation," *International Journal of Non- Linear Mechanics, ,* **70** pp 73 - 84, 2014.

[3]   M. Wiercigroch, "A new concept of energy extraction from oscillations via pendulum systems.". Patent UK Patent application.

[4]   M. Wiercigroch, A. Najdecka and V. Vaziri, "Nonlinear Dynamics of Pendulums System for Energy Harvesting, Vibration Problems ICOVP 2011," *Springer,* 2011.

[5]   X. Xu, M. Wiercigroch and M. P. Cartmell, "Rotationg orbits of a parametrically excited pendulum," *Chaos, Solitons and Fractals,* vol. **23**, no. 5, pp. 1537 - 1584, 2005.

[6]   X. Xu, Nonlinear dynamics of parametric pendulum for wave energy extraction. PhD, Aberdeen: University of Aberdeen, 2005.

[7] B. W. Horton, X. Xu and M. Wiercigroch, "Transient tumbling chaos and damping identification for parametric pendulum," *Philos. Tran. R. Soc.,* vol. A **366**, pp. 767 - 784, 2008.

[8] X. Xu, E. Pavloskaia, M. Wiercigroch, F. Romeo and S. Lenci, "Dynamic interactions between parametric pendulum and electro-dynamical shaker.," *Z. Angew Math. Mech,* vol. **87**, pp. 172-186, 2007.

[9] X. Xu and M. Wiercigroch, "Approximate analytical solutions for oscillatory and rotational motion of a parametric pendulum," *Nonlinear Dynamics,* vol. **47**, pp. 311-320, 2007.

[10] S. Lenci, G. Rega, E. Pavloskaia and M. Weircigroch, "Rotating solutions and stability of parametric pendulum by perturbation method," *Journal of Sound Vibrations,* vol. **310**, pp. 243-259, 2008.

[11] S. C. Jong, Nonlinear Dynamics of a Vibro-Impact System Subjected to Electromagnetic interactions, Ph.D.Thesis, Semenyih, Malaysia: University of Nottingham Malaysia Campus, 2014.

[12] R. W. Leven and B. P. Koch, "Chaotic behaviour of a parametrically excited damped pendulum," *Physics Letters,* vol. **86**A, no. 2, pp. 71-74, 1981.

[13] H. J. T. Smith and J. A. Blackburn, "Experimental study of an inverted pendulum," *American Journal of Physics,* vol. **60**, pp. 909-911, 1992.

[14] J. A. Blackburn and G. L. Baker, "A comparison of commercal chaotic pendulums," *American Journal of Physics,* vol. **66**, pp. 821-830, 1998.

[15] S. Y. Kim, S. H. Shin, J. Yi and C. W. Jang, "Bifurcations in a paramterically forced magnetic pendulum.," *Physical Review E,* vol. 56, pp. 6613-6619, 1997.

[16] P. J. Bryant and J. W. Miles, "On a periodically forced, weakly damped pendulum Part 3: Vertical forcing," *Journal of the Australian Mathematical Society,* vol. 37, no. Series B, pp. 42-60, 1990.

[17] M. J. Clifford and S. R. Bishop, "Locating oscillatory orbits of the parametrically-excited pendulum," *Journal of the Australian Mathematical Society,* vol. 37, no. Series B, pp. 309-319, 1996.

[18] J. Isohätälä, K. N. Alekseev, L. T. Kurki and P. Pietiläinen, "Symmetry breaking in a driven and strongly damped pendulum," *Physical Review E,* vol. 71, no. 066206-6, 2005.

[19] S. R. Bishop and M. J. Clifford, "Approximating the escape zone for the parametrically excited pendulum," *Journal of Sound and Vibration,* vol. 172, no. 4, pp. 572-576, 1994.

[20] I. W. Stewart and T. R. Faulkner, "Estimating the escape zone for a parametrically excited pendulum-type equation," *Physical Review E,* vol. 62, pp. 4856-4861, 2000.

[21] D. Capecchi and S. R. Bishop, "Periodic oscillations and attracting basins for a parametrically excited pendulum," *Dynamics and Stability of Systems,* vol. 9, no. 2, pp. 123 - 143, 1994.

[22] H. J. Smith and J. A. Blackburn, "Multiperiodic orbits in a pendulum with a vertically oscillating pivot," *Physical Review E,* vol. 50, pp. 539-549, 1994.

[23] W. Szemplińska-Stupnicka, E. Tyrkiel and A. Zubrzycki,, "The global bifurcations that lead to transient tumbling chaos in a parametrically driven pendulum," *International Journal of Bifurcation and Chaos,* vol. 10, no. 9, pp. 2161-2165, 2000.

[24] W. Szemplińska-Stupnicka and E. Tyrkiel, "Common features of the onset of the persistent chaos in nonlinear oscillators: a phenomenological approach," *Nonlinear Dynamics,* vol. 27, no. 3, pp. 271-293, 2002.

[25] R. Kobes, J. Lui and S. Peleš, "Analysis of a parametrically driven pendulum," *Physical Review E,* vol. 63, no. 036219-17, 2000.

[26] S. Y. Kim and K. Lee, "Multiple transitions to chaos in a damped parametrically forced pendulum," *Physical Review E,* vol. 53, pp. 1579-1586, 1995.

[27] S. R. Bishop, A. Sofroniou and P. Shi, "Symmetry-breaking in the response of the parametrically excited pendulum model," *Chaos, Solitons and Fractals,* vol. 25, no. 2, pp. 257-264, 2005.

[28] J. M. Thompson, "Chaotic phenomena triggering the escape from a potential well," *Proceedings of Royal Society of London A,* vol. 421, no. 1862, pp. 195-225, 1989.

[29] J. H. Ho, V. D. Nguyen and K. C. Woo, "Non linear dynamics of a new electro-vibro- impact system," *Nonlinear Dynamics,* vol. 63, pp. 35-49, 2011.

[30] S. H. Teh, K. C. Woo and H. Demrdash, "Rotating orbits of pendulum in stochastic excitation," *Journal of Theoretical and Applied Mechanics,* 2015.

[31] L. Meirovitch, Elements of Vibrtion Analysis.

[32] S. Tsaplin, Vibratory impact mechanisms for road and bridge construction, Autotranzidat, 1953.

[33] S. C. Jong, V. C. Lee and K. C. Woo, "Electromagnetic force interactions in forward progressive motion," *Acta Mechanica Sinica.*

[34] K. C. Woo, V. D. Nguyen and E. Pavloskaia, "Experimental study and mathematical modelling of a new of vibro-impact moling device," *International Journal of Non-Linear Mechanics.*

[35] V. D. Nguyen, MSc Nonlinear Dynamics of Electromechanical machines Vibro − Impact machines, 2007.

[36] H. Y. Hu, "Primary resonance of a harmonically forced oscillator with a pair of symmetric set − up elastic stops," *Journal of Sound and Vibration,* vol. 207, no. 3, pp. 393-401, 1997.

[37] B. Blazejczyk-okolewska and F. Peterka, " An investigation of the dynamic systems," *Chaos, Solitons and Fractals,* vol. 9, no. 8, pp. 1321-1338, 1998.

[38] H. P. Lok, R. D. Neilson and A. A. Rodger, "Computer − based model of vibro − impact diving," *Proceedings of ASME DETC: Symposium on Nonlinear dynamics in Engineering Systems,* 1999.

[39] M. A. Aziz, A. E. Vakakis and L. I. Manevich, "Exact solutions of the problem of the vibro-impact oscillations of a discrete system with a two degrees of freedom," *Journal Appl. Maths Mechs,* vol. 63, no. 4, pp. 527-530, 1999.

[40] S. A. Kember and V. I. Babitsky, "Excitation of vibro-impact systems by periodic impulses," *Journal of Sound and vibration,* vol. 227, no. 2, pp. 427-447, 1999.

[41] G. W. Luo and Y. Zhang, "Analyses of impact motions of harmonically excited systems having rigid amplitude constraints," *Internation Journal of Impact,* no. doi: 10.1016/j.ijimpeng.2006.10.0014,2006..

[42] S. G. Kryzhevich and V. A. Pliss, " Chaotic modes of oscillation of a vibro − impact system," *Journal of applied mathematics and mechanics,* vol. 69, pp. 13-26, 2005.

[43] W. Hana, D. P. Jina and H. Y. Hu, "Dynamics of an oblique-impact vibrating system of two defrees of freedom," *Journal of Sound and Vibration,* vol. 216, no. 3, pp. 435-439, 1998.

[44] B. Blazejczyk-okolewska and T. Kapitaniak, "Co-existing attractors of impact oscillator," *Chaos, Solitons and Fractals,* vol. 9, no. 8, pp. 1439-1443, 1998.

[45] G. W. Luo, "Period doubling bifurcations and routes to chaos of thevibratory system contacting stops," *Physics Letters A,* vol. 323, pp. 210-217, 2004.

[46] G. W. Luo and J. H. Xie, "Bifurcations and chaos in a system with impacts," *Physica D,* vol. 148, pp. 183-200, 2001.

[47] G. W. Luo and J. H. Xie, "Hopf bifurcations and chaos of a two deree vibro-impact systems in two strong resonance cases," *International Journal of Non-Linear Mechanics,* vol. 37, pp. 19-34, 2002.

[48] G. W. Luo, "Hopf-flip bifurcations of vibratory systems with impacts," *Nonlinear Analysis: RealWorld Applications,* vol. 7, pp. 1029-1041, 2006.

[49] B. Blazejczyk-Okolewska, T. Kapitaniak, J. Wojewoda and R. Barron, "Experimental Observation of intermittent chaos in a mechanical system with impacts," *Journal of Sound and Vibration,* vol. 178, no. 2, pp. 272-275, 1994.

[50] J. C. Sprott and A. Maus, "LagSpace 1.3," [Online]. Available: http://sprott.physics.wisc.edu/chaos/maus/lagspace.htm.

[51] S. S. Rao, Mechanical Vibrations, Fourth edition in SI units, 2005.

[52] "Motor gears," [Online]. Available: https://www.pinterest.com/pin/453315518718892865/.

[53] J. A. Yorke, "Dynamics; the program," [Online]. Available: yorke.umd.edu/dynamics.

[54] "Lagspace," [Online]. Available: http://sprott.physics.wisc.edu/chaos/maus/lagspace.htm.

[55] Abadi, "On self-excited auto-parametric systems," *Nonlinear Dynamics,* vol. 24, pp. 147 - 166, 2001.

[56] P. Alevras, I. Brown and D. Yurchenko, "Experimental investigation of a rotating parametric pendulum," *Nonlinear Dynamics,* pp. 1-13, 2015.

[57] P. Alevras and D. Yurchenko, "Stochastic rotational response of a parametric pendulum coupled with an SDOF system," *Probabilistic Engineering,* vol. 37, pp. 124-131, 2014.

[58] G. L. Baker, J. A. Blackburn and H. J. Smith, "A stochastic model of synchronization for chaotic pendulums," *Physics Letters A,* vol. 252, no. 3, pp. 191 - 197, 1999.

[59] S. R. Bishop and M. J. Clifford, "The use of manifold tangencies to predict orbits, bifurcations and estimate escape in driven systems," *Chaos, Solitons and Fractals,* vol. 7, no. 10, pp. 1537-1553, 1996.

[60] S. R. Bishop and M. J. Clifford, "Zones of chaotic behaviour in the parametrically excited pendulum," *Journal of Sound and vibration,* vol. 189, no. 1, pp. 142-147, 1996.

[61] J. A. Blackburn, "Noise activated transitions among periodic states of a pendulum with a vertically oscillating pivot, mediated by a chaotic attractor,"

Proceedings of the Royal Society of London A: Mathematical, Physical amd Engineering Sciences, vol. 462, no. The Royal Society, 2006.

[62] J. A. Blackburn, N. Granbech-Jensen and H. J. Smith, "Stochastic noise and chaotic transients," *Physical review letters,* vol. 74, no. 6, p. 908, 1995.

[63] J. J. Blakley, "A linear oscillating feeroresonant machine," *IEEE transactions on magnetics,* vol. 19, no. 4, pp. 1574 - 1579, 1983.

[64] P. J. Bryant and J. W. Miles, "On a periodically forced, weakly damped pendulum Part 1: Applied torque," *The journal of the Australian Mathematical Society. Series B,* vol. 32, no. 01, pp. 1-22, 1990.

[65] P. J. Bryant and J. W. Miles, "On a periodically forced, weakly damped pendulum Part 2: Horizontal forcing," *The Journal of the Australian Mathematical Society. Series B.,* vol. 32, no. 01, pp. 23-41, 1990.

[66] P. Brzeski, P. Perlikowski, S. Yanchuk and T. Kapitaniak, "The dynamics of the pendulum suspended on the force duffing oscillator,," *Journal of Sound and Vibration,* vol. 331, pp. 5347-5357, 2012.

[67] B. F. Feeny and J. W. Liang, "A decrement method for simultaneous estimation of coulomb and viscous friction," *Journal of Sound and Vibration,* vol. 195, no. 1, pp. 149-154, 1996.

[68] W. Garira and S. R. Bishop, "Rotating solutions of the parametrically excited pendulum," *Journal of Sound and Vibration,* vol. 263, pp. 233-239, 2003.

[69] O. Gomis-Bellmunt, S. Galceran-Arellano, A. Sudria-Anderu, D. Montesinos-Miracle and L. F. Campanile, "Linear electromagnetic actuator modeling for optimization of mechatronic and adaptronic systems," *Mechatronics,* vol. 17, no. 2, pp. 153-163, 2007.

[70] A. Gus'kov, G. Y. Panovko and C. Van Bin, "Analysis of the dynamics of a pendulum vibration absorber," *Journal of Machinery Manufacture and Reliability,* vol. 37, pp. 321-329, 2008.

[71] J. H. Ho, V. D. Nguyen and K. C. Woo, "Approximate analytical solution to oscillations of a conductor in a magnetic field," *Nonlinear Dynamics,* vol. 64, pp. 315-330, 2011.

[72] M. J. Clifford and S. R. Bishop, "Approximating the escape zone for the parametrically excited pendulum," *Journal of Sound and Vibration,* vol. 172, pp. 572-576, 1994.

[73] M. J. Clifford and S. R. Bishop, "Rotating periodic orbits of the parametrically excited pendulum," *Physics Letters A,* vol. 201, pp. 191-196, 1995.

[74] A. de Paula, M. A. Savi, V. Vaziri, M. Wiercigroch and E. Pavloskaia, "Numerical and experimental bifurcation control in a parametrically excited pendulum," *Proceedings of the XV International Symposium on Dynamic Problems of Mechanics, ABCM,* 2013.

[75] B. W. Horton and M. Weircigroch, "Effects of heave excitation on rotations of pendulum for wave energy extraction," *in: IUTAM Symposium on fluid-structure interaction in ocean engineering, Springer,* 2008.

[76] J. Ing, E. Pavloskaia and M. Wiercigroch, "Complex nonlinear response of a piecewise linear oscillator: Experiment and simulation," *in: IUTAM Symposium on Dynamics Modelling and Interaction Control in Virtual and Real Environments, Springer,* 2011.

[77] M. P. John and V. M. Nandakumaran, "Chaotic oscillations in a piecewise linear spring-mass system," *Theoretical and Applied Mechanics Letters,* vol. 2, no. 5, p. 053002, 2012.

[78] E. Kallenbach, H. Kube, V. Zoppig, K. Feindt, R. Hermann and F. Beyer, "New polarized electromagnetic actuators as integrated mechatronic components- design and application," *Mechatronics,* vol. 9, no. 7, pp. 769-784, 1999.

[79] K. Kecik and J. Warminski, "Dynamics of an autoparametric pendulum-like system with a nonlinear semiactive suspension," *Mathematical Problems in Engineering 2011,* vol. 451047, 2011.

[80] S. H. Kellert, "In the wake of chaos: Unpredictable order in dynamical systems," *University of Chicago press,* 1994.

[81] B. P. Koch and R. W. Leven, "Subharmonic and homoclinic bifurcations in a parametrically forced pendulum," *Physica D 16,* pp. 1-13, 1985.

[82] B. P. Koch, R. W. Leven, B. Pompe and C. Wilke, "Experimental evidence for chaotic behaviour of a parametrically forced pendulum," *Physics Letters A,* vol. 96, no. 5, pp. 219-224, 1983.

[83] W. K. Lee and C. S. Hsu, "A global analysis of an harmonically excited spring-pendulum system with internal resonance," *Journal of Sound and Vibration,* vol. 171, pp. 335-359, 1994.

[84] S. Lenci, M. Brocchini and E. Lorenzoni, "Experimental rotations of a pendulum on water waves.," *Journal of Computational and Nonlinear Dynamics,* vol. 7, p. 011007, 2012.

[85] S. Lenci, E. Pavloskaia, G. Rega and M. Wiercigroch, "Rotating solutions and stability of parametric pendulum by perturbation method,," *Journal of Sound and Vibration,* vol. 310, pp. 243-259, 2008.

[86] S. Lenci and G. Rega, "Competing dynamic solutions in a parametrically excited pendulum: attractor robustness and basin integrity," *Journal of Computation and Nonlinear Dynamics,* vol. 3, p. 041010, 2008.

[87] S. Lenci and G. Rega, "Experimental versus theoretical robustness of rotating solutions in a parametrically excited pendulum: A dynamic integrity perspective.," *Physica D,* vol. 240, pp. 814-824, 2011.

[88] R. W. Leven, B. Pompe, C. Wilke and B. P. Koch, "Experiments on period and chaotic motions of a parametrically forced pendulum," *Physica D: Nonlinear Phenomena,* vol. 16, no. 3, pp. 371-384, 1965.

[89] MathWorks, "MATLAB/Simulink R2011a," 2011. [Online]. Available: http://-www.mathworks.com.

[90] A. Maus and J. C. Sprott, "Evaluating lyapunov exponent spectra with neural networks," *Chaos,Solitons&Fractals,* vol. 51, pp. 13-21, 2013.

[91] J. Miles, "on resonant rotation of a weakly damped pendulum," *Journal of sound and vibration,* vol. 280, no. 1, pp. 401-406, 2005.

[92] F. C. Moon, "Chaotic vibrations: An introduction for applied scientist and engineers," *Wiley-Interscience,* 2004.

[93] A. Najdecka, "Rotating dynamics of pendula systems for energy harvesting from ambient vibrations," *Ph.D. thesis, University of Aberdeen,* 2013.

[94] A. Najdecka, T. Kapiataniak and M. Wiercigroch, "Synchronous rotational motion of parametric pendulums," *International Journal of Non-Linear Mechanics,* vol. 70, pp. 84-94, 2015.

[95] A. Najdecka, S. Narayanan and M. Wiercigroch, "Rotary motion of the parametric and planar pendulum under stochastic wave excitation," *International Journal of Non-Linear Mechanics,* vol. 71, pp. 30-38, 2015.

[96] A. Najdeck, V. Vaziri and M. Wiercigroch, "Dyamics, synchronization and control of parametric pendulums, in: IUTAM Symposium on Nonlinear Dynamics for Advanced Technologies and Engineering Design," *Springer,* 2013.

[97] K. Nandakumar, M. Wiercigroch and A. Chaterjee, "Optimum energy extraction from rotational motion in a parametrically excited pendulum," *Mechanics Research Communications,* vol. 43, pp. 7-14, 2012.

[98] D. Yurchenko and P. Alevras, "Stochastic dynamics of a parametrically base excited rotating pendulum," *Procedia IUTAM,* vol. 6, pp. 160-168, 2013.

[99] D. Yurchenko and P. Alevras, "Dynamics of the n-pendulum and its application to wave energy converter concept," *International Journal of Dynamics and Control,* vol. 1, no. 4, pp. 290-299, 2013.

[100] J. M. Thompson and H. B. Stewart, "Nonlinear dynamics and chaos," *John Wiley & Sons,* 2002.

[101] E. A. Mendrela and Z. J. Pudlowski, "Transients and dynamics in a linear reluctance self-oscillating motor.," *IEEE Transactions on Energy Conversion,* vol. 7, pp. 183-191, 1992.

[102] V. D. Nguyen, K. C. Woo and E. Pavloskaia, "Experimental study and mathematical modelling of a new vibro-impact moling device," *International Journal of Non-Linear Mechanics,* vol. 43, pp. 542-550, 2008.

[103] V. D. Nguyen and K. C. Woo, "Nonlinear dynamic responses of new electro-vibroimpact system," *Journal of Sound and Vibration,* vol. 310, no. 4, pp. 769-775, 2008.

[104] V. D. Nguyen and K. C. Woo, "New electro vibro-impact system," *Proceedings of the institution of Mechanical Engineers, Part C: Journal of Mechanical Engineering Science,* vol. 222, no. 4, pp. 629-642, 2008.

[105] R. Meiers, "Coolterm," [Online]. Available: https://freeware.the-meiers.org/CoolTerm_Readme.txt.html.

[106] Micro Epsilon, [Online]. Available: www.micro-epsilon.co.uk/service/download/.

[107] W. Szemplińska-Stupnicka and E. Tyrkiel, "The oscillation-rotation attractors in the forced pendulum and their peculiar properties," *International Journal of Bifurcation and Chaos,* vol. 12, pp. 159-168, 2002.

[108] A. Tondl, T. Ruijgrok, F. Verhulst and R. Nabergoj, "Autoparametric resonance in mechanical systems," *Cambridge University Press,* 2000.

[109] G. Litak, M. Wiercigroch, B. W. Horton and X. Xu, "Transient chaotic behaviour versus periodic motion of a parametric pendulum by recurrence plots.," *ZAMM Journal of Applied Mathematics and Mechanics,* vol. 90, no. 1, pp. 33-41, 2010.

[110] A. Sofroniou and S. R. Bishop, "Breaking the symmetry of the parametrically excited pendum," *Chaos, Solitons & Fractals,* vol. 28, no. 3, pp. 673-681, 2006.

[111] E. Pavloskaia, B. W. Horton, M. Wiercigroch, S. Lenci and G. Rega, "Approximate rotational solutions of pendulum under combined verical and

horiontal excitation," *Internation Journal of Bifurcation and Chaos,* vol. 46, pp. 436-442, 2011.

[112] V. Vaziri, A. Najdecka and M. Wiercigroch, "Experimental control for initiating and maintaining rotation of parametric pendulum," *The European Physical Journal Special Topics,* vol. 223, no. 4, pp. 795-812, 2014.

[113] D. Yurchenko, A. Naess and P. Alevras, "Pendulum's rotational motion governed by a stochastic mathieu equation," *Probabilistic Engineering Mechanics,* vol. 31, pp. 12-18, 2013.

[114] M. J. Ogorzalek, "Taming chaos- part i: synchronization," *IEEE Trans. Circuits Syst. I: Fundamental Theo. Appl,* vol. 40, no. 10, pp. 693-699, 1993.

Appendices

Appendix A : List of figures
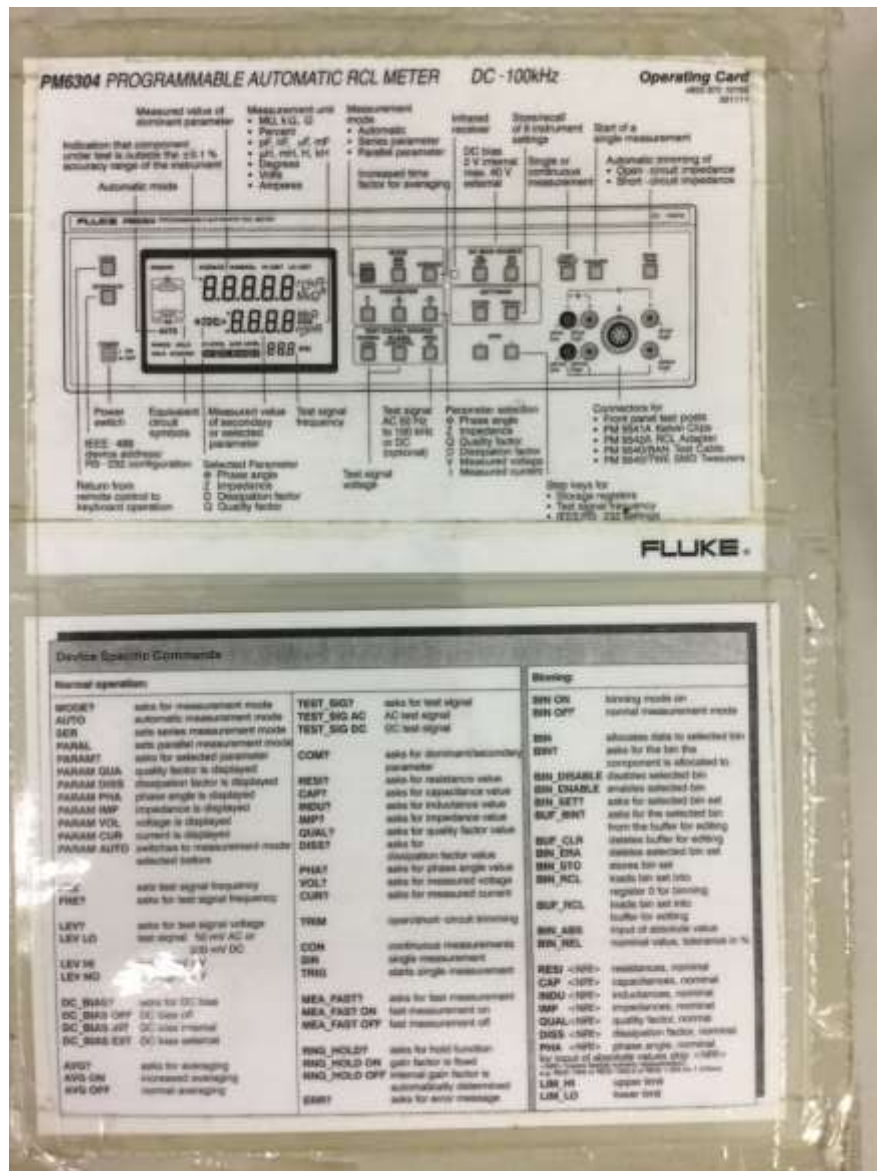
Fig A. 1 Data Manual for the automatic RCL meter

Fig A. 2 The RCL meter, along with the measurements

Fig A. 3 Measurement device for the inductance graph.

Upon running the equation, with the results determined from signal express and the resistance obtained from Fluke. The result equates to 0.0526 J when running in 20 seconds with the use of the toy motor.

The power output resulted with the use of the motor indicates that it is not an efficient energy device. However, this case only occurs due to the used motor as well as the spur gear used. Multiple factors are taken into an account and the proceeding solutions are factors such as, adapters for the motor in order to deploy or use larger gears that reduce unwanted friction and noise. A longer shaft to hold the pendulum as well as the gear.

Fig A. 4 The resistance and inductance is displayed when connected to the solenoid.

Fig A. 5 PXI connected to the NI USB 4432 to get the result from the motor

Picture	Name	RPM (With Load)	RPM (Without Load)	Torque	Power Consumed
	FA-130 Motor	9900	13800	10 g-cm	1100
	Touch Dash	11200	15000	10 g-cm	1300
	Torque Tuned	12000	13600	14.5 g-cm	1200
	Atomic Tuned	13700	15700	10 g-cm	1300
	Rev Tuned	14300	17600	10 g-cm	1500
	Hyper Dash	17200	19300	10 g-cm	1600
	Hyper Dash 2	?	?	10 g-cm	1600
	Mach Dash	20800	23400	15 g-cm	1900
	Jet Dash	23000	28000	22 g-cm	4000
	Ultra Dash	24000	29000	20 g-cm	4000
	Plasma Dash	25000	29000	20 g-cm	4100

Fig A. 6 Motor details and the type of motor
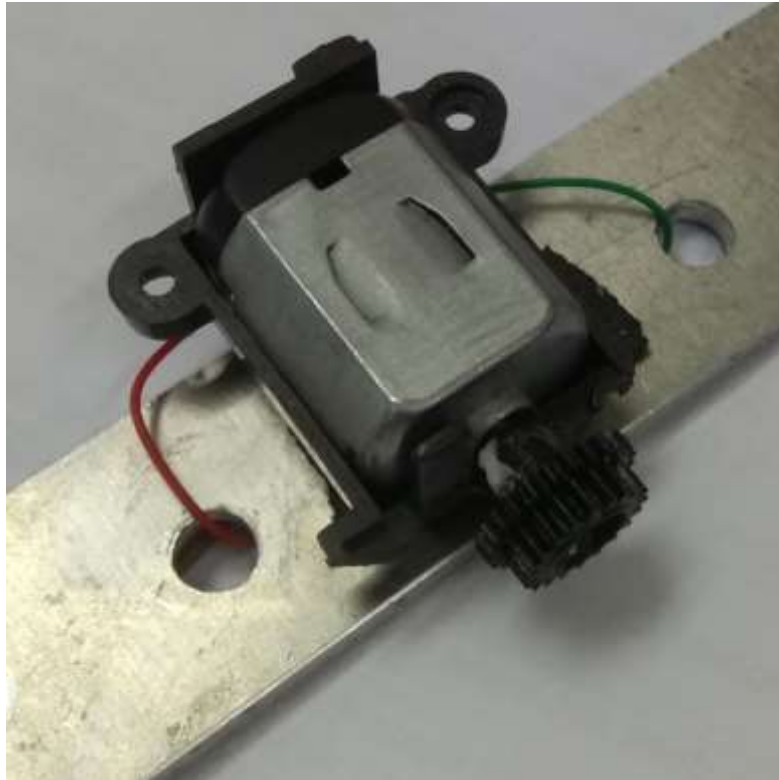
Fig A. 7 Motor used to extract energy taken from a toy vehicle

- Operating Temperature: -10°C ~ +60°C

- Rated Voltage: 6.0VDC

- Rated Load: 10 g*cm

- No-load Current: 70 mA max

- No-load Speed: 9100 ±1800 rpm

- Loaded Current: 250 mA max

- Loaded Speed: 4500 ±1500 rpm

- Starting Torque: 20 g*cm

- Starting Voltage: 2.0

- Stall Current: 500mA max

- Body Size: 27.5mm x 20mm x 15mm

- Shaft Size: 8mm x 2mm diameter

- Weight: 17.5 grams

The code from the encoder as extracted from the manual is as follows:

Appendix B : LabView results to test experimental vibrations

Graphs obtained from labview with the use of the configuration assembled to test vibrations

Appendix B.1 Practical
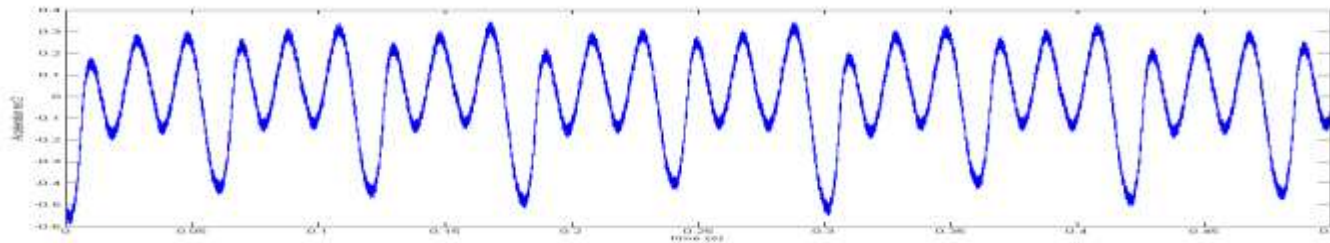
Fig A. 8 8 cycles
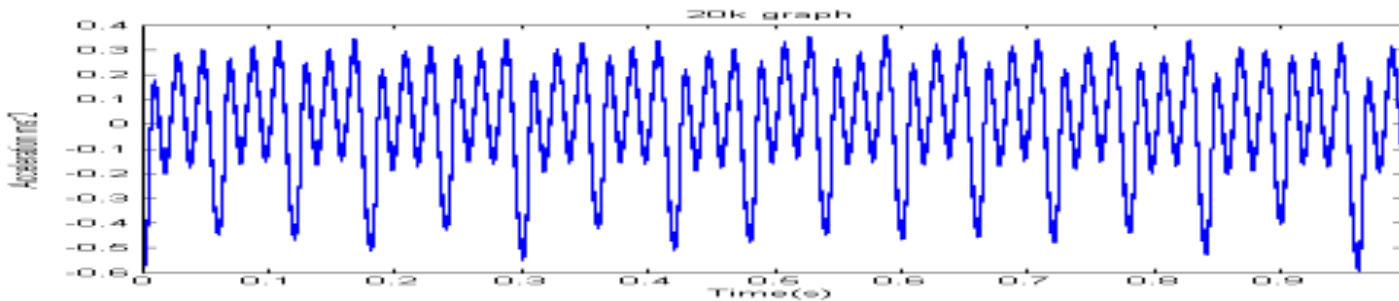
Fig A. 9 20,000 points
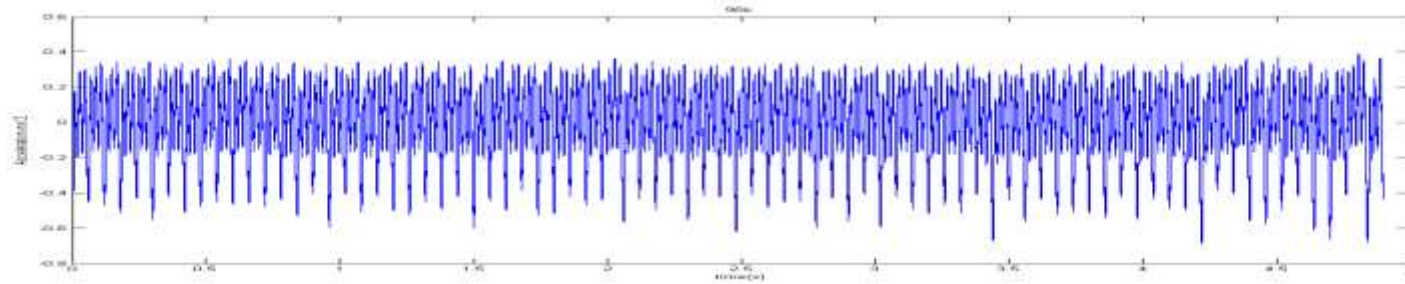
Fig A. 10 98000 points
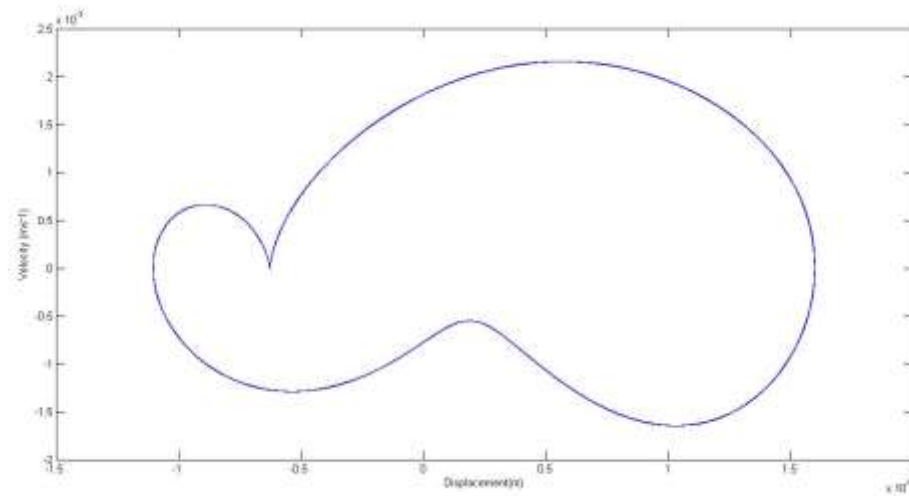
Fig A. 11 poincaré map
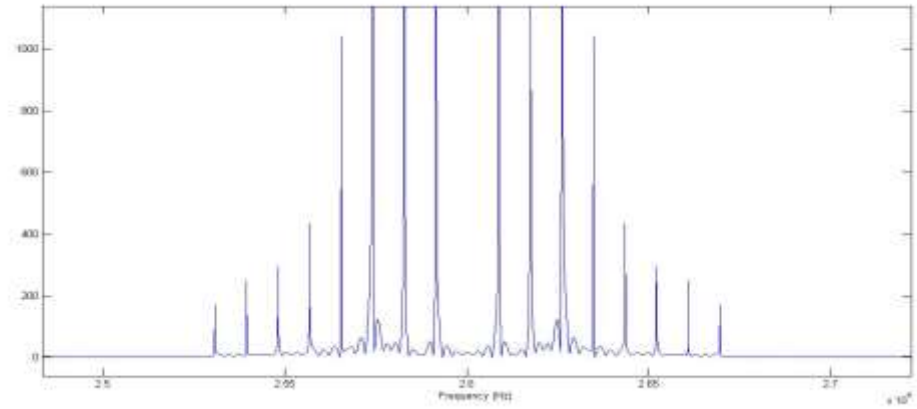
Fig A. 12 frequency spectrum

Appendix B.2: Simulation and Experimental from previous Vibro – Impact Device
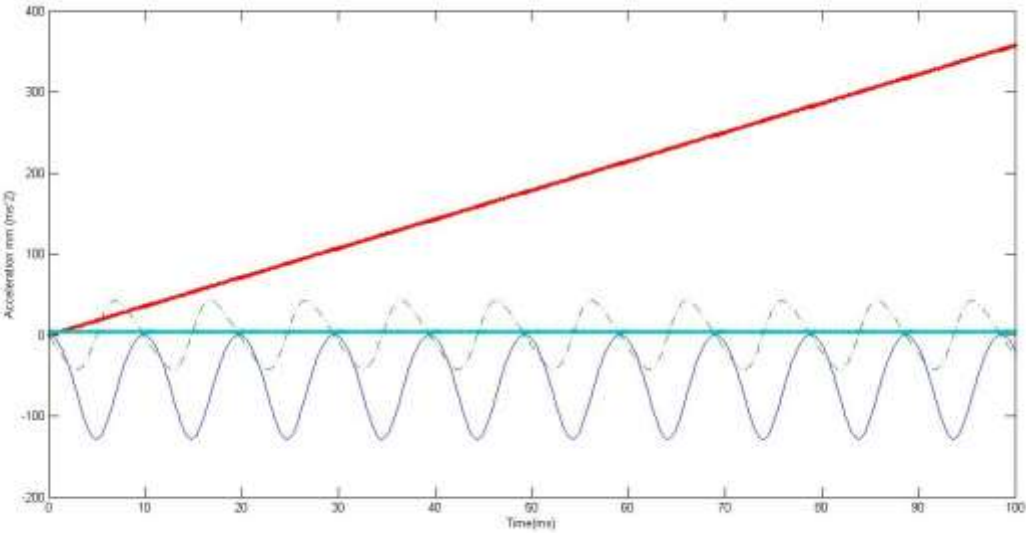
Fig A. 13 the dark blue graph is dx(1), the dotted line graph is dx(2), the red graph is dx(3) and the blue straight line is dx(4) "the acceleration".
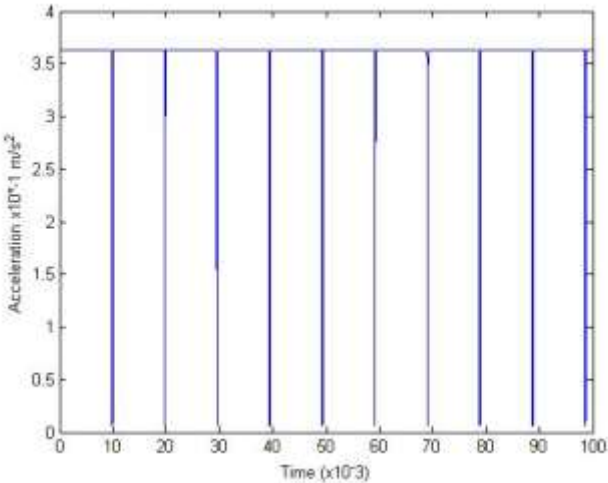
Fig A. 14 zoomed in of the acceleration graph.
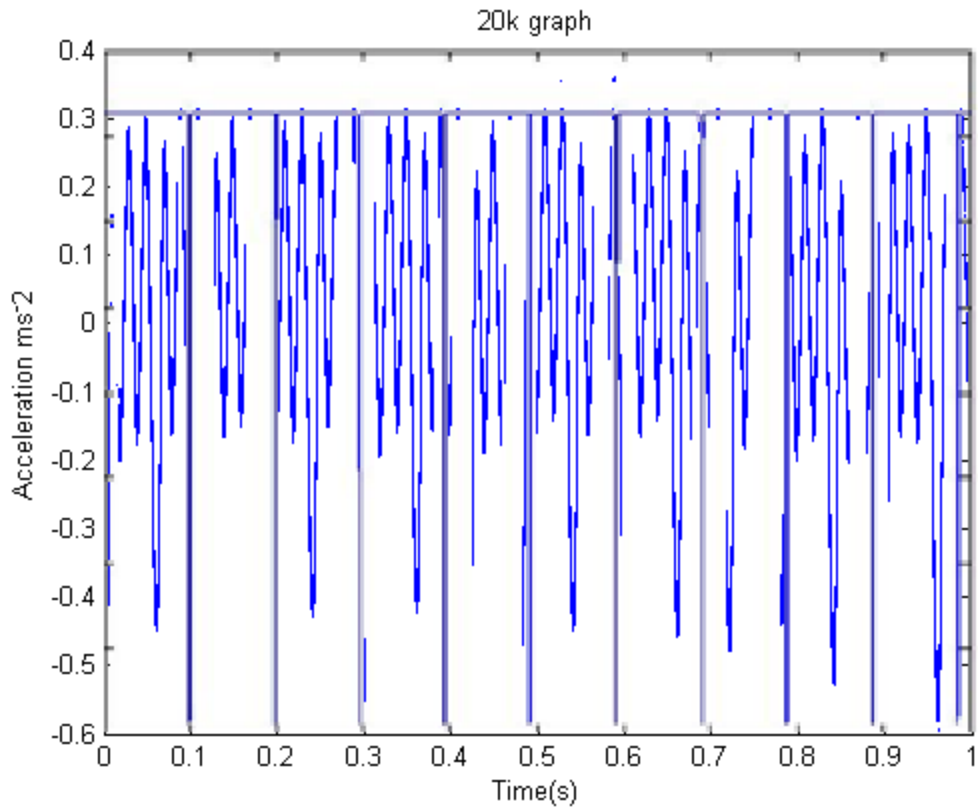
Fig A. 15 comparison of the graphs, the spike is the experimental, whereas the square shape is

the simulated.

Appendix C : MATLAB, Simulink model, and Arduino codes

Fig A. 16 Labview model as a whole with subsystems.
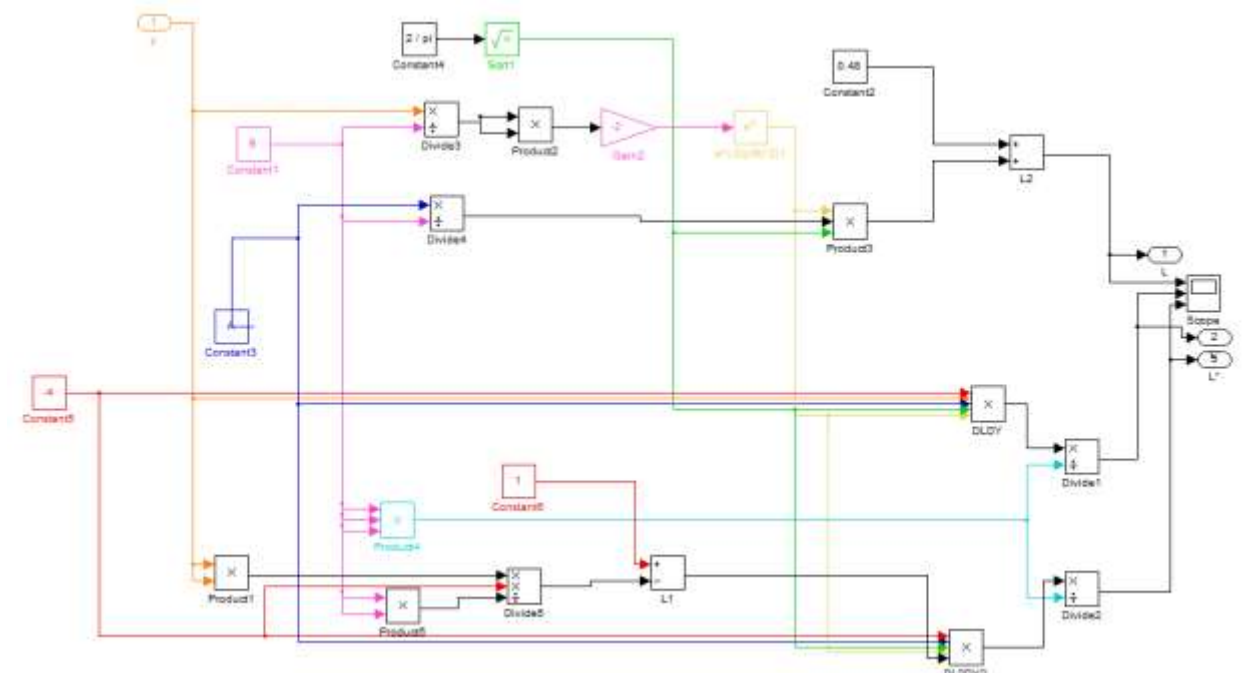
Fig A. 17 Inductance view

The Simulink model that describes the mathematical model base on the equation (8).
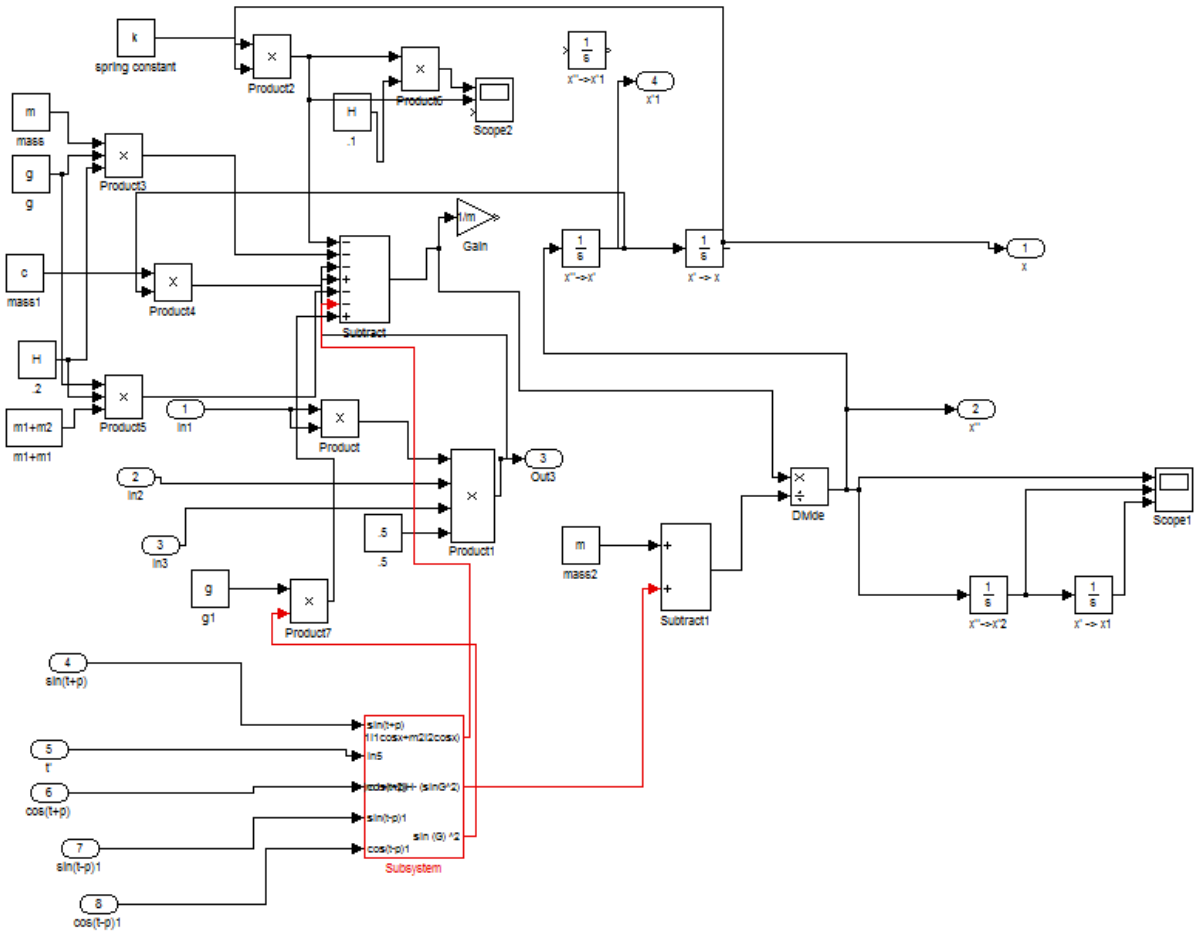
Fig A. 18 Oscillator Simulink subsystem

179
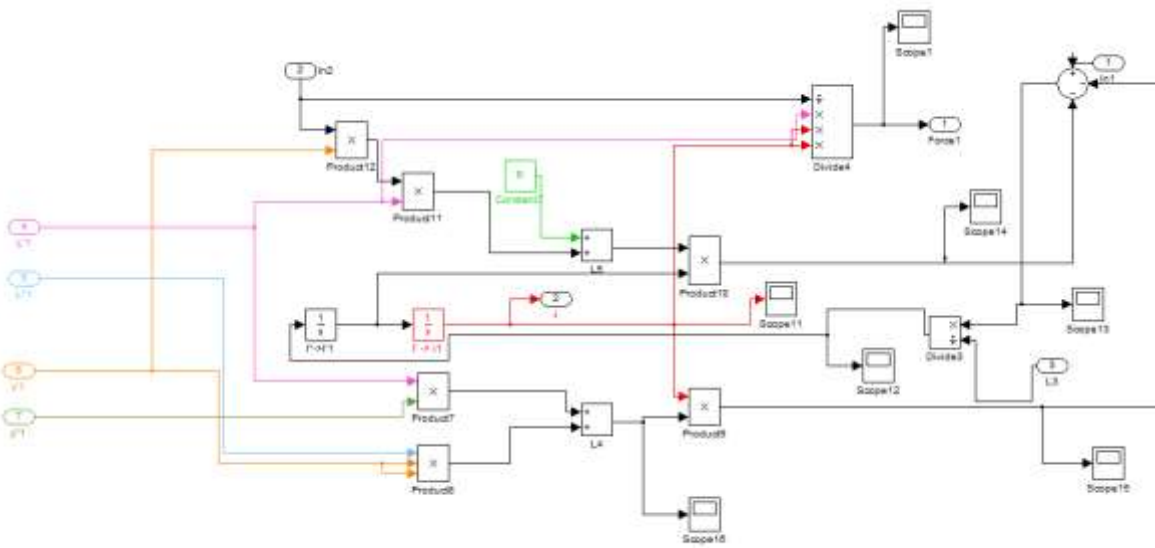
Fig A. 19 Current equation Simulink subsystem
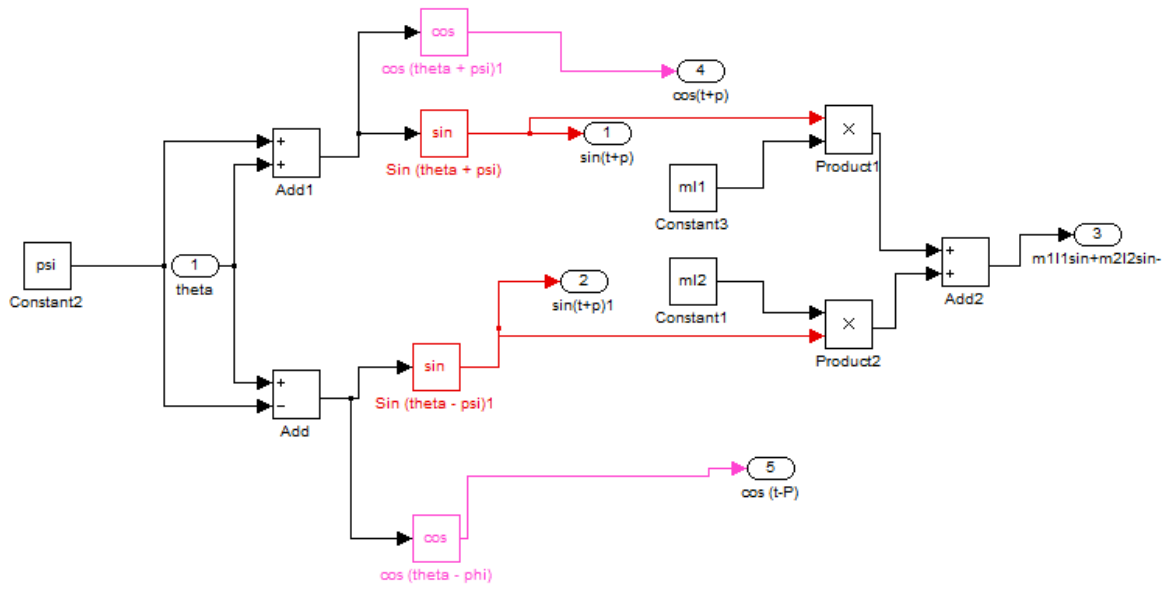
Fig A. 20 Angular relation subsystem
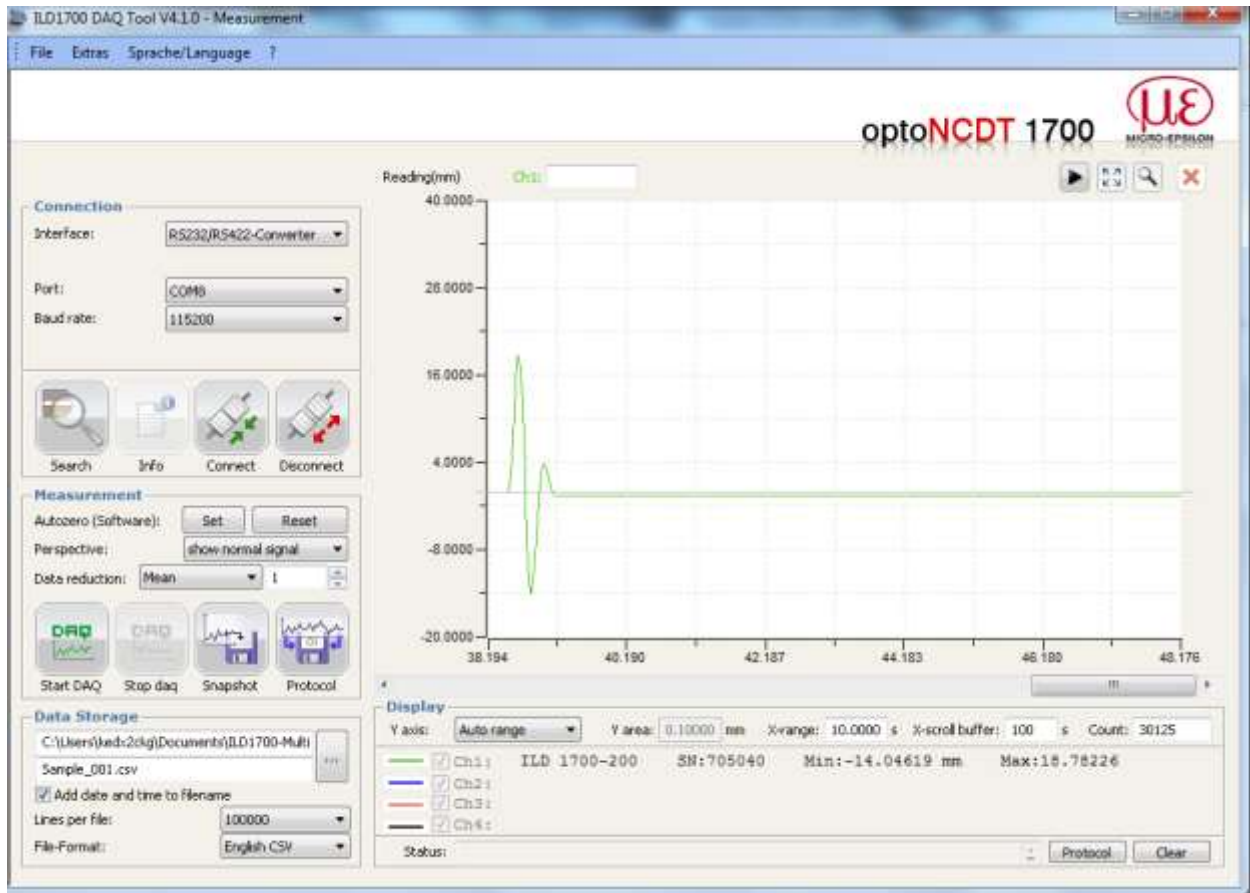
Fig A. 21 Vertical damping oscillators

```
%function dbifurc

global A  B L_0 l f m k R V C_z C_theta phi I g sigma_z sigma_theta %Making the variables

in dfile to be able to pass explicitly to the workspace




%Defining global variables%

A= 0.000028;        %Coefficient

B=0.01;            % Standard deviation

L_0=0.0019*10^-2;        % Initial inductance of the solenoid in unit H
```

```
g=9.81;          % Gravitational acceleration in unit m/s^2

l=0.34;          % Length of pendulum in unit m

I=((1.6314*10^-5)+(1.8073*10^-5)); % Total second moment of inertia in unit kgm^2

m=1.4;           % Total mass in unit kg

f=5;             %Frequency in unit Hz

V=18;            % Voltage of AC power supply in unit V

R=25;            % Resistance, unit in Ohm

C_z=0.3366;      % Damping coefficient of the vertical axis in unit Ns/m

C_theta=1.501*10^-5;   % Damping coefficient of the angular axis in unit Nms/rad

k=95;            % Capacitance, in unit F

phi=pi/2;

sigma_z=0.2618;

sigma_theta= 2.2*10^-3;% Subtended angle in unit rad


%Generating Time Histories and Phase Portrait

x0=[0 0 0 7.25*pi 0 0];%Change this for altering frequency

options=odeset('RelTol',1e-16);

[t,x] = ode15s(@testrun2,[0:1/(2*pi*f*500):2],x0,options);

%

% for a = 1:1:5

%

%  hold off

% for count=1:100 %increase the frequency value
```

```matlab
%    dt=0.01;

%    t(count+1)=t(count)+dt;

% [T x] = ode15s(@testrun2, [t(count+1)], [0 0 0 10 0 0]);

%

%    plot(a,x(cnt,3),'.','MarkerEdgeColor','k');

%    xlabel('a')

%    ylabel('x') % plotting on the bifurcation diagram

%    hold on;

%    %cnt=cnt+1;

% end

% a=a+count/100

% count

% hold on

% end


% =====BACKUP====

% a = 1;

%

%  hold off

% for count=1:100 %increase the frequency value

%    [T x] = ode15s(@testrun2, [0:2*pi/(100*a):10], [0 0 0 10 0 0]);

% for cnt=50:100 %plot points for a single value of a

%    plot(a,x(cnt,3)); % plotting on the bifurcation diagram
```

```matlab
%     hold on;

%      %cnt=cnt+1;

% end

% a=a+count/100

% count

% hold on

% end


% figure;

% plot(t,(x(:,3)),'k');

% title('theta vs t')

% xlabel('t (s)');

% ylabel('theta (deg)');

% axis square

% figure;

% plot(x(:,3),x(:,4));

% xlabel('theta');

% ylabel('theta_dot');

% axis square


 figure;

%%plot(t(:,1),mod(((x(:,3))*(180/pi)),360),'k');axis([8 10 -1 7]);

H = (2*pi);
```

```
x2 = mod (x(:,3), H);

plot (t,x2);axis ([5 7 -1 7]);

%%plot(t(:,1),mod(((x(:,3))*(180/pi)))); axis([5 7 -10 370]);

title('theta vs t')

xlabel('t (s)');

ylabel('theta (deg)');

axis auto

axis square
```

Table A. 1 The equation in matlab software

```
m = 1.6 +.375 ;

k = 285;

dl = 1;

i = 1;

f = 3.2;

g = 9.81;

c = 1;

m1 = 0.018;

m2 = 0.019;
```

```
phi = (22.5/360) * 2 * pi;

l1 = 0.034 ;

l2 = 0.035;

j1 = 0.00002;

j2 = 0.00005;

H= (m1*l1)^2 + (m2*l2)^2 + j1 + j2 ;

Hm = H* (m1+m2);

ml1 = m1*l1;

ml2 = m2*l2;

A= 0.000028;       %Coefficient

B=0.01;           % Standard deviation

L_0=0.0019;        % Initial inductance of the solenoid in unit H

R = 25;

psi = 22.5 * ((2*pi)/360);

V = 15;

ct_z = 0;

%ct_z = 0.192;
```

Table A. 2 Input data

```
y1 = theta.Data;

x1 = theta.Time;

y3= vertical.Data;

x3 = vertical.Time;

K = (2*pi);

y2 = mod (y1, K);

plot(x1,y2);axis([25 29 -1 7]);

%plot(x3,y3);axis([25 29 -1 7]);

%%plot(x1,y2);axis([38 42 -1 7 ]);

%%plot(x1,y2);axis([50 56 -1 7]);

%%when initial angular velocity is x<7.25pi period 2 oscillation can be found

%%in the system. when the angular velocity is 7.25pi period 4 rotation can be

%%found, when the angular velocity is 7.5pi period 2 rotation can be found,

%%and when the angular velocity is 10pi = period 1 rotation is found, an

%%extra speed can found when increasing the angular velocity to 12pi.
```

Table A. 3 Drawing code from Simulink data

```
freq=0.0000005;


t=0:0.005:10;

y=randn(2001,1);
```

```
z=zeros(2001,1);

x= square(2*pi*freq*t);

for cnt2=1:2001

 z(cnt2,1)= z(cnt2,1)+1000*square(2*pi*freq*t(cnt2),100*y(cnt2,1));

 if z(cnt2,1)> 0;

   z(cnt2,1) = z(cnt2,1);

 else

   z(cnt2,1) = 0;

end

end

plot(t,z)


fid=fopen('example4.dat','w');

fprintf(fid,'L%5.0f,',z);

fclose(fid);
```

Table A. 4 Stochastic distribution number generator

```
clc; clear;

global F w A B C

F = 0.177;

A = 0.168;

B = 0.5;

C = 0.5;
```

```matlab
w = 2000 *2*pi;


x0 = 1;

v0 = 0;

[t,x] = ode45(@chan,[0 200],[x0 v0]);


figure(1)

plot(t,x(:,1)) %displacement,x over time,t

xlabel('time')

ylabel('displacement')


figure(2)

plot(t,x(:,2)) %velocity,v over time,t

xlabel('time')

ylabel('velocity')


figure(3)

plot(x(:,1),x(:,2)) %poincare map

xlabel('displacement')

ylabel('velocity')


G = x(:,2)* 1000 * 1000;

%% G=x(:,1);
```

```matlab
%%z=0:0.005:10;

%%y=randn(2001,1);

%%for cnt2=1:2001

 %%G(cnt2)= G(cnt2)+1000*square(2*pi*freq*z(cnt2),100*y(cnt2));

%%end


figure(4)

plot(t,G) %displacement,x over time,t

xlabel('time')

ylabel('input')

J = G;


%%for cnt2=1:1746577

%%if J(cnt2,1)>0

 %%  J(cnt2,1) = 1000;

%%elseif J(cnt2,1) == 0

 %%  J(cnt2,1) = 0;

%%else

 %%  J(cnt2,1)= -1000;

%%end

%%end


figure(5)
```

```
plot(t,J) %displacement,x over time,t

xlabel('time')

ylabel('input')

%%for cnt2=1:2501

 %%J(cnt2,1)= J(cnt2,1)+1000*square(2*pi*freq*t(cnt2),100*y(cnt2,1));

%%end

K = J(1:10000);

%%J = J(1,10000);

fid=fopen('examplechan3.dat','w');

fprintf(fid,'L%5.0f,',K);

fclose(fid);
```

Table A. 5 Duffing's Equation

```
function [dx] = chan(t,x);



global F w A B C

dx = zeros(2,1);

dx(1) = x(2);

dx(2) = F*sin(w*t) - A*x(2) + B*x(1) - C*(x(1).^3);
```

Table A. 6 Global buffering data

```
// Read in 10-bits Magnetic Encoder AEAT-6010-A06  into Arduino Uno

// RobinL


// Declarate


const int CSn = 4; // Chip select

const int CLK = 7; // Clock signal

const int DO = 8; // Digital Output from the encoder which delivers me a 0 or 1, depending on

the bar angle..

int analogPin = 3;

int val = 0;

int s=0;

int tix = 0;

int sec=0;

int minutes=0;

int initialHours = 02;//variable to initiate hours

int initialMins = 0;//variable to initiate minutes

int initialSecs = 00;//variable to initiate seconds

unsigned int sensorWaarde = 0;

void setup() {

  Serial.begin(115200);

  pinMode(CSn, OUTPUT);
```

```
  pinMode(CLK, OUTPUT);

  pinMode(DO, INPUT);

  digitalWrite(CLK, HIGH);

  digitalWrite(CSn, HIGH);

}

int seconds()

{

   s = initialHours*3600;

   s = s+(initialMins*60);

   s = s+initialSecs;

   s = s+(millis()/1000);

   return s;

}

//assign seconds

int secs()

{

   sec = seconds();

   sec = sec%60;

   return sec;

}

//assign milliseconds

int tim()

{
```

```
  tix = millis();

  tix = tix%1000;

  tix = abs(tix);

  return tix;

}

//assign minutes

int mins()

{

   minutes = seconds();

   minutes = minutes/60;

   minutes = minutes%60;

   return minutes;

}


//To capture data from the function generator

void loop() {

 val = analogRead(analogPin);

 sensorWaarde = readSensor();

 delayMicroseconds(1); //Tcs waiting for another read in

}

unsigned int readSensor() {

 unsigned int dataOut = 0;

 digitalWrite(CSn, LOW);
```

```
  delayMicroseconds(1); //Waiting for Tclkfe

 //Passing 10 times, from 0 to 9

 for (int x = 0; x < 10; x++) {

   digitalWrite(CLK, LOW);

   delayMicroseconds(1); //Tclk/2

   digitalWrite(CLK, HIGH);

   delayMicroseconds(1); //Tdo valid, like Tclk/2

   dataOut = (dataOut << 1) | digitalRead(DO); //shift all the entering data to the left and past
the pin state to it. 1e bit is MSB

  }

//Data output

 digitalWrite(CSn, HIGH); //

  Serial.print(mins());

  Serial.print(" ");

  Serial.print(secs());

 Serial.print(" ");

  Serial.print(tim());

 Serial.print(" ");

 Serial.print(dataOut);

 Serial.print("");

 Serial.print(" ");

 Serial.println(val);

 Serial.print(" ");
```

```
//delayMicroseconds(4750);

 delay (2);

 return dataOut;

}
```

Table A. 7 Code generated from the Arduino Uno

Appendix D : Extra experimental results, and bifurcation table

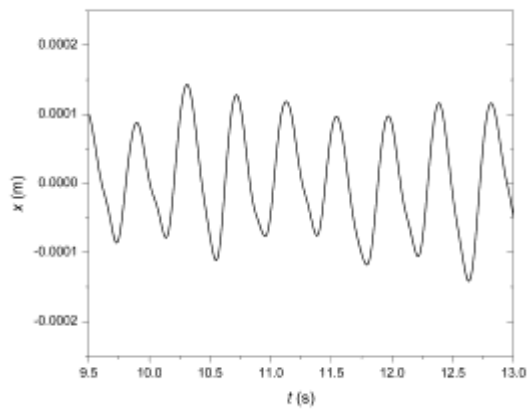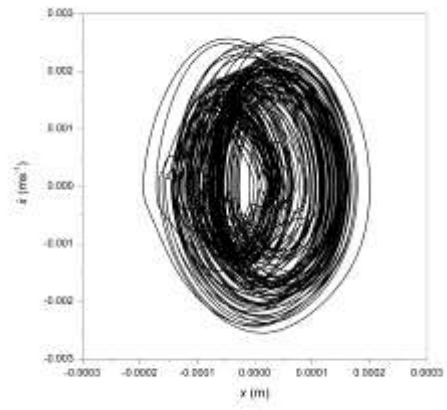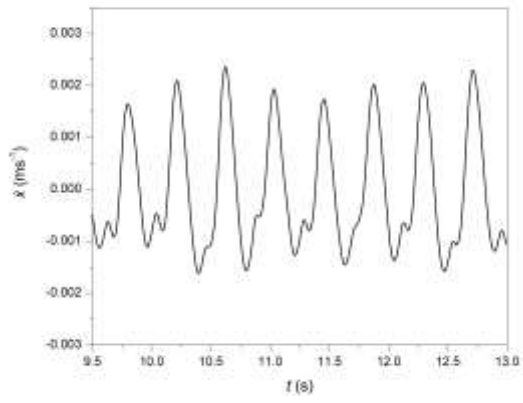Graphical responses
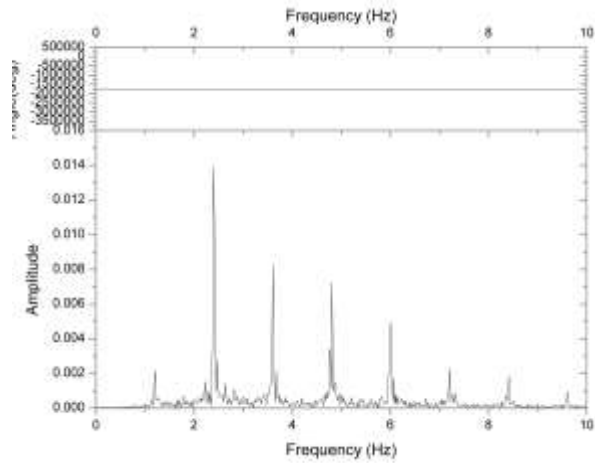
Rotation 21/4/14
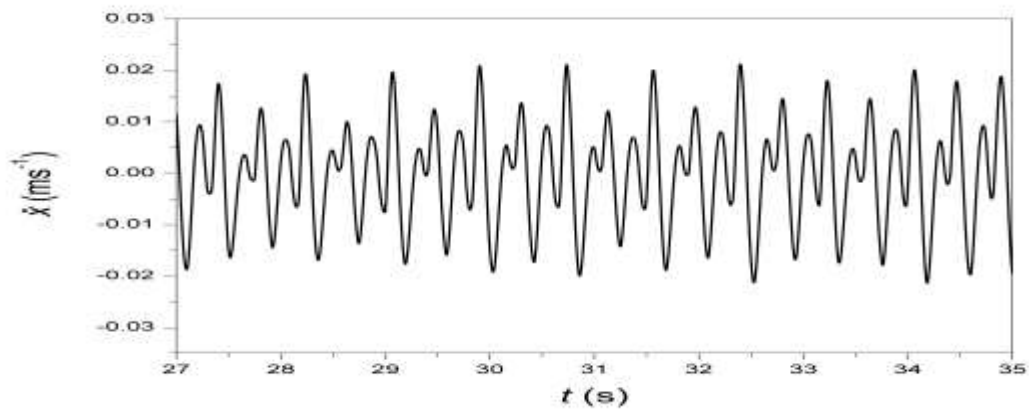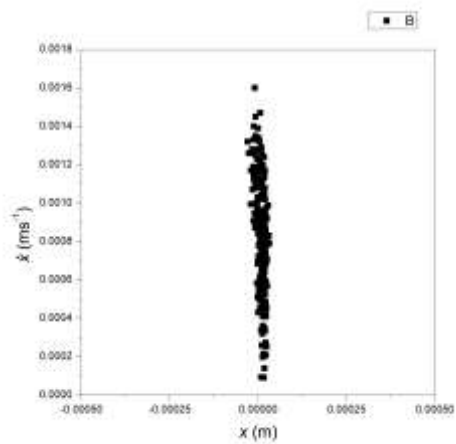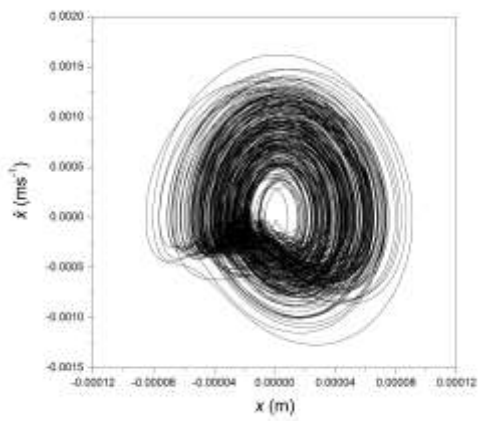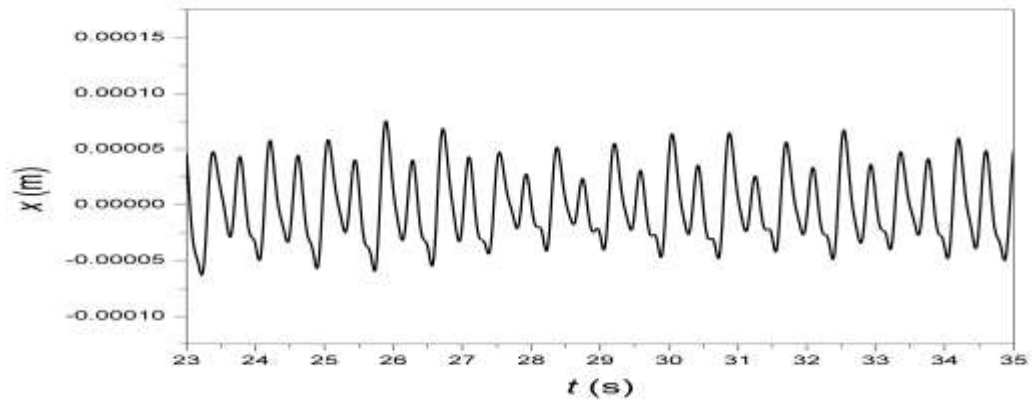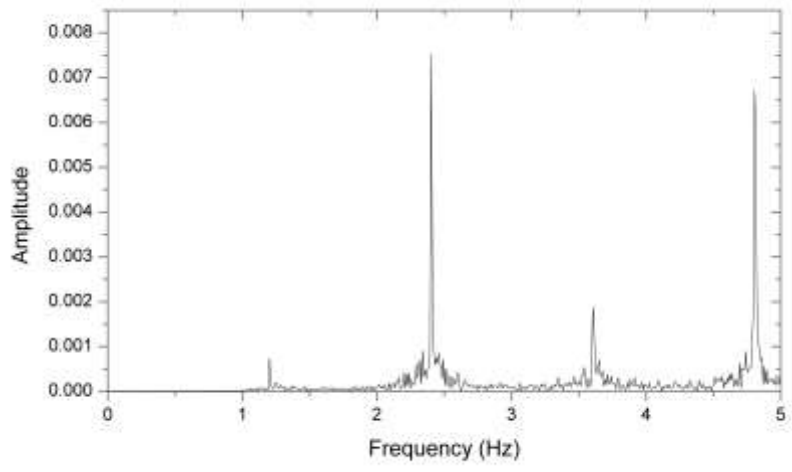
Oscillation
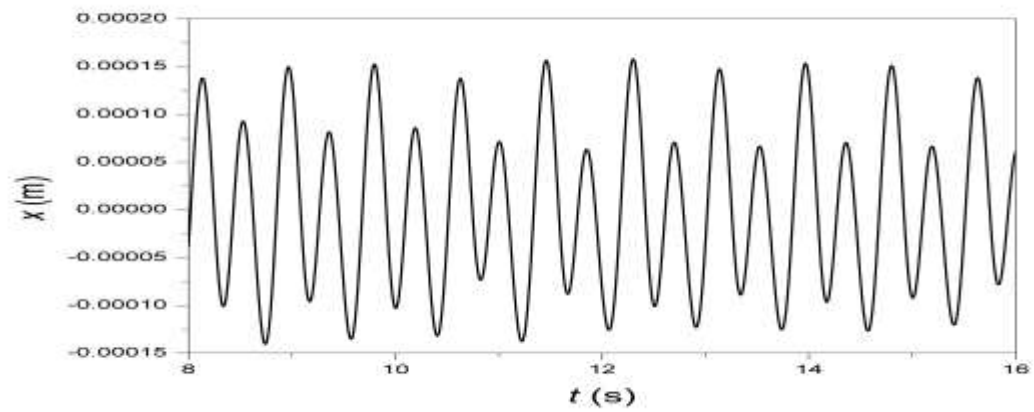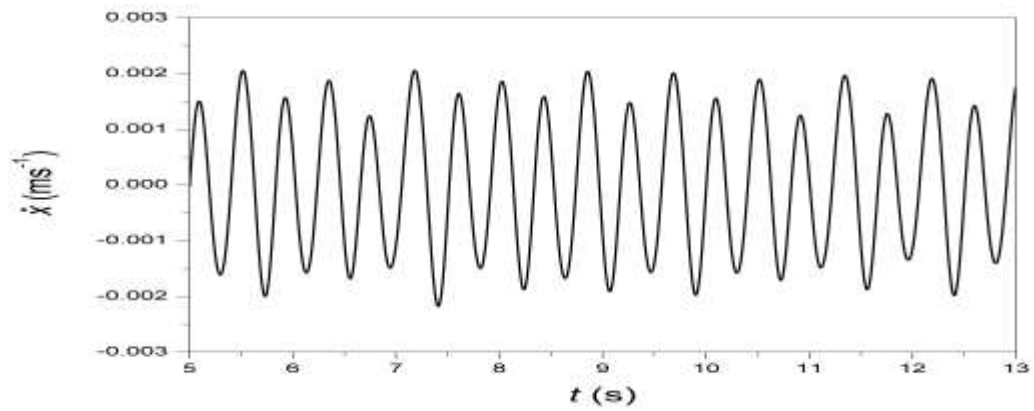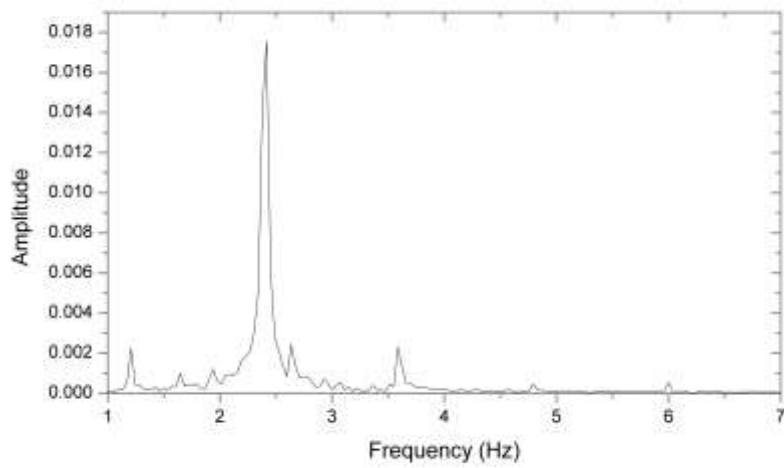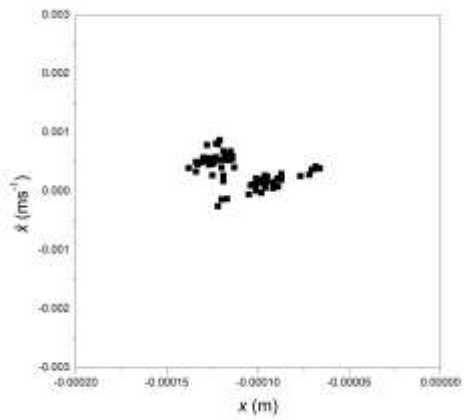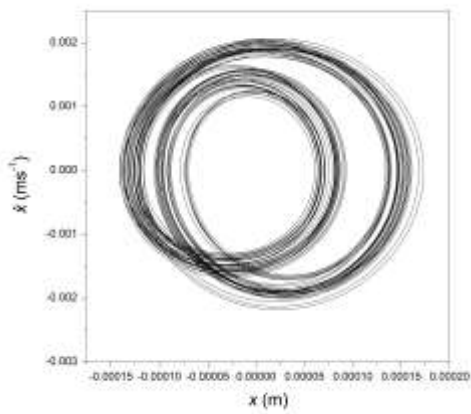
2.4156 Hz Responses when input 120 V with an angle to generate rotations.
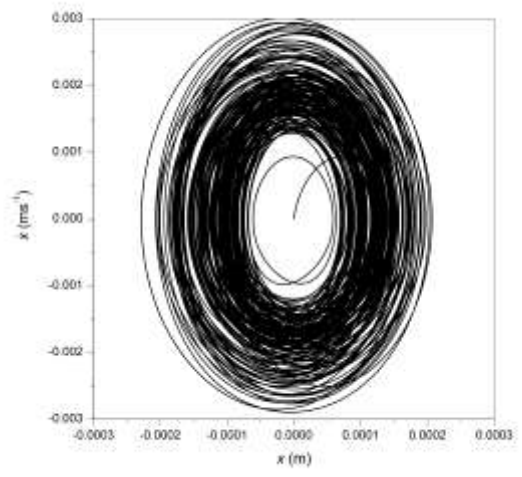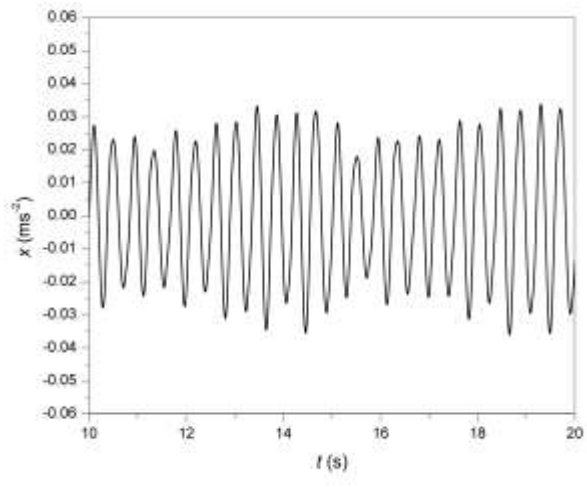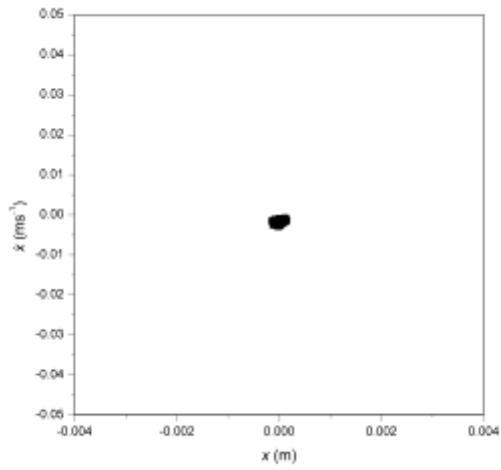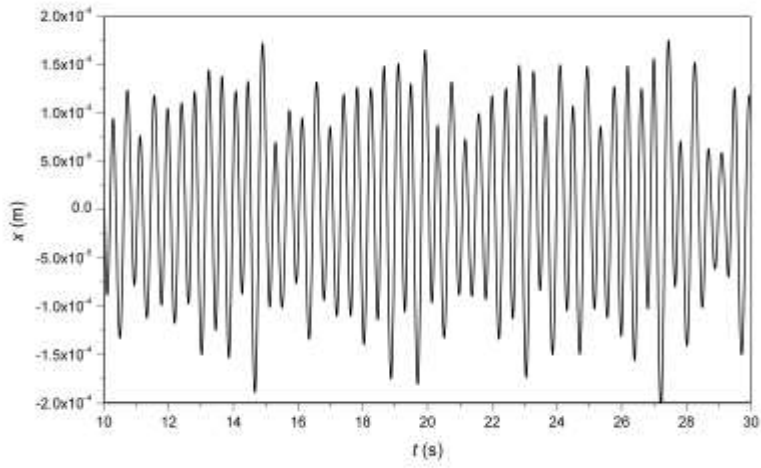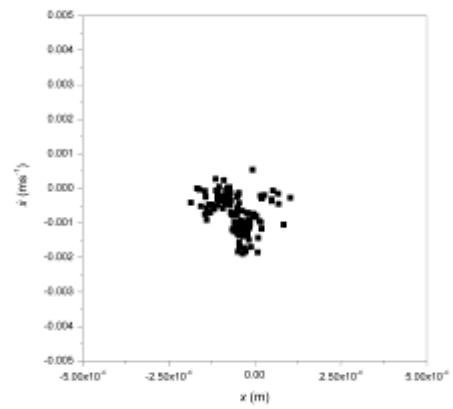
Bifurcation investigation

Bifurcation table

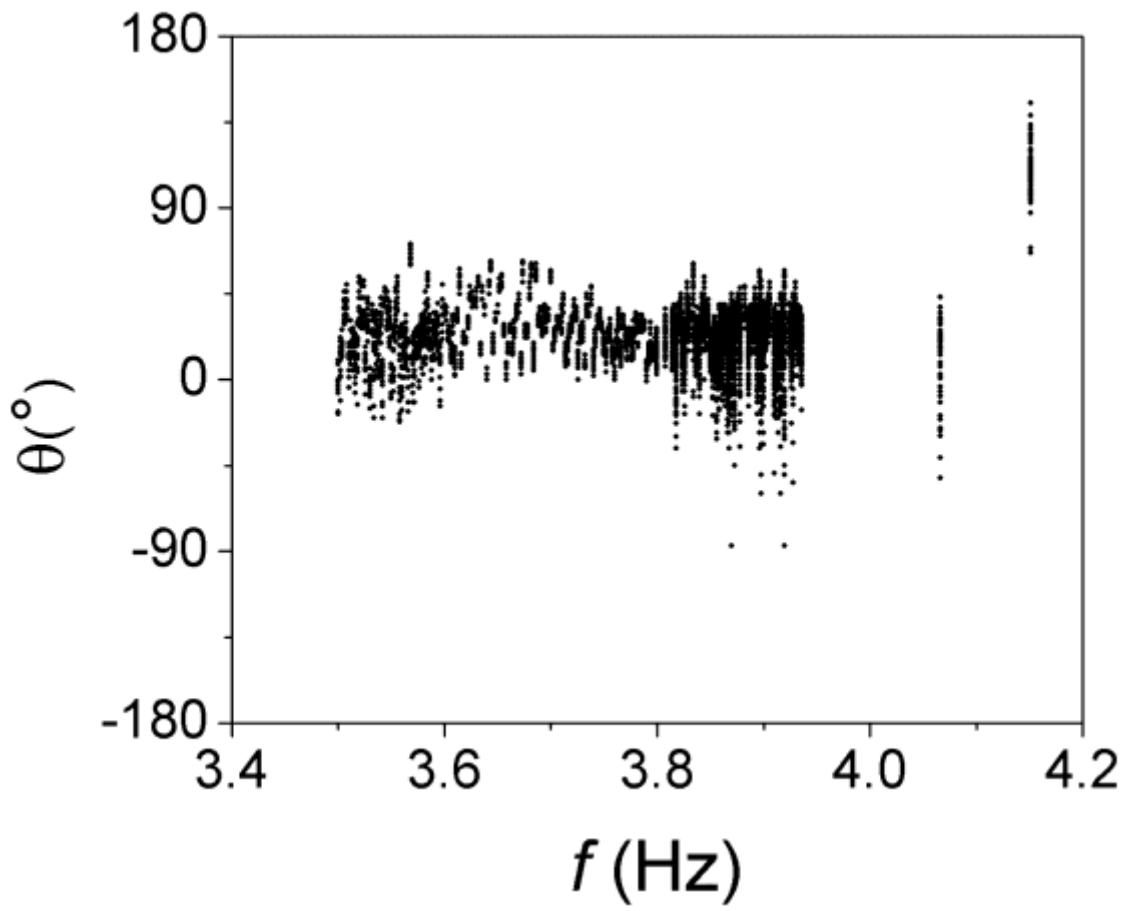The bifurcation was investigated however, due to the experimental result not being accurate, it was not presented. The graph is shown below:

Fig A. 22 Bifurcation Diagram